Title
Fast Times: Excitatory Effect of GABA in Axonal Compartments in the Cerebellar Molecular Layer

Author
Luo, Ray

Publication Date
2012

Peer reviewed|Thesis/dissertation

UNIVERSITY OF CALIFORNIA

Los Angeles

Fast Times:

Excitatory Effect of GABA in Axonal Compartments in the Cerebellar Molecular Layer

A dissertation submitted in partial satisfaction of the

requirements for the degree Doctor of Philosophy

in Neuroscience

by

Ray Luo

2012

ABSTRACT OF THE DISSERTATION

Fast Times:

Excitatory Effect of GABA in Axonal Compartments

in the Cerebellar Molecular Layer

by

Ray Luo

Doctor of Philosophy in Neuroscience

University of California, Los Angeles, 2012

Professor Thomas S. Otis, Chair

While exploring the functions of individual cells in a circuit, we can often overlook the importance of specialized subcellular compartments organized within one neuron. We probe the former with techniques like optogenetics, optical imaging, and (multi) cell recordings, while the latter can be clouded with mystery that have only begun to resolve in recent years. We explore these seemingly remote and difficult-to-record-from places in a well-mapped circuit in the cerebellum that is also relevant to behavior. Granule cells of the cerebellar cortex carry information associated with the context of a motor movement to the Purkinje cells, which as the sole output of the cerebellar cortex, is a major site of motor learning. Traditionally thought to be inhibitory, $GABA_A$

receptors ($GABA_A$Rs) in granule cells, although inhibitory in the soma, have been found to be excitatory in the axons. These axons, the parallel fibers, are too thin to record from, and methods to study them include population recordings like calcium imaging and fiber volley detection, computational modeling, and voltage sensitive dyes.

We first studied the presynaptic terminals of parallel fibers using calcium imaging, and showed that $GABA_A$R activation leads to increased amplitude of stimulus-evoked calcium transients. This excitation appears to bring axons closer to firing threshold, recruiting addition fibers as opposed to increasing calcium levels on a per fiber basis. Blocking the transporter that accumulates chloride reduces the effect, suggesting that high chloride concentration in the axons is the mechanism behind this effect.

To gain better temporal resolution, we used GABA uncaging to probe extracellular fiber volleys and found that GABA not only increases fiber volley amplitudes, but also increases conduction velocity on parallel fibers. We showed that δ-subunits are not required for $GABA_A$R-mediated excitation and that endogenous GABA in a slice is sufficient to excite parallel fibers. Using a computational model of the granule cell, we showed how GABA-mediated excitation on the axons can influence cell spiking, and that properties of sodium channel inactivation determine whether there's an excitatory effect of GABA on threshold for spiking and on conduction velocity.

Finally we described a novel method for detecting voltage in subcellular compartments utilizing fluorescence transfer between a lipophilic tracer dye and a voltage sensitive compound. This two-component system is seen to produce some of the biggest voltage sensing signals in the literature, and is capable of recording

submillisecond voltage fluctuations in subcompartments of a Purkinje cell. We propose to use this system to record voltage from parallel fibers and determine the effect of GABA on action potential shape and subthreshold voltage fluctuations.

The dissertation of Ray Luo is approved.

_____
Dean V. Buonomano

_____
Felix E. Schweizer

_____
Julio L. Vergara

_____
Thomas S. Otis, Committee Chair

University of California, Los Angeles

2012

To Mom, and Clarice.

"St. Augustine, like a great artist, had worked from multiplicity to unity, while [I], like a small one, had to reverse the method and work back from unity to multiplicity."

Henry Adams, *The Education of Henry Adams*, 1919.

"If I want to learn the art of loving, I must strive for objectivity in every situation, and become sensitive to the situations where I am not objective. I must try to see the difference between *my* picture of a person and his behavior, as it is narcissistically distorted, and the person's reality as it exists regardless of my interests, needs, fears."

Erich Fromm, *The Art of Loving*, 1956.

"We don't see things as they are, we see them as we are."

Anaïs Nin, *Seduction of the Minotaur*, 1958.

TABLE OF CONTENTS

FIGURE LIST

ACKNOWLEDGEMENTS

My mother Connie has been there for me no matter what my temperament, and no matter what turn life has taken for me. I wish to thank her.

My adviser Dr. Tom Otis leads me by the example he sets as an insightful scientist, a caring mentor, and an inspiring communicator. I wish to thank him.

My colleague Dr. Shlomo Dellal has donated most of his time and energy to this project, and importantly, has inspired a healthy self-skepticism. I wish to thank him.

My laboratory associates Dr. Meera Pratap, Dr. Martin Wallner, Dr. Movses Karakossian, Dr. Paul Mathews, Dr. Joyce Wondolowski, Dr. Ka Hung Lee, Dr. Matthew Shtrahman, Dr. Lawrence Kruger, Dr. Paul Dodson, Dr. Viji Santhakumar, Jaione Maiz, Alex Reeves, Patty Araj, Mariam Al-Hamad, and Vivy Tran have fueled me with their scientific ideas, selfless and generous help, and friendship. I wish to thank them.

My program director and manager Dr. Michael Levine and Suzie Vader have provided the infrastructure and aid for my continuing studies. I wish to thank them.

My committee members Dr. Dean Buonomano, Dr. Felix Schweizer, and Dr. Julio Vergara have supported me with guidance and encouragement. I wish to thank them.

My friends TY, DC, AC, DH, CI, SN, BC, QC, who inspired. I wish to thank them.

Chapter II is adopted from (Luo, Dellal et al. 2012) in preparation to PLOS One. Chapter III is adopted from (Dellal, Luo et al. 2012) in Journal of Neurophysiology. Chapter IV is adopted from (Bradley, Luo et al. 2009) in Journal of Neuroscience.

Funding sources include Eugene V. Cota-Robles fellowship (UCLA) and Neural Microcircuits training grant (NIH).

VITA

2012 University of California, Los Angeles, Ph. D. Program in Neuroscience.

2005 University of California, Berkeley, B. S. EECS, Minor Mathematics.

2003 Harvey Mudd College, Claremont, Major CS, Mathematics, Psychology.

BIOGRAPHICAL SKETCH

2012 Graduate Student Researcher, Tom Otis Laboratory, UCLA.

2010 Editor-in-chief, The Mental Note Online Newsletter, UCLA.

2009 Arts and Entertainment Editor, Pacific Ties News Magazine, UCLA.

2006 Teaching Assistant, Department of Chemistry and Biochemistry, UCLA.

2006 Teaching Assistant, Life Sciences Core Curriculum, UCLA.

2006 Rotation Student, Istvan Mody Laboratory, UCLA.

2006 Rotation Student, David Krantz Laboratory, UCLA.

2005 Intern, Stottler Henke Artificial Intelligence Consulting, California.

2005 Contributor, UC Berkeley Scientific Journal, UC Berkeley.

2005 Research Associate, Cognition and Action Lab (Richard Ivry), UC Berkeley.

2005 Research Intern, Palo Alto Research Institute (David Fleet), California.

2005 Teaching Assistant, Electrical Engineering Department, UC Berkeley.

2004 Research Programmer, Group for User Interface Research, UC Berkeley.

2003 Research, Visualization and Intelligent Systems (Bir Bhanu), UC Riverside.

2003 Research Associate, Pomona College Psychology (Bill Banks), California.

2002 Intern, HRL Laboratories Information Sciences (Pete Tinker), California.

PUBLICATIONS AND PRESENTATIONS

Dellal, S. S.*, Luo, R.*, Otis, T. S. (2012) $GABA_A$ receptors increase excitability and conduction velocity in cerebellar parallel fiber axons. J. Neurophysiology, doi: 10.1152/jn.01028.2011 (* - these authors contributed equally to this work.)

Luo, R. (2011) Axonal excitation by GABARs facilitates initiation and propagation of action potentials. Interdepartmental Neuroscience Program retreat talk, UCLA.

Luo, R., Dellal, S. S., Otis, T. S. (2010) Mechanism and consequence of parallel fiber excitation by $GABA_A$ receptor activation in the cerebellum. FENS poster, Holland.

Luo, R. (2010) California neuroscientists hike up Montreal for Cognitive Neuroscience conference. CNS article, Canada, http://thementalnote.ucla.edu/?p=104.

Luo, R., Dellal S. S., Otis, T. S. (2009) RIKEN BSI summer poster colloquium.

Bradley, J., Luo, R., Otis, T. S., DiGregorio, D. A. (2009) Submillisecond optical reporting of membrane potential *in situ* using a neuronal tracer dye. J. Neuroscience, 29(29):9197-9209.

Luo, R., Dellal S. S., Otis, T. S. (2009) Dynamics of Neural Microcircuits poster.

Luo, R., Dellal, S. S., Otis, T. S. (2008) Axonal measurements of calcium implicate $GABA_A$ receptors in mediating parallel fiber excitation. SfN poster, Wash DC.

Luo, R. (2005) Learning categories using semantic priming in a Bayesian framework. California Engineer, 81(2):18-23.

Poon, E., Luo, R., Fleet, D. (2005) Tracking people with edge statistics and hybrid Monte Carlo filtering. Palo Alto Research Center research symposium poster.

Luo, R., Fleet, D. (2004) Empirical likelihoods for visual tracking. PARC abstract.

CHAPTER I

Introduction

Each of us serves a unique function in our society, specializing in what we do best and communicating with those whom we rely on. Each cell serves a unique function in a microcircuit, processing information of some modality and transmitting signals to other units downstream. Does each *part* of a cell also serve a unique function analogous to the way each individual specializes in its community of interacting units? How can we explore the subcellular structures of a neuron to investigate its functional significance? We will attempt to bridge this gap between cellular physiology and molecular neuroscience by using different techniques and applying diverse perspectives to analyze one well-mapped system that has proven behavioral relevance.

We focus on a circuit in the cerebellar cortex critical for motor learning in paradigms such as eyeblink conditioning, vestibulo-ocular reflex, and saccade adaptation. In particular, we examine the cerebellar granule cell, which at around 50 billion, make up the largest neuron population in the brain (Haines 2008). These 6 μm diameter neurons transmit sensory information received from the cerebral cortex to the error correcting output of the cerebellum, the Purkinje cells. Granule cells possess up to 6 mm long axons called parallel fibers that ascend into the molecular layer to innervate both the output Purkinje cells as well as interneurons that secret GABA (Palay and Chan-Palay 1974). These 0.3 μm diameter fibers are difficult to study one-on-one, and often bulk signals of population activity are the only feasible means of inferring conduction and release modulation in them. What are the functional consequences of modulating parallel fiber activity? How do we study these subcellular structures in the context of the function of granule cells in a motor learning circuit?

The computations carried out by the cerebellum can be read out as Purkinje cell output, which is in turn influenced by the modulation of parallel fiber activity by GABA (Stell, Rostaing et al. 2007; Pugh and Jahr 2011). In this chapter, we set the stage by introducing the cerebellar circuit and the place of granule cells within it, as well as some techniques for studying them at the macro and micro levels. In the second chapter, we examine presynaptic calcium release at parallel fiber terminals and how they are affected by GABA modulation. We see that GABA has an excitatory effect on calcium transients in the molecular layer and that this effect depends on the chloride gradient established by a balance of transporters on these fibers. In the third chapter, we move one step backward to investigate the conduction of action potentials along parallel fibers. Using a temporally more precise method of introducing GABA as well as a computational model for carrying out physiologically inaccessible experiments, we show that GABA decreases spike threshold and increases conduction velocity on parallel fibers. In the fourth chapter, we continue the theme of using novel techniques to uncover activity in inaccessible compartments by introducing an optical two-component voltage sensing technique, and show how it would allow us to examine modulation of individual action potential as in the parallel fibers. Finally, in chapter five, we conclude with a summary of our results, and speculate on how parallel fiber excitation contributes to cerebellar processing, and how it may generalize to other types of compartmental specialization in neuronal systems.

BRIEF HISTORY

Although both the Greek Galen and the Roman Vesalius described the cerebellum, it wasn't until the 1600s and 1700s when fine structures were identified by Raymond de Vieussens (deep nuclei) and Vincenzo Malacame (folia differentiation) (Glickstein, Strata et al. 2009). Phrenologists actually took cerebellum as an organ associated with sexuality, and it wasn't until Pierre Flourens studied cerebellar lesions that the organ's function in motor coordination began to be illuminated. In the 1900s, Lodewijk Bolk and others mapped cerebellar structure in different mammals and created a nomenclature still used today to codify the lobules common to all mammals.

When Jan Evangelista Purkinje first looked into the cells of the cerebellar cortex that now takes his name, he also laid down the foundation of what would be called the neuron doctrine, that idea that individual separate units make up the nervous system. Camillo Golgi oppsed this idea, maintaining instead that nerve elements formed an interconnected reticular network. Ironically it is Golgi's eponymous silver nitrate stain that allowed Santiago Ramon y Cajal to first identify subcellular structures like spines and growth cones (Ramón y Cajal 1905). Cajal's descriptions of mossy fiber and climbing fiber inputs to the cerebellum were given functional significance by Gerbrandus Jelgersma, who first suggested that the Purkinje cells provide a corrective signal based on these sensory and executive inputs (Glickstein, Strata et al. 2009).

In the 1960s, modern cerebellar physiology was ushered in by Sir John Eccles, who mapped the functional architecture of the cerebellum (Eccles 1967). Eccles and colleagues identified the basic excitatory and inhibitory cell types in the cerebellar

cortex, such as Purkinje cells and molecular layer interneurons, which received innervation from granule cells via parallel fibers. While the organization of the cerebellum is well-understood, the precise computation undertaken and the manner in which the computation is organized are still mysterious. David Marr put the physiological results in a theoretical framework, proposing that the mossy fiber-granule cell pathway provides patterns of contextual motor activities that are corrected by inferior olive-climbing fiber innervation of Purkinje cells (Marr 1969). James Albus modified this theory to account for the need for depression of Purkinje cell activity (Albus 1971) and Masao Ito provided experimental evidence for this model when he discovered climbing fiber mediated long term depression (LTD) of the parallel fiber-Purkinje cell synapse (Ito, Sakurai et al. 1982). We will now review the functional architecture of the cerebellum gleaned from these physiological studies.

CEREBELLUM ORGANIZATION

The cerebellum possesses a well-defined microstructure where the inputs, outputs, and relaying cell types are all well-organized. The input to the cerebellum comes from two sources. The mossy fiber pathway arises from the cerebral cortex, the spinal cord, the pons, and other brain stem areas, and synapses onto cerebellar granule cells at a structure known as the glomerulus (Kandel 2000). Each of the four claw-like dendrites of the granule cells populates a different glomerulus, expanding the mossy fiber inputs into a combinational code for finer discrimination. The mossy fiber input is

traditionally thought to carry information about the state of movement and environment, and this contextual information is recorded by the granule cell and relayed to Purkinje cells (25 to 75 μm in diameter) via its axon, the parallel fiber. The divergence of input from mossy fibers to granule cells converge again at the Purkinje cell, as each granule cell innervates only 400 Purkinje cells, but each Purkinje cells receives about 10,000 granule cell inputs (Palay and Chan-Palay 1974).

The second source of cerebellar input, the climbing fiber, originates in the inferior olive, and terminates on Purkinje cells on a one-to-one basis. Calcium spikes generated by climbing fiber excitation of Purkinje cells lead to a burst of action potentials known as the complex spike, which has been suggested to be an error signal for the coincident parallel fiber inputs coding for contextual motor signals. Firing spontaneously at 50 to 100 hz, Purkinje cells form the sole output of the cerebellar cortex and tonically inhibit the deep cerebellar nuclei (Hausser and Clark 1997). Climbing fiber-mediated complex spikes are followed by a characteristic pause in Purkinje cell firing, notably relieving the inhibition of the deep nuclei, which in turn project to brain stem and thalamic areas involved in movement control (Raymond, Lisberger et al. 1996).

In addition to Purkinje cells, granule cells also project via parallel fibers to molecular layer interneurons: basket cells and stellate cells, each of which inhibits Purkinje cells that usually lie outside the beam of parallel fiber activation. Parallel fibers also innervate a third type of inhibitory neurons, the Golgi cells, which provide feedback inhibition of granule cells.

Parallel fibers are axons of granule cells. They include the ascending axon, usually 70 μm long, as well as a T-junction at the molecular layer where the ascending segment splits into two branches (Palay and Chan-Palay 1974). Upon bifurcating in the molecular layer, these unmyelinated axons travel up to 2 mm in either direction while synapsing onto dendrites of Purkinje cells and molecular layer interneurons, often junctioning many times with the complex dendritic arbor of a single Purkinje cell. One is tempted to inquire whether modulation of excitability this far from the cell body would affect processing of orthodromic spikes from the granule cell itself.

CEREBELLAR PLASTICITY

Synaptic plasticity as a model for learning was given an experimental foundation by the discovery of Long Term Potentiation (LTP) in recording field potentials in the hippocampus (Bliss and Lomo 1973). These long lasting changes (hours to days) in synaptic efficacy caused by periods of brief trains of stimulation have an analog in the cerebellum in the form of Long Term Depression (LTD) of the parallel fiber to Purkinje cell synapse (Ito, Sakurai et al. 1982; Ito 1984). Cerebellar LTD is thought to involve a postsynaptic decrease of AMPA receptors in the active zone following climbing fiber-mediated calcium accumulation. The climbing fiber is thought to encode a teaching signal that suppresses the coincidence mossy-fiber to parallel fiber to Purkinje cell encoding. What's more, there're LTD and LTP at other points in the circuit worth noting, including LTP of the parallel fiber to stellate cell connection that would facilitate Purkinje

cell inhibition (Rancillac and Crepel 2004) and presynaptic LTP of parallel fiber to Purkinje synapses that do not require climbing fiber activity (Salin, Malenka et al. 1996).

The cellular plasticity in the cerebellar cortex has been given physiological relevance by a form of classical conditioning called eyeblink conditioning. In the task, a conditioned eyeblink reflex results from a tone (the conditioned stimulus) paired with an airpuff (the unconditioned stimulus). The cerebellar cortex is necessary for the precise timing required for the acquisition of eyeblink conditioning (Kim and Thompson 1997). Moreover, the mossy and climbing fiber inputs encode the conditioned and unconditioned stimulus, respectively (Steinmetz, Rosen et al. 1986). The mossy fiber carries sensory and movement-related input from the pons to the granule cells, which feed into the Purkinje cells. The climbing fiber carries the error correcting code associated with the puff from the inferior olive to the Purkinje cell, where the convergent inputs and resultant complex spike lead to a pause in spontaneous Purkinje cell firing, thus disinhibiting the deep nuclei, allowing it to activate facial movements via red nucleus control. Two compelling evidences for this claim are that cerebellar cortex lesions disrupts the timing of learned responses in eyeblink conditioning (Perrett, Ruiz et al. 1993), and that inferior olive stimulation can substitute for the unconditioned stimulus in eyeblink conditioning (Mauk, Steinmetz et al. 1986).

Plasticity in the cerebellar cortex is bidirectional. Receptive fields of Purkinje cells are decreased when parallel fiber stimulation was paired with climbing fiber activity, and increased when parallel fiber stimulation is unpaired (Jorntell and Ekerot 2002). For interneurons, receptive fields are expanded when parallel fiber activity is paired with

climbing fiber, and vice versa. However, since Purkinje cells fire spontaneously at 50 to 100 hz even without parallel fiber input (Hausser and Clark 1997), it is natural to wonder if parallel fiber LTD makes a substantial difference in learning. Alternatively, pauses in Purkinje cell firing following complex spikes are known to occur *in vivo* (Medina, Garcia et al. 2000), and may be crucial in disinhibiting the deep nuclei, although these occur in *response* to the error signals rather than anticipate them.

SUBCELLULAR ORGANIZATION

Just as the cerebellum and other nervous system structures are organized by their input and output pathways, the neuron itself is divided into its own functional compartments. We begin with the dendrite, which can have wide varying attenuated voltages depending on where one records from, so that identical synaptic inputs are amplified differently, especially in the case of complex dendritic structures such as those of neocortical pyramidal cells (Stuart and Spruston 1998). In the same way, inhibition is stronger near the soma than in the distal dendrites, allowing the dendrite to sum over a broader base of inputs (Pouille and Scanziani 2001). Moreover, in some cells such as the Purkinje cell, action potentials are not generated in the dendrite, but rather spread back to the dendritic tree passively following initiation in the axon initial segment (Stuart and Hausser 1994). In the Purkinje cell, dendritic spikes do not propagate well to the soma, and do not directly trigger the complex spike following climbing fiber input, but does regulate the post-complex spike pause, making the dendrite a functionally

distinct compartment from the rest of the cell (Davie, Clark et al. 2008). Unlike Purkinje cells, in CA1 pyramidal cells, action potentials can actively backpropagate to the dendrite, depending on the frequency of spiking and branch points in the dendrite (Spruston, Schiller et al. 1995). Back propagating spikes can even gate the induction of LTP in CA1 neurons (Magee and Johnston 1997). Thus the dendrite can act like an axon in conducting regenerative spikes to presynaptic boutons.

The study of axonal compartments can be divided into work on spike initiation and work on spike propagation. Direct verification that the axon initial segment is the site of action potential initiation was conducted using voltage-sensitive dyes, showing that in layer 5 pyramidal cells, spikes are generated at the distal end just before the first internode (Palmer and Stuart 2006). One reason for this localization is the high density of sodium channels in the proximal axon (Bender and Trussell 2012). Repetitive activity in axons leads to a period of reduced conduction velocity due to the refractory period following spiking, followed subsequently by a period of increased velocity (Bullock 1951), as seen in parallel fibers (Gardner-Medwin 1972). Increased extracellular potassium concentration, I-h, and resurgent sodium currents have all been implicated in the depolarization that leads to increased excitability (Bucher and Goaillard 2011), but it may also be the case that two spikes traveling at different speeds are equilibrating in the process of interval locking (Moradmand and Goldfinger 1995). This activity-dependent increases in excitability, termed supernormal excitability, has been shown to occur *in vivo* (Gardner-Medwin 1972; Malenka, Kocsis et al. 1983), and has been attributed to potassium channel inactivation. Activity-independent forms of spike

propagation modulation is also possible. These can result from noise, non-uniform channel distribution, and impedance mismatch, and can lead to ectopic spike generation and spike failures, especially at branch points (Debanne, Guerineau et al. 1997). However, due to the difficulty in recording from axons, ion channel distribution in one cell type cannot be used to infer generally about other cell types.

Modulation of channels at the axons may also influence other compartments. Axonal depolarizations can either decrease (Zhang and Jackson 1993), or facilitate transmitter release (Jang, Nakamura et al. 2006). Moreover, subthreshold membrane fluctuations at axonal terminals can change the threshold for generating action potentials (Paradiso and Wu 2009). Even the firing patterns of cells may be affected based on activity leading to depolarization or hyperpolarization in the axon. Together, this suggests that axons may be acting as a dendrite to integrate subthreshold signals to affect cell spiking at the axon initial segment.

SUBCELLULAR TECHNIQUES

To investigate different compartments of a cell in addition to different neurons in a circuit, methods other than traditional electrode-based recording techniques are necessary. Two techniques stand out for observing/understanding subcellular activities and for manipulating subcellular conditions: voltage-sensitive dyes and compartmental modeling.

Traditional patch clamp techniques cannot easily probe subcellular compartments like axons, while calcium imaging techniques are not fast enough to report individual action potentials or their spike shapes. One technique for reporting activity in small subcellular compartments is by using a voltage sensor. Protein-based voltage sensors offer the promises of genetic encoding and *in vivo* imaging capability (Mutoh, Perron et al. 2011), whereas synthetic dyes generally have better signal to noise for imaging parts of small compartments (Djurisic, Antic et al. 2004). Voltage-sensitive dyes can provide submillisecond resolution with signals up to 60% ΔF/F per 100 mV, faster and bigger than those of genetically encoded sensors, but can also be toxic and create background fluorescence (Dreosti and Lagnado 2011). In contrast, dyes that do not have enough temporal resolution include pH sensitive dyes and FM dyes, the former having concentration-dependent intensities, while the latter stains all membranes.

One possibility is to combine genetic targeting using a genetically encoded fluorescence acceptor with a lipophilic anion as a fluorescence donor in a FRET-based approach to voltage sensing (Chanda, Blunck et al. 2005). In order to obtain the highest signal to noise available, we can pair the anion with a lipophilic tracer dye targeted to the inner leaflet of the plasma membrane. This tracer dye, DiO does not affect excitability (Honig and Hume 1989), and together with the voltage-sensitive anion dipicrylamine (DPA), allows depolarizations to be read out as a decrease in the fluorescence via voltage-dependent DPA-mediated quenching of DiO. Such a system allows us to trace not only action potentials in cell assemblies, but also individual spikes in inaccessible locations like axons and dendrites. Moreover, detailed information like

spike shape, spike threshold, propagation velocity, and subthreshold depolarizations would become available.

Another way to infer functional consequences of manipulations of a cell in a circuit or a channel within a subcellular compartment is by using computational modeling. One of the earliest conceptualizations is the integrate and fire model, which abstracts over a cell's diverse conductances to directly model its input-output characteristics (Lapicque 2007). If you in turn take a homogeneous population of excitatory and inhibitory cells and consider only their population firing rates, you arrive at a further abstraction modeled by coupled differential equations (Wilson and Cowan 1972). This type of abstraction is taken further by cascade models, which use mathematical primitives to understand neural coding mechanisms. Linear time-invariant filters like integrators and differentiators can be complemented by nonlinear processes like sigmoid activation functions. For example, information-theoretic optimization can be used to estimate nonlinear neural modules for understanding adaptation in the visual cortex (Sharpee, Sugihara et al. 2006). An even more general methodology is to use probability theory to model a neuron's efficient coding strategy, as opposed to differential equations (Herz, Gollisch et al. 2006). Here, the spikes represent an information-theoretic efficient code that has shown to possess features similar to that seen in, for example, auditory nerve fibers (Smith and Lewicki 2006). Probabilistic models can also bridge the gap between firing rate models and phenomenological models, leveraging insight regarding a priori encodings and observed spiking to update a temporal prior that efficiently represents the phenomenon at hand.

The other side of computational modeling reaches for descriptive detail instead of generalizability. Starting from the cable equations (Rall 1959), we can connect individual cylinders together for arbitrary complexity. Compartmental models are based on anatomical considerations, and can involve a large set of equations due to the large number of parameters to be estimated. For instance, a 1600 compartment model of the Purkinje cell and its dendrites was used to examine synaptic and intrinsic voltage-gated currents, generating realistic *in vivo* firing patterns (Jaeger, De Schutter et al. 1997). Compartmental models often attempt to recreate all the relevant conductances seen in a specific type of neuron. In one model of the granule cell, five types of potassium conductances and an enriched sodium conductance are placed in the axon hillock in simulating spike initiation and backpropagation (Diwakar, Magistretti et al. 2009). Multi-compartment models can be computationally expensive, thus reduced compartment models and single compartment models are often used. The classic Hodgkin-Huxley model is a single compartment reduced representation of a cell's sodium and potassium conductances (Hodgkin and Huxley 1952). Using a reduced model can allow for greater flexibility and generalizability, because one is not tied to the specific conductances of a specific cell type.

CHAPTER II

Presynaptic increase in calcium mediated by GAB_AA receptor activation in the cerebellar molecular layer is dependent on chloride accumulation

SUMMARY

A predominant source of inhibition in the nervous system is provided by $GABA_A$ receptors ($GABA_ARs$), although recent evidence suggests that GABA may play an excitatory role in development and in subcellular compartments. In the cerebellum, studies have shown that Purkinje cell EPSCs frequencies are increased by GABA application in the molecular layer, and that conduction velocity at the parallel fibers is increased by $GABA_AR$ activation. To bridge these results, we used calcium imaging to monitor presynaptic calcium influx to parallel fiber terminals, and found that a $GABA_AR$ agonist increases the amplitude of stimulus-evoked calcium transients, and that this effect is blocked by the $GABA_AR$ blocker gabazine. To investigate the subunit composition of $GABA_ARs$ required for this effect, we applied both a broad spectrum modulator and a modulator specific to the γ-subunit, and found that the γ-subunit does not participate in $GABA_AR$-mediated presynaptic calcium increases, narrowing the range of possible receptor subtypes to those not containing γ_2 or those with α_6 and γ_2. To probe the mechanism behind this effect, we increased stimulus intensity to activate more fibers, and found that the $GABA_AR$-mediated effect is abolished, suggesting that $GABA_AR$ activation serves to recruit additional fibers by bringing them closer to threshold. To test whether the chloride gradient is responsible for this effect, we applied a blocker for the chloride accumulating transporter NKCC1, and showed that the $GABA_AR$-mediated calcium increase is reduced over time. Taken together this evidence suggests that $GABA_AR$ activation excites parallel fiber terminals, and that this effect is due to accumulation of chloride in parallel fibers.

INTRODUCTION

Propagation of signals from the mossy fiber pathway to the Purkinje cell output layer of the cerebellum is critical for climbing-fiber mediated learning of conditioned cues, as demonstrated in eyeblink conditioning (Kim and Thompson 1997; Ohyama and Mauk 2001). Transmission of motor-related mossy fiber signals to the Purkinje cell requires exquisite fidelity in the transmission of action potentials in granule cells and their axons the parallel fibers, which may be up to 5 mm long (Palay and Chan-Palay 1974). One of the ways signals may be modulated in the conduction of granule cell spikes through the parallel fiber is the presence of receptors responsive to ambient transmitters such as GABA.

Early studies of presynaptic GABA receptors suggest that they reduce postsynaptic EPSPs by depolarizing afferents (Eccles, Eccles et al. 1961). The view that GABA only inhibits presynaptic elements has been challenged by observations that GABA increases IPSC frequencies in granule cells (Kaneda, Farrant et al. 1995), that $GABA_A$Rs mediate increases in glutamate release in development at the calyx of Held (Turecek and Trussell 2002), that GABAergic axo-axonic cells in the cortex can depolarize pyramidal cells (Szabadics, Varga et al. 2006), and that $GABA_A$Rs depolarize nerve terminals in the posterior pituitary due to a depolarized reversal potential for chloride (Zhang and Jackson 1995). In the cerebellum, increased EPSCs have been recorded from Purkinje cells and molecular layer interneurons in response to $GABA_A$R activation of the parallel fibers (Stell, Rostaing et al. 2007). Increased release probability at parallel fiber synapses (Pugh and Jahr 2011) and increased parallel fiber

conduction velocity due to $GABA_AR$ activation have also been found, suggesting that GABA excites parallel fibers.

Perforated patch studies in the calyx of Held (Price and Trussell 2006) and recordings from the posterior pituitary (Zhang and Jackson 1995) have shown that internal chloride concentration can be locally upregulated in presynaptic compartments up to 21 mM, which can be five times its concentration in cell bodies. While activity-dependent changes like high frequency stimulation can lead to chloride accumulation (Lu and Trussell 2001), persistent upregulation of internal chloride may rely on the presence of the chloride accumulating NKCC1 transporter, as it occurs early in development (Dzhala, Talos et al. 2005). In adults, the chloride extruding KCC2 transporter renders GABA inhibitory (Rivera, Voipio et al. 1999), but recent evidence suggests that the lack of KCC2 in adults may underlie the excitatory effect of GABA in certain GABAergic cells (Szabadics, Varga et al. 2006). Since both NKCC1 and KCC2 are expressed in cerebellar granule cells (Mikawa, Wang et al. 2002), excitation and inhibition in different subcellular compartments may be possible through differential regulation of these two transporters.

Previous studies have recorded from cells downstream from parallel fibers (Stell, Rostaing et al. 2007) or granule cells themselves (Pugh and Jahr 2011). To directly test whether GABA affects presynaptic excitability, we filled bundles of parallel fiber axons with a calcium indicator, and found that a $GABA_AR$ agonist increases calcium transients elicited by brief extracellular current stimulations. This effect is sensitive to a $GABA_AR$ blocker, showing that $GABA_ARs$ on parallel fiber terminals excite presynaptic elements.

To examine the subunit composition of these extrasynaptic receptors, we used both a broad spectrum modulator and a modulator specific to the γ subunit, and found that calcium signals are enhanced by the former and left unchanged by the latter. $GABA_AR$ activation may lead to increases in calcium influx in individual axons or to an increase in the number of excited axons. To disambiguate the two possibilities, we applied different stimulus intensities, and saw that at high stimuli, the $GABA_AR$-mediate effect is abolished, consistent with the hypothesis that $GABA_AR$ activation works to recruit more fibers. To understand the mechanism for this $GABA_AR$-mediated increase in excitability, we manipulated internal chloride concentrations by using a blocker specific to the NKCC1 transporter, and showed that the phenomenon is reduced over time, consistent with the idea that accumulation of chloride enables GABA to excite parallel fiber terminals.

METHODS

Brain slice physiology

Transverse cerebellar slices 275 to 300 μm in thickness were cut from isoflurane-anesthetized 20 to 37 days old Sprague-Dawley rats and C57BL6 mice using a Leica VT1000 vibratome (Leica Microsystems, Wetzlar, Germany). The ice cold solution used during cutting consisted of (mM) 85 NaCl, 2.5 KCl, 0.5 $CaCl_2$, 4 $MgCl_2$, 1.25 NaH_2PO_4, 24 $NaHCO_3$, 25 glucose, 75 sucrose. Upon cutting, the slices were transferred to a 35 °C waterbath and stored for 15 to 30 minutes in external solution consisting of (mM) 119

NaCl, 2.5 KCl, 2 $CaCl_2$, 1 $MgCl_2$, 1 NaH_2PO_4, 26.2 $NaHCO_3$, 25 glucose. The same solution was used after the incubation period, when the slices were allowed to sit at room temperature for 15-30 minutes before the calcium indicator was applied. Solutions were bubbled with 95% O_2 / 5% CO_2 continuously during all phases of the experiment, which also took place in room temperature unless otherwise indicated. Slices were transferred to a chamber and visualized using a Zeiss Axioskop setup (Göttingen, Germany) during dye application. Drugs were purchased from Sigma-Aldrich (St. Louis, MO), Tocris Bioscience (Ellisville, MO), or Invitrogen (Carlsbad, CA).

Labeling protocol

First 20 µl of 25% pluronic acid solution in DMSO was added to 50 µg packages of Oregon Green 488 BAPTA-1 AM to aid the loading process. Saline consisting of the external solution shown above was then added to get to 75-100 µM labeling solution, to which a trace amount of Alexa Fluor 594 was applied for visualizing the plume (both from Invitrogen). Similar to the procedure detailed in (Regehr and Atluri 1995), one pipette (5-8 µm, 2-4 MΩ, less than 10 psi) was filled with the solution and lowered into the molecular layer. Another pipette (1-3 MΩ) was held above the slice and connected to an equilibrated vacuum to serve as suction for the plume. As dye was pushed out of the smaller pipette by pressure application, a plume could be visualized as the dye flows through the slice and into the suction pipette (**Figure II-1B**). In 30-50 minutes, 250 µm label of the parallel fibers could be seen emanating perpendicular to the flow of the dye.

Stimulation and calcium imaging

A bipolar theta stimulating electrode was lowered onto the surface of the slice at least 100 µm away from the loading site and used to generate 250 µs current pulses at 0.5 hz using an ISO Flex stimulator (AMPI, Jerusalem, Israel). Sometimes an extracellular recording pipette (3-5 MΩ) was placed at least 100 µm away near the imaging site to detect population electrical artifact. Fluorescence signals were captured at least 200 µm away from the stimulation site using a custom made photodiode connected to an Axopatch 1D amplifier (Axon Instruments, Foster City, CA). The fluorescence source was from a HBO 100 mercury lamp attached to a Zeiss Axioskop 2 (Göttingen, Germany). Muscimol was delivered via a puffer pipette (2-4 MΩ) lowered just above the site of imaging and delivered through a Picospritzer microinjector (Parker, Cleveland, OH). Calcium transients were action potential dependent, as they are blocked by TTX (500 nM).

Data analysis

Calcium signals were indicated by increases in fluorescence of the dye Oregon Green BAPTA-1 AM, but the polarity of the photodiode showed a downward deflection on our amplifier; hence all traces are flipped before analysis. Data was acquired using an Axon Digidata 1320A and a computer running pClamp 8 and 9 (Molecular Devices, Sunnyvale, CA) sampling at 4 khz. Fluorescence transients ΔF were divided by the baseline fluorescence F, and these values were then normalized to the mean ΔF/F of

trials before muscimol delivery (10 responses, 20 seconds). Paired t-tests were used to compare peak of the response with the first response before muscimol application in **Figure II-1**. Paired t-tests were also used to compare peak of the muscimol-induced increase in each modulator versus the peak of the increase without the modulators in **Figure II-2**. Two-sample t-test were used to compare high and low baseline conditions in **Figure II-3A**, and paired t-tests were used to compare peak amplitudes in each bumetanide condition (30 minutes, 75 minutes) with control.

RESULTS

$GABA_AR$ agonist muscimol enhances presynaptic calcium transients

The calcium indicator Oregon Green BAPTA-1 was loaded into the molecular layer using a selective delivery technique (Regehr and Atluri 1995) (**Figure II-1B**). With parallel fibers labeled, a bipolar stimulus was placed away from the loading site and used to elicit calcium transients detected using a photodiode placed at least 200 μm away along the fibers (**Figure II-1A**). A pipette containing the $GABA_AR$ agonist muscimol was placed just above the imaging spot, and $GABA_AR$ specific agonist muscimol (10 μM) was puffed 20 seconds into a 0.5 hz stimulus train for 20 seconds (**Figure II-1C)**. Stimulus-evoked calcium transients amplitudes were increased by muscimol application with a peak response above 150% of pre-muscimol period (paired t-test, $p<0.002$, $n=10$) (**Figure II-1D**). When 50 μM gabazine (SR95531) was washed in, the same muscimol application has no effect on calcium signals (paired t-test,

p>0.05, n=10). In three of these experiments, gabazine was washed out of the bath for at least an hour, and the muscimol responses were recovered.

$GABA_AR$ γ subunit is not required for GABA-mediated presynaptic calcium increases

GABARs can be categorized into two broad classes. The γ-containing GABARs are low-affinity receptors that are activated in a phasic manner by synaptic vesicle release while the δ-containing GABARs are high affinity extrasynaptic receptors that respond to tonic activation (Brickley, Cull-Candy et al. 1996; Farrant and Nusser 2005). To investigate the type and composition of $GABA_A$Rs responsible for presynaptic parallel fiber excitation, we first used the broad spectrum modulator etomidate, which has positive allosteric modulatory effect on all β_2 or β_3 containing (but not β_1) $GABA_A$Rs, regardless of δ or γ presence (Belelli, Lambert et al. 1997). Etomidate (5 μM) application increased the muscimol-induced rise in amplitude of calcium transients by up to 100% ($p<0.002$, n=5), and this effect was consistent across different experiments (**Figure II-2AB**).

To more specifically narrow down the possible $GABA_A$R subtypes responsible for the effect, we applied diazepam, a selective agonist for γ-subunit containing $GABA_A$Rs that also lack α_4 and α_6 (Klein and Harris 1996). Diazepam (1 μM) application had no effect on the muscimol-induced amplitude enhancement ($p>0.4$, n=4) (**Figure II-2CD**), suggesting that γ_2-containing receptors are not major contributors to GABA-mediated parallel fiber excitation. These results are consistent with a receptor composition of α_6 γ_2 (Santhakumar, Hanchar et al. 2006; Dellal, Luo et al. 2012).

Presynaptic calcium increase results from GABA-mediated recruitment of parallel fibers

Increase in calcium levels arising from muscimol application can be due either to an increase in the amount of calcium influx in a single fiber, or to the recruitment of more fibers. If calcium influx per fiber is indeed increased by muscimol application, then at high stimulus intensities, more fibers would be activated, and muscimol would have a greater effect overall due to its greater effect per fiber. If on the other hand muscimol simply brings fibers closer to the threshold for firing by depolarization, then when additional fibers are activated by high stimulus intensity, the muscimol induced increase would subside (Stell 2011).

In order to ensure that the dye is not saturated at calcium levels where we expect to see an increase, we interleaved control trials in which a pair of stimulus pulses separated by 50 ms were given at both low (80 μA) and high (120 to 200 μA) stimulus intensities. The second pulse always gave rise to a calcium influx, and the ratio of second pulse amplitude to first pulse amplitude is unchanged at low and high fluorescence baselines ($p>0.1$, $n=3$ at low, 4 at high baseline, single experiment), indicating that Oregon Green BAPTA-1 was not saturated at these calcium levels (**Figure II-3A**). When stimulus intensity was high, resulting in a high baseline ΔF/F, the muscimol effect was significantly reduced from an average of 130% at low baseline to 107% at high baseline ($p<0.006$, $n=4$ each). Thus $GABA_AR$ activation is serving to depolarize parallel fibers, bringing them closer to the threshold for firing action

potentials, and when axons are already firing at high stimulus intensities, the effect of $GABA_AR$ activation is reduced.

Blocking chloride accumulation reduces $GABA_AR$-mediated presynaptic calcium increase

Previously depolarizing effect of GABA has been associated with accumulation of chloride in subcellular compartments (Price and Trussell 2006). Since both the chloride extruding transporter KCC2 and the chloride accumulating transporter NKCC1 are expressed in granule cells (Mikawa, Wang et al. 2002), we hypothesized that $GABA_AR$-mediated increases in presynaptic excitability result from chloride accumulation by NKCC1 on parallel fibers. The NKCC1 specific blocker bumetanide reduces E_{GABA} *in vitro*, suppressing epileptiform activity in hippocampus slices (Dzhala, Talos et al. 2005). Application of bumetanide (10 to 20 μM) in the bath reduces muscimol-induced increases in presynaptic calcium transient amplitudes (by 30 minutes $p<0.04$, by 75 minutes $p<0.03$, $n=5$). The average peak amplitude during muscimol puffs is reduced from 172% in control to 152% after 20 to 30 minute bumetanide application, and to 137% after 60 to 75 minute bumetanide application (**Figure II-3B**). This result is consistent with the hypothesis that chloride accumulation in the axons is the mechanism behind $GABA_AR$ excitation of parallel fiber terminals.

DISCUSSION

Using a calcium dye to image cerebellar parallel fiber terminals, we have shown that a $GABA_AR$ agonist increases the amplitude of stimulus-evoked calcium transients, that this effect does not require γ-subunit-containing $GABA_ARs$ that do not include ·. subunits, that it involves recruitment of parallel fibers by $GABA_AR$-mediated depolarization, and that maintenance of a high internal chloride concentration is crucial for this effect. This work extends results by (Pugh and Jahr 2011), which also saw an increase in release probability at parallel fiber synapses, as well as (Dellal, Luo et al. 2012), which described conduction velocity increases, both due to $GABA_AR$ activation. We have described the middle step of the pathway, after action potential has arrived at the terminal, and before transmitter is released, and found that population measurements of calcium at presynaptic terminals also suggests the excitatory effect of $GABA_ARs$.

The depolarizing effect of GABA has been attributed to the accumulation of chloride in subcellular compartments (Zhang and Jackson 1995; Price and Trussell 2006), although whether the depolarization leads to excitation or inhibition depended on the system studied. Modeling work has suggested that the voltage dependence of sodium channel inactivation may be critical in determining whether depolarization leads to propagation block (Jackson and Zhang 1995) or to facilitation (Dellal, Luo et al. 2012). In either case, theoretical work also predicts different sized effects of $GABA_AR$ mediated depolarization depending on the chloride reversal potential present, a feature

that depends critically on the spectrum of chloride transporters available and how they are regulated.

Previously, the lack of the chloride-extruding transporter KCC2 on axon initial segments has been implicated for the depolarizing effect of GABA on axoaxonic cells in the cortex (Szabadics, Varga et al. 2006). However another group recorded from subcellular compartments of these same cells and found using NKCC1 knockout mice that chloride accumulation at the axon initial segment gives rise to GABA-mediated depolarization effects (Khirug, Yamada et al. 2008). We corroborate these findings, showing that the presence of the chloride-accumulating transporter NKCC1 on axons must also contribute to GABA-based excitation. In cerebellum, KCC2 colocalizes with β_2, β_3 containing $GABA_A$Rs, and staining has been found both in the granule cell layer and the molecular layer (Williams, Sharp et al. 1999). Given that both NKCC1 and KCC2 are expressed in granule cells (Mikawa, Wang et al. 2002), it is likely that reduction of KCC2 levels in the granule cell axons can fully explain the chloride gradient that enables GABA to depolarize. More likely it is a fine tuning of the balance of NKCC1 and KCC2 in axonal compartments that determine whether GABA depolarizes and how much it depolarizes. Modeling work has shown that a difference of only 5 mV difference in the reversal potential for chloride can increase the spike threshold twicefold, and indeed can turn depolarization into shunting inhibition (Dellal, Luo et al. 2012).

The inhibitory action of $GABA_A$Rs on parallel fiber axons has been observed in room temperature experiments that applies a $GABA_A$R agonist for over 10 seconds (Stell 2011). Although the specific configuration of the fibers with respect to the slice could

matter, inhibition appears to occur only when $GABA_A$Rs are activated strongly over a long time range. Since inhibition does not correlate with conduction velocity increases (Dellal, Luo et al. 2012), it may occur as a result of prolonged chloride channel opening that leads to a shift in the reversal potential for chloride.

The lack of effect of diazepam on calcium transient increases modulated by muscimol suggests either the presence of α_6, and/or the absence of γ_2 in $GABA_A$R mediated excitation. Since $GABA_A$R induced fiber volley amplitude increases are still seen in δ knock-out mice (Dellal, Luo et al. 2012), and given that etomidate in our experiment has a facilitatory effect, it is likely that α_1 and/or α_6 subunits, which are found in cerebellar granule cells (Pirker, Schwarzer et al. 2000), are linked to the excitatory response. It is also possible that the $GABA_A$R under question is made up entirely of α and β subunits. Given these observations, we propose that the most likely subunit subtype of the $GABA_A$R of interest are made up of both α_6 and γ_2 subunits (Schmid, Bonanno et al. 1999).

We have seen that $GABA_A$R activation leads to an increase in presynaptic calcium transient amplitudes, that this effect is gabazine and etomidate sensitive, and that it appears to work by recruiting additional fibers, bringing them closer to threshold. The chloride gradient is likely a key component in determining the size of the depolarizing effect, since blocking the chloride accumulating transporter stunts the excitatory action of $GABA_A$Rs. Manipulating chloride concentrations using different native solutions and pharmacology provides a promise for better understanding the correlation between the chloride gradient and whether $GABA_A$R induced excitation or inhibition occurs. The

recording of voltage in these fine compartments would allow us to better examine how action potentials and subthreshold voltage changes are affected by GABA.

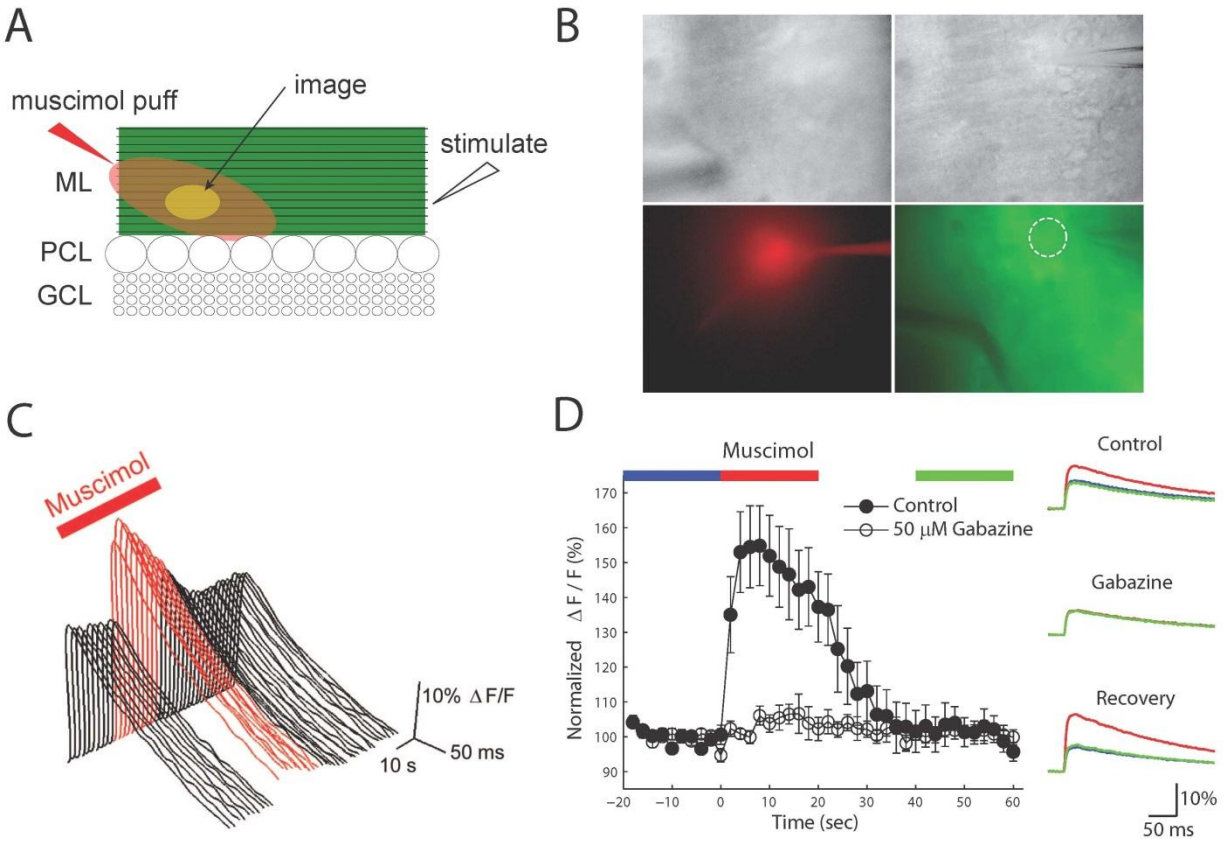

Figure II-1. Presynaptic calcium transients are enhanced by GABAAR agonist muscimol. A) Diagram of the experimental setup with Oregon Green BAPTA-1 loaded onto the fibers. ML molecular layer, PCL Purkinje cell layer, GCL granule cell layer. B) Labeling process in action. DIC images of the suction pipette above the slice (upper left), loading pipette containing Oregon Green BAPTA-1 on the slice (upper right). Fluorescence image of the plume with a Texas Red filter showing Alexa 594-containing calcium solution flowing from the loading pipette to the suction pipette upon traversing through the slice (lower left). After labeling, a bipolar stimulus electrode is placed 300 to 500 μm away, and a 60-100 μm spot in the molecular layer is imaged during stimulation at 0.5 hz, in the middle of which muscimol is puffed from a nearby pipette (lower right). C) Representative example of delivery of 40 pulses of bipolar current stimuli at 0.5 hz producing calcium transients that are enhanced by a 20 second muscimol (10 μM, red) puff application delivered 20 seconds into the train. Traces are inverted to show decrease in ΔF/F as an increase in calcium signal. D) Muscimol (10 μM, red) increases the amplitude of stimulus-evoked calcium transients ($p<0.002$, $n=10$). Summary data (left) showing control condition (black) and $GABA_AR$ block condition (white) where gabazine (SR95531, 50 μM) is added to the bath. For each trial, ΔF/F is normalized to the mean of the ΔF/F values before (blue) muscimol application. Example traces (10 trace average over the intervals showed on the left) before (blue), during (red), and 20 seconds after (green) muscimol application.

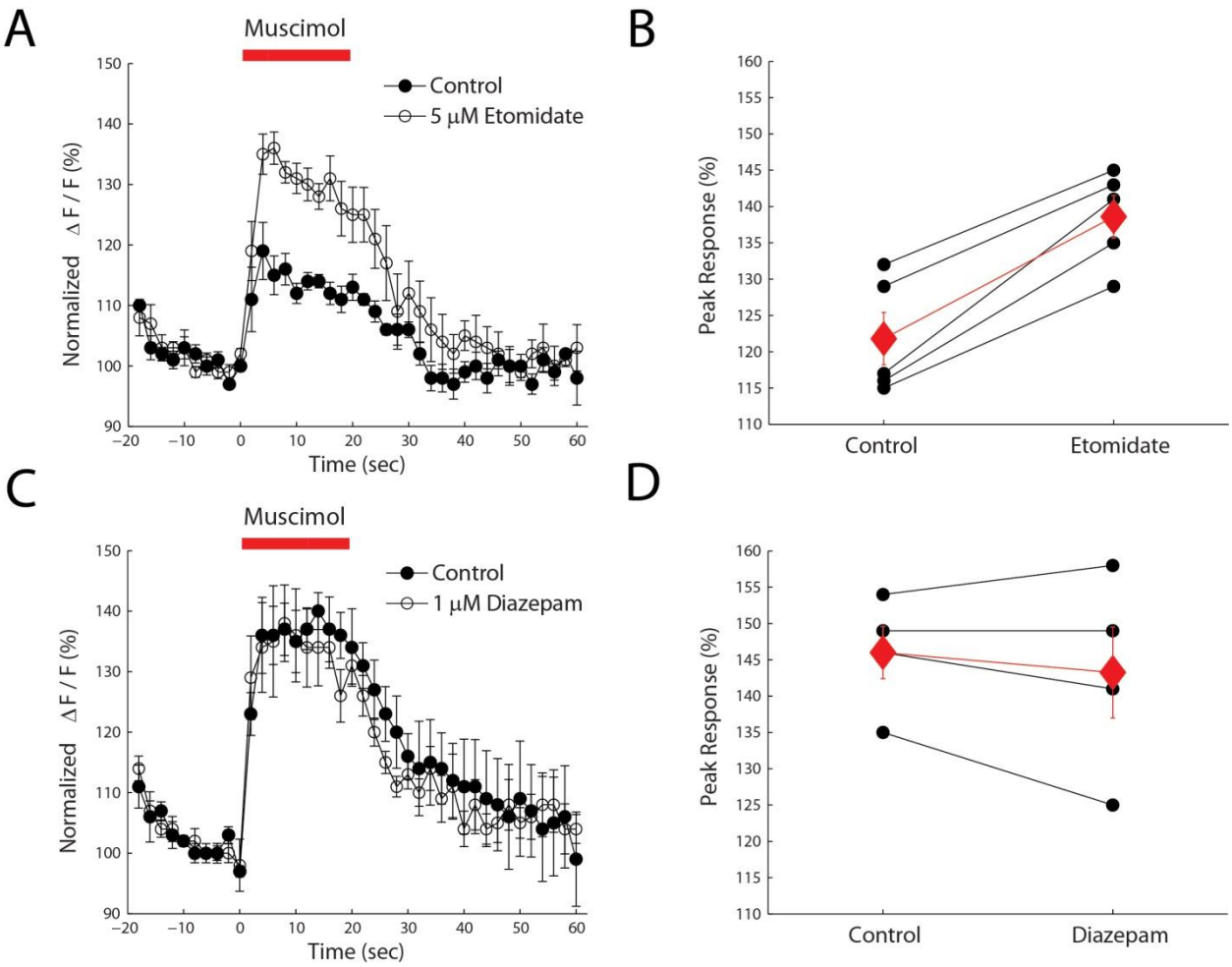

Figure II-2. GABAAR mediated enhancement of presynaptic calcium transients are sensitive to etomidate but not diazepam. A) Broad spectrum modulator etomidate (5 μM, circle) increases the effect of the muscimol-mediated enhancement of stimulus-evoked calcium transients ($p<0.002$, $n=5$). Muscimol (red) is applied at 0 seconds for 20 seconds. B) Peak amplitudes during muscimol application for each experiment pairing before and after etomidate application. Averages are shown in red. C) γ-subunit specific modulator diazepam (1 μM, circle) has no effect on the muscimol-mediated enhancement of stimuls-evoked calcium transients ($p>0.4$, $n=4$). Muscimol (red) is applied at 0 seconds for 20 seconds. D) Peak amplitudes during muscimol application for each experiment pairing before and after diazepam application. Averages are shown in red.

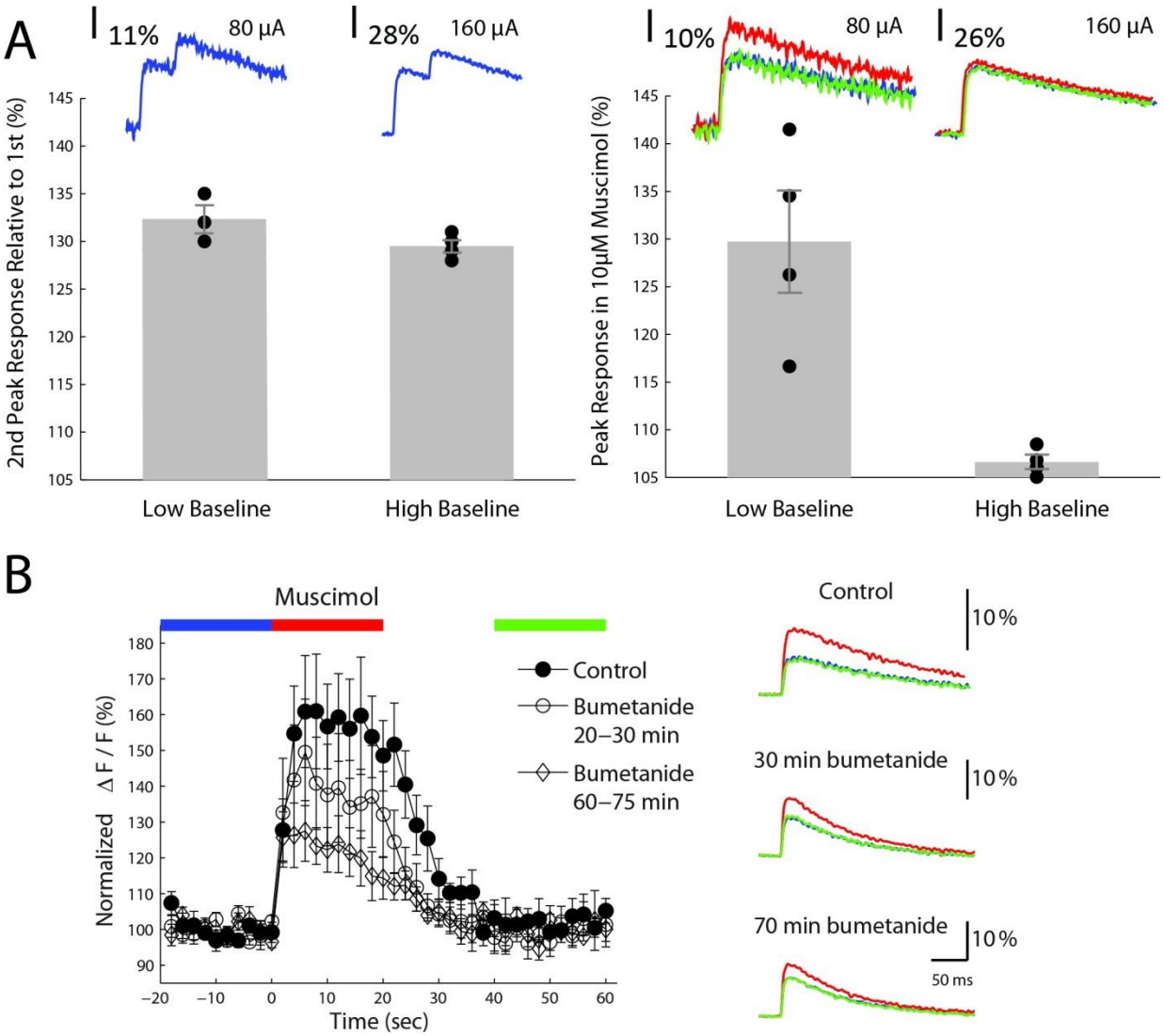

Figure II-3. GABAAR mediated excitation is reduced by high stimulus intensity and by NKCC1 transporter blocker. A) $GABA_AR$ driven enhancement of calcium transients is dependent on baseline ΔF/F, but not on dye saturation. Two stimulus trials (left) were interleaved with single stimulus trials (right) with 20 second long muscimol application 20 seconds into a train (same protocol as **Figure II-1**). Individual measurements from a single experiment are shown. Second peak response is not reduced by higher stimulus intensity ($p>0.1$, n=3 at low, 4 at high baseline). Muscimol-induced increase in amplitude is reduced by higher stimulus intensity ($p<0.006$, n=4 each). Low baseline is 19% to 26% ΔF/F. High baseline is 43% to 64% ΔF/F. Example single traces are from 80 µA and 160 µA stimulus trials. B) Muscimol (10 µM, red) induced enhancement in amplitude of stimulus-evoked calcium transients is reduced by 10 to 20 µM bath-applied bumetanide (by 30 minutes $p<0.04$, by 75 minutes $p<0.03$, n=5). Summary data (left) showing control condition (black) and bumetanide conditions (cirlces and diamonds). Example traces (right) are 10 trace averages from before (blue), during (red), and after (green) muscimol application.

CHAPTER III

$GABA_A$ receptors increase excitability and conduction velocity of cerebellar parallel fiber axons

SUMMARY

In the adult mammalian brain, $GABA_A$ receptors ($GABA_ARs$) are responsible for the predominant forms of synaptic inhibition but these receptors can excite neurons when the chloride equilibrium potential (E_{Cl}) is depolarized. In many mature neurons, $GABA_ARs$ are found on presynaptic terminals where they exert depolarizing effects. To understand whether excitatory GABA action affects axonal function, we used transverse cerebellar slices to measure the effects of photolysis of caged GABA on the initiation and propagation of compound parallel fiber (PF) action potentials (APs). Photolysis of caged GABA increased the amplitude and conduction velocity of PF APs; GABA reuptake blockers and a positive modulator of $GABA_ARs$ enhanced these effects. In contrast, a modulator selective for δ-subunit-containing $GABA_ARs$ did not enhance these effects and responsiveness remained in $\delta^{-/-}$ mice, arguing that δ-subunit containing $GABA_ARs$ are not required. Synaptically-released GABA also increased PF excitability indicating that the mechanism is engaged by physiological signals. A Hodgkin-Huxley style compartmental model of the PF axon and granule cell body was constructed and this model recapitulated the GABA-dependent decrease in AP threshold and the increase in conduction velocity, features that were sensitive to E_{Cl} and to the voltage dependence of sodium channel inactivation. The model also predicts that axonal $GABA_ARs$ could affect orthodromic spike initiation. We conclude that GABA acting on cerebellar PFs facilitates both spike generation and propagation, allowing axons of granule cells to passively integrate signals from inhibitory interneurons and influence information flow in the input layer to the cerebellar cortex.

INTRODUCTION

The classical studies of muscle afferent inputs to spinal motor neurons that gave rise to the concept of presynaptic inhibition also eventually led to the first identification of presynaptic $GABA_A$Rs (Eccles, Schmidt et al. 1963). Subsequent work by many laboratories demonstrated that this $GABA_A$R-mediated presynaptic inhibition results from a depolarizing action of GABA on presynaptic afferent terminals (Rudomin and Schmidt 1999). Since those initial findings, $GABA_A$Rs have been observed on presynaptic terminals in a variety of brain regions including auditory brainstem, ventral tegmental area, hypothalamus, amygdala, hippocampus, cerebellum, and cortex and in most of these locations GABA has been found to be depolarizing (Zhang and Jackson 1993; Turecek and Trussell 2002; Szabadics, Varga et al. 2006; Woodruff, Monyer et al. 2006; Alle and Geiger 2007; Stell, Rostaing et al. 2007; Trigo, Chat et al. 2007; Xiao, Zhou et al. 2007; Khirug, Yamada et al. 2008; Pugh and Jahr 2011). Cell attached and perforated patch clamp approaches applied to large axon terminals in brainstem auditory nuclei, anterior pituitary, and hippocampus indicate that depolarizing effects of GABA can be attributed to a depolarized E_{Cl} (Zhang and Jackson 1993; Price and Trussell 2006; Ruiz, Campanac et al. 2010).

While there have been many studies on the consequences of presynaptic $GABA_A$Rs on synaptic transmission, relatively little is known about whether these receptors affect axonal excitability. In order to directly test whether transient activation of $GABA_A$R affects axonal excitability we have taken advantage of transverse cerebellar slices which preserve PF axons, allowing compound APs to be recorded as fiber volleys.

Prior studies of GABA action on PFs have established that activation of axonal $GABA_A$Rs increases the frequency of synaptic currents recorded in postsynaptic targets of PFs (Stell, Rostaing et al. 2007). This increased excitability is accompanied by increases in calcium transients in PF axonal bundles (Stell 2011) and in single *en passant* PF synaptic boutons (Pugh and Jahr 2011). Electron microscopy (EM) data demonstrates that $GABA_A$R subunits are present on PF presynaptic boutons and likely on axons as well (Stell, Rostaing et al. 2007). The experiments presented here extend this work to examine how $GABA_A$Rs affect axonal excitability.

We find that UV photolysis of CNB-caged GABA increases both the amplitude and conduction velocity of PF volleys, effects that are inhibited by $GABA_A$R antagonists, enhanced by blocking GABA reuptake, and enhanced by broad spectrum modulators of $GABA_A$Rs. Trains of stimuli generate increases in axonal excitability that are blocked by $GABA_A$R antagonists and enhanced by GABA reuptake inhibitors suggesting that these mechanisms are engaged by physiological activity. Recognizing the prominent extrasynaptic $GABA_A$R conductance present in granule cell bodies we tested whether $GABA_A$R mediated excitation of PFs persists in δ-subunit knock-out mice and found no differences from wild type indicating that extrasynaptic $GABA_A$Rs composed with this subunit are not required.

Construction of a compartmental model of the PF axon and granule cell body allowed us to examine the effects of different chloride gradients in the axon. With a depolarized E_{Cl}, the model reproduced the GABA-dependent decrease in spike initiation threshold and increase in conduction velocity. The magnitude of E_{Cl} relative to the

resting potential and the voltage dependence of sodium channel inactivation were critical factors in the model behavior. The model indicated that PF axons could act like dendrites to passively integrate $GABA_AR$-mediated depolarization and influence AP initiation at the spike initiation zone.

Together these observations show that depolarizing $GABA_ARs$ can robustly influence the electrical behavior of axons. Interestingly, the GABA- and activity-induced increases in excitability that we describe here show many similarities to a phenomenon termed "supernormal excitability" identified in PF axons *in vivo* (Gardner-Medwin 1972; Malenka, Kocsis et al. 1983). Our results suggest that $GABA_ARs$ contribute to this activity-induced increase in conduction velocity and excitability and that this mechanism allows molecular layer inhibitory interneurons to influence the timing and strength of information emanating from the granule cell layer, the principal input layer of the cerebellum.

METHODS

Brain slice electrophysiology

After inducing deep anesthesia with isoflurane, mice were decapitated, in accordance with a protocol approved by the University of California, Los Angeles Institutional Animal Care and Use Committee. The cerebellum vermis was removed and placed in an ice-cold cutting solution containing (in mM): 85 NaCl, 2.5 KCl, 0.5 $CaCl_2$, 4 $MgCl_2$, 1.25 NaH_2PO_4, 24 $NaHCO_3$, 25 glucose, and 75 sucrose. Transverse slices (300

μm) were cut from 19- to 35-day old C57/Bl6 wild type or $\delta^{-/-}$ mice with a Leica VT1000 vibratome (Leica Microsystems, Wetzlar, Germany) and stored in external recording solution containing (in mM): 119 NaCl, 2.5 KCl, 2 $CaCl_2$, 1 $MgCl_2$, 1 NaH_2PO_4, 26.2 $NaHCO_3$, and 25 glucose, warmed to 35°C for 15-20 min, after which the solution was allowed to reach room temperature. All solutions were continuously bubbled with 95% O_2 / 5% CO_2. All drugs and reagents were purchased from Sigma-Aldrich (St. Louis, MO), Tocris Bioscience (Ellisville, MO), Ascent Scientific (Princeton, NJ), or Invitrogen (Carlsbad, CA). Recordings were made at room temperature with a Dagan BVC-700A (Dagan, Minneapolis, MN), Axopatch 200A, or 200B (Axon Instruments, Foster City, CA) amplifier. Data was acquired with pClamp software (Axon Instruments).

External solutions during recordings contained CGP 35348 (100 μM) to block $GABA_B$ receptors and O-(CNB-caged) GABA (100 μM) in the photolysis experiments. CGP 35348 (100 μM) was also included in the stimulus train experiments. All experiments were conducted at room temperature and under recirculation of the external solution (7-10 ml total volume) at a flow rate of 2-4 ml/min. Extracellular population spike (fiber volley) recordings were carried out as follows. A bipolar stimulating electrode (FHC, Bowdoin, ME) was placed in the molecular layer and a recording electrode (1-3 MΩ) was placed in the same molecular layer 80-500 μm distal to the stimulating electrode. Single stimuli ranging in duration from 40-400 μsec and intensity from 15-350 μA were delivered to the stimulating electrode via an Iso-Flex stimulator (A.M.P.I, Jerusalem, Israel) to elicit the fiber volley. All fiber volleys were AP-dependent as they were eliminated by TTX (0.5-1 μM).

Photolysis of caged GABA

Photolysis of caged GABA was accomplished with a 2 sec UV flash from an epifluorescence lamp using a center wavelength 366, full-width half maximum 17 nm excitation filter, a 409 nm dichroic mirror (both filters from Semrock, Inc., Rochester, NY), and either a 40x, N.A. 0.8 or a 60x, N.A. 0.9 objective, as described previously (Dittman and Regehr 1997), and shuttered by a digital pulse from a Master-8 interval generator (A.M.P.I., Jerusalem, Israel).

A prior study which used photolysis of 150 μM CNB-caged GABA in transverse cerebellar slices estimated a peak GABA concentration of approximately 10 μM (Dittman and Regehr 1997). Although similar in many respects to our experiments (same preparation, same objective lens, same caged GABA at a similar concentration), this study used a different UV source (flash lamp rather than an arc lamp) and applied GABA locally to the slice, reducing extinction effects caused by UV absorption of caged GABA when it is circulating in the bath. Nonetheless, their estimates are consistent with maximal peak concentrations in the range of tens of micromolar at the slice surface. Due to the high UV absorption of cerebellar tissue (DiGregorio, Rothman et al. 2007) it is expected that progressively lower concentrations would be achieved with depth in the slice.

UV light has been reported to have direct effects on many ion channels including $GABA_A$ receptors (Chang, Xie et al. 2001). With this in mind we performed a number of control experiments including testing the effects of UV light pulses in the absence of

caged GABA, testing UV pulses with $GABA_A$ receptor antagonists present (**Figure III-1**), and testing the effects of endogenous GABA (**Figure III-8**). These experiments confirmed that UV-induced transient potentiation of fiber volleys and of conduction velocity were dependent on both the presence of caged GABA and of functional $GABA_A$Rs.

Endogenous GABA excitation

To elicit endogenous GABA release, 20 Hz stimulus trains were delivered for 1.5 to 3 seconds. Stimulus intensity (100-200 µA, 40-150 µs) was fixed throughout a single experiment and all experiments were conducted in the $GABA_B$R blocker CGP-35348 (100 µM). Using a blinded experimental design we compared the effects of control solution with a solution containing 100 µM cadmium chloride. In each experimental group PTX (100 µM) was applied to isolate the PTX-sensitive response to the train.

Experiments examining the effects of NNC-711 (10 µM) were not blinded. In these experiments NNC-711 was applied followed by PTX allowing the PTX-sensitive responses to be calculated for both control and for NNC-711. PTX-sensitive control responses in this experiment were statistically indistinguishable from the control responses in the prior blinded design and so the control data have been pooled in **Figure III-8**.

Data Analysis and Statistics

Unless otherwise noted, error bars represent the S.E.M. and significance was tested by a one-tailed Student's t-test. The choice of a one-tailed as opposed to a two-tailed test was justified because we had an *a priori* expectation of the direction of the effect. In cases where distributions failed tests of normality by the Shapiro-Wilk test, the Mann-Whitney Rank Sum (MWRS) test was used as indicated. Data analysis was carried out with Excel, SigmaPlot, and with routines written in Matlab R2008.

In all experiments involving photolysis, we defined excitation as the maximum value reached in the 6 s window from the start of the UV flash; this is for all parameters measured i.e. volley amplitude, latency, and velocity. Inhibition was defined as the minimum value reached in the 11 s window from the start of the UV flash, since the inhibition occurs on a longer time scale than the excitation (Stell 2011). Using this definition, a value for inhibition can be obtained for every experiment, as it is simply the minimum value. This is to be distinguished from the inhibition described in **Figure III-3 A-B**, where there was no excitation measured. In the GABA uptake blockade experiments (**Figure III-5**), cumulative value differences were calculated by summing the normalized values in the 11 s time window from the start of the UV pulse.

In the experiments involving stimulus intensity variation (**Figure III-4**), responses were extremely variable at the lowest stimulus intensities (<10% maximum) with coefficients of variation in baseline amplitude and response that were 80 to 320% larger than at higher intensities. For this reason we chose to display data from the range 10% to 100% of normalized baseline amplitude.

In the stimulus train experiments, traces were averaged from four trials per experiment, normalized to the first pulse amplitude, and peak values from each pulse in PTX conditions were subtracted from peak values in control, NNC-711, and cadmium conditions. Due to the temporally correlated nature of these subtracted time series, we chose to test the significance of the cumulative amplitude differences as a time series in each condition. In this case, statistical tests are conducted at successive time points which reflect cumulative differences from the beginning of the train. Repeated measures Analysis of Variance was also performed post hoc.

NEURON modeling

The compartmental model of the granule cell was constructed in NEURON using mammalian Hodgkin-Huxley channels (Wang, Liu et al. 2003). The soma has diameter 5.8 μm and area 105.68 μm^2, with resistivity of 1000 Ω/cm^2, capacitance 1 $\mu F/cm^2$, Na^+ channel conductance 45 mS/cm^2, K^+ channel conductance 18 mS/cm^2, and leak conductance 30 $\mu S/ cm^2$. The axon has the same conductive properties, but is 0.3 μm in diameter, with each compartment a single segment 2.5 μm in length. The ascending branch of the fiber is 70 μm in length, and branches into two segments, 750 μm and 250 μm each. For all compartments, the reversal potentials are V_{Na} = 50 mV, V_K = -77 mV, and V_L = -70 mV. Temperature is set at 30°C as in (Wang, Liu et al. 2003) and (Diwakar, Magistretti et al. 2009), however additional experiments (**Figure III-12**) conducted at room and physiological temperatures both show spike facilitation and velocity increases of 108.33% (24 °C) and 111.00% (37 °C). In addition to the

standard leak conductance and voltage-gated Na^+ and K^+ conductances, we introduced a tonic chloride conductance (G_{GABA}) used to model $GABA_A$Rs. At the soma, this conductance is constant at 100 μS/cm^2, with a reversal potential of -70 mV. Given a 5.8 μm diameter cell body this corresponds to a conductance of 423 pS, within the range reported for tonic current in granule cells (Brickley, Revilla et al. 2001). In the axons, the conductance is $GABA_A$R-gated, i.e. it is zero in control and 100 μS/cm^2 when active, with reversal potentials varying from -75 to -60 mV. Output from NEURON was analyzed using custom routines written in Matlab R2008.

RESULTS

Compound APs in parallel fibers are enhanced by photolysis of caged GABA

In order to test whether parallel fiber excitability was directly enhanced by $GABA_A$ receptor activation, we performed extracellular recordings of stimulus-evoked population spike activity (fiber volleys) in the molecular layer of acute cerebellar cortical slices cut in a transverse/coronal plane (**Figure III-1A**). An extracellular stimulating electrode and a recording electrode were placed at distances of 80 to 500 μm apart and fiber volleys were elicited by single stimulus pulses at a frequency of 1 Hz. The external solution contained 100 μM CGP 35348 to block $GABA_B$ receptors and 100 μM CNB-caged GABA. Photolysis of caged GABA transiently enhanced the amplitude (**Figure III-1B-C**) and this amplitude increase was blocked by either 50 μM SR 95531 (SR) or 100 μM picrotoxin (PTX) (n=95 for control, n=68 for antagonists, $p<0.001$, MWRS test, **Figure**

III-1C) confirming that this resulted from the action of GABA at $GABA_A$ receptors. UV excitation in the absence of CNB-GABA had no significant effects on the volley amplitude (101.9 ± 0.6 % peak amplitude in UV, 99.0 ± 0.6 % minimum amplitude in UV; $p>0.26$, Paired two-tailed test for the average, minimum, and maximum values reached during the 6 s after the UV versus the 6 s before the UV, n = 9 measurements from 6 slices).

AP conduction velocity is increased by photolysis of caged GABA

We also noticed that the GABA photolysis decreased the latency of the evoked fiber volley and that this effect was sensitive to $GABA_AR$ antagonists (control, 136 ± 7 μs advancement relative to pre-UV period; antagonists, 49 ± 6 μs advancement, n=95 and 68 respectively, $p<0.001$, MWRS test). In the absence of CNB-GABA in the bath solution, UV excitation alone slightly decreased the volley latency (24 ± 7 μs advancement, n=9 measurements from 6 slices), similar to the photolysis responses in $GABA_A$ antagonists ($p=0.12$, two-tailed t-test).

These decreases in volley latency suggested to us that GABA increased fiber volley conduction velocity. To get a more accurate measurement of conduction velocity, two recording electrodes and a stimulating electrode were positioned in the molecular layer along a beam of parallel fibers so that fiber volley propagation could be recorded (**Figure III-1D**). Conduction velocity was then estimated by dividing the spatial separation of electrodes by the temporal difference in volley onset. The average conduction velocity we measured in this manner is 0.231 +/- 0.046 m/s (n=16), similar

to that reported previously (Vranesic, Iijima et al. 1994). Photolysis of caged GABA increased conduction velocity, an effect sensitive to $GABA_AR$ antagonists (control, 107 ± 1.0 %, n=16; $GABA_AR$ antagonists, 103 ± 0.8 %, n=13 antagonists, p=0.002, unpaired t-test, **Figure III-1E**).

Tonic GABA levels in cerebellar slices activate extrasynaptic forms of $GABA_ARs$ (Santhakumar, Hanchar et al. 2006). To assess whether ambient GABA levels in slices tonically increase PF axonal excitability, we tested whether $GABA_AR$ antagonists change baseline volley amplitude. No significant effects of $GABA_AR$ antagonists were found (n=68, p=0.73, MWRS test, **Figure III-1F**) suggesting that basal levels of GABA in the vicinity of parallel fibers do not increase axonal excitability either because they are not high enough to activate $GABA_ARs$ or because a persistent presence of GABA is ineffective (Bright, Renzi et al. 2011).

In these experiments GABA was deliberately photolysed in a large volume in order to influence as large a population of PFs as possible; this approach has the potentially complicating consequence that $GABA_ARs$ on granule cell bodies may be activated. To test whether the effects of GABA photolysis on fiber volleys are influenced by somatic $GABA_A$ receptors we carried out a series of experiments in which we surgically removed the granule cell layer, completely severing the connections between granule cell bodies and PF axons (see **Figure III-2A-B**). **Figure 2C-D** summarize the excitatory actions of GABA photolysis on fiber volley amplitude (127 ± 8.1 %, n=5) and latency (advancement of 113 ± 7.9 μs, n=5) in this reduced slice. $GABA_AR$ antagonists significantly inhibited these effects (p=0.024 for amplitude and

p=5.2 x 10^{-4} for latency). Statistical comparison of these data with the main data set plotted in **Figure III-1** indicated that they are not significantly different (p=0.11 for amplitude; p=0.47 for latency, two-tailed t-tests).

A slow inhibitory phase was observed in some slices

There have been reports in several brain regions, including in cerebellar PFs, of axonal $GABA_A$Rs mediating inhibition (Zhang and Jackson 1995; Ruiz, Fabian-Fine et al. 2003; Glickfeld, Roberts et al. 2009; Stell 2011). When data from all slices were examined there was evidence of a biphasic effect which manifested as a slight depression in the fiber volley amplitude following the initial peak enhancement. The average minimum reached for all measurements was 95 ± 0.5 % (n=95), a significant reduction from the pre-UV pulse baseline (p=0.042, MWRS test). Although significant, because peak depression occurs with a variable latency in different slices it is barely discernible in the average time course in **Figure III-1C**.

In a minority of slices (6 out of 70) we observed monotonic decreases in the volley amplitude with photolysis and this inhibition was reduced by $GABA_A$R antagonists (control, 86 ± 2.0 %; antagonists, 92 ± 1.3 %, n=8 measurements, Paired t-test, p=0.026, see Methods for how this was calculated, **Figure III-3A**). However, inhibition of fiber volley amplitude in this subset of experiments was not accompanied by delays of the volley arrival or decreases in fiber volley velocity. In fact, it was associated with significantly increased conduction velocity (latency: 161 ± 31 μs, n=11 measurements in 8 slices; velocity: 107 ± 1 %, n=3 slices; Paired t-tests, p<0.02).

This "pure" inhibition decreased in older animals (**Figure III-3B**), a developmental profile distinct from that exhibited by excitation (**Figure III-3C**).

$GABA_B$ receptors on PF axon terminals inhibit calcium influx but have been reported to modestly inhibit parallel fiber volley amplitudes recorded with voltage sensitive dyes (Dittman and Regehr 1997; Sabatini and Regehr 1997). All experiments presented to this point included the $GABA_B$ receptor antagonist CGP 35348. To test whether $GABA_B$ receptors influence the fiber volley and conduction velocity or may contribute to the slow inhibitory effects, we compared photolysis responses prior to and after addition of the $GABA_B$ receptor antagonist CGP 35348. We observed similar excitatory actions of GABA photolysis on fiber volley amplitude and latency in the absence of CGP 35348, and no significant change after addition of the antagonist (Normalized Volley Amplitude: control, 123 ± 2.8 %; CGP 35348, 126 ± 3.8 %, p=0.11, Paired t-test; Relative Volley Latency: control, 84 ± 14.6 µs; CGP 35348, 89 ± 13.5 µs, p=0.18, Paired t-test, n=5). Inhibitory actions were also unaffected (control, 92 ± 2.5%; CGP 35348, 91 ± 2.9%, Paired two-tailed t-test, p=0.58). Taken together these results show that the inhibitory effects are relatively small and slow as compared to the excitatory effects and are dependent on $GABA_A$Rs but are unrelated to $GABA_B$ receptors.

Recruitment of more axons accounts for the increase in fiber volley amplitude

To further explore the mechanism underlying GABA mediated excitation of PFs we carried out experiments similar to those described above but using a range of electrical stimulus intensities. If the excitatory effect of GABA increases the probability

of eliciting a spike in individual axons, then as the electrical stimulus intensity is raised, the increase of volley amplitude evoked by GABA photolysis should be smaller since there will be progressively smaller pools of axons to recruit. We found a robust, inverse correlation between percent enhancement and baseline fiber volley amplitude (**Figure III-4A**), consistent with the view that GABA is increasing the probability that an axon is brought to threshold at a given stimulus intensity. No correlation was observed for inhibition versus baseline volley amplitude (**Figure III-4B**). We also tested whether the magnitude of the conduction volley increase varied with stimulus intensity and found no correlation consistent with a mechanism that does not depend on fiber recruitment (**Figure III-4C**).

The magnitude of the photolysis effect was dependent on the clearance rate of GABA from the extracellular space surrounding the axons. Blockade of the GABA transporter GAT-1 by NNC-711 (10 μM) significantly increased the peak enhancement of volley amplitude by photolysis and prolonged the time course of the photolysis increase ($n=14$, $p=0.0007$, Paired 2-tailed test comparing cumulative amplitudes of control vs. drug, **Figure III-5A-B**). NNC-711 did not significantly increase the peak enhancement of velocity but it did prolong the time course of velocity increase, although this effect did not reach significance ($n=5$, $p=0.059$, Paired 2-tailed test, **Figure III-5C-D**). Two other GABA transporter isoforms, GAT-2 and GAT-3, are not expressed in the cerebellar cortex (Clark, Deutch et al. 1992; Durkin, Smith et al. 1995). Consistent with this, the GAT-2 and GAT-3 specific antagonist, SNAP-5114 had no significant effect on the photolysis enhancement of volley amplitude (Cumulative amplitude change: control, 79

± 18 %, SNAP-5114, 54 ± 16 %, p=0.15, Paired, two-tailed test; n = 9 measurements, 5 slices from 4 animals).

Subunit requirement of axonal $GABA_A$ receptors mediating excitation

To obtain insight into the molecular composition of the axonal $GABA_A$ receptors mediating this excitatory effect we tested a series of drugs which target different $GABA_AR$ subtypes. We first tested etomidate, a widely used intravenous anesthetic which enhances currents from all $GABA_A$ receptors containing either a β_2 or β_3 receptor, independent of whether γ or δ subunits are present (Belelli, Lambert et al. 1997; Meera, Olsen et al. 2009). Etomidate (5 μM) increased the excitatory effect of GABA photolysis on volley amplitude (p=0.038, Paired t-test, n=8, **Figure III-6A-B**). In addition, etomidate enhanced the inhibition that followed the initial excitation (**Figure III-6A**, p=0.006, Paired t-test).

We then tested the more specific allosteric modulator diazepam, a benzodiazepine which enhances currents from $GABA_ARs$ which both lack the α_4 and α_6 subunits and contain a γ subunit (Mohler, Crestani et al. 2001). Diazepam (1 μM) had no significant effects on either the excitatory or inhibitory actions of GABA photolysis on volley amplitude (Excitation: p=0.65, MWRS test, n=9, Inhibition: p=0.39, Paired t-test, **Figure III-6C-D**). As discussed in the Methods section, photolysis-induced GABA concentration transients within the slice are unlikely to saturate $\alpha_1\beta_{2/3}\gamma_2$ receptors, the only receptor subtypes that would be diazepam sensitive (Santhakumar, Hanchar et al. 2006) and even if there were saturation, the decay rate of the effects would likely be

prolonged by diazepam. Thus, the lack of diazepam sensitivity rules out $\alpha_1\beta_{2/3}\gamma_2$ receptor subtypes as major contributors to the potentiating effect of GABA on PF axons.

The $GABA_A$ receptor δ subunit has been shown to be extrasynaptically localized in the cerebellum, hippocampus, and other brain regions (Brickley, Cull-Candy et al. 1996; Farrant and Nusser 2005). Also, δ-containing $GABA_A$ receptors are reported to be expressed at mossy fiber terminals in the hippocampal dentate gyrus, where they mediate a depolarizing action of GABA (Ruiz, Campanac et al. 2010). To determine whether the excitatory GABA effects on parallel fibers require the δ subunit, we first tested the drug DS2 which has been shown to be a specific positive allosteric modulator of $GABA_A$Rs containing the δ subunit (Wafford, van Niel et al. 2009; Shu, Bracamontes et al. 2011). There were no significant effects of DS2 (10 μM) on the excitatory phase of volley amplitude (p= 0.11, Paired t-test, **Figure III-7A-B**, n=8), however, DS2 enhanced the inhibitory phase (p=0.03, Paired t-test, **Figure III-7A**).

We then carried out the same photolysis experiments in cerebellar slices from mice lacking the δ subunit gene. These mice lack tonic $GABA_A$R-mediated currents in the cell bodies (i.e., granule cells) of PF axons (Stell, Brickley et al. 2003; Meera, Wallner et al. 2011). Photolysis of GABA in slices from $GABA_A$R antagonists significantly inhibited the response in $\delta^{-/-}$ slices (n=10, p=0.032, MWRS test, **Figure III-7C**). Photolysis of GABA in slices from $\delta^{-/-}$ mice was statistically indistinguishable from that observed in slices from wild type mice (n=12 for $\delta^{-/-}$ group, p=0.25, MWRS test, **Figure III-7C**), indicating that the δ subunit is not required for this excitatory action of GABA.

Endogenously released GABA can excite PFs

To determine whether endogenous GABA released by molecular layer interneurons can also excite parallel fibers, we carried out experiments in which stimulus trains (20 Hz) were delivered to the molecular layer while fiber volleys were recorded 300-500 µm away in the presence of a $GABA_BR$ blocker (**Figure III-8A**). As compound APs, fiber volley amplitudes varied during trains, typically increasing in amplitude steeply during the first 0.4 seconds, and reaching a steady state amplitude approximately 1 s into the train (**Figure III-8B**). In order to isolate the $GABA_AR$-dependent effects we compared trains in the absence and presence of the $GABA_AR$ antagonist PTX and calculated the $GABA_AR$-dependent change in fiber volley amplitude during the train normalized to the amplitude of the first pulse (**Figure III-8C**). To assess whether $GABA_AR$-dependent increases in fiber volley amplitude are due to GABA released from interneurons, we used a blinded experimental design to compare responses in control solution with responses in solution containing the calcium channel blocker cadmium (100 µM). After the initial 0.4 second transient rising phase, there was a significant PTX- sensitive response in the control condition but not in the cadmium condition (control, $n = 6$, $0.027 < p < 0.050$; cadmium, $n=6$, $0.17 < p < 0.490$, **Figure III-8C**). Since the measurements are repeated, a repeated measure ANOVA was used to show that amplitudes in control differ in time ($F = 1.82$, $p < 0.2$) but not in cadmium ($F = 1.56$, $p > 0.05$). These results demonstrate that synaptic transmission is required for the $GABA_AR$-dependent effect, and imply that fiber volley amplitudes are altered by the release of GABA from molecular layer interneurons.

We next examined whether the GABA uptake blocker NNC-711 further enhanced this effect. Analysis of the cumulative PTX-sensitive change in the time period from 0 to 0.75 seconds showed significant increases in the control condition; as this control was indistinguishable from the control condition above (Kolmogorov-Smirnov 2 sample test, $0.08 < p < 0.82$ for time points between 0 and 1.2 s), control data have been pooled in **Figure III-8C**. For both control and NNC-711 conditions, PTX-sensitive responses were significantly enhanced from no change (Fig 8C, control in black, n=10, $p = 0.042$; NNC-711 in blue, n=10, $p = 0.004$). Comparing with the cadmium condition using a repeated measures ANOVA, group and interaction effects were only significant in the NNC-711 condition ($F = 7.33$ and 1.88, $p < 0.2$). Although there was a trend to larger increases throughout the train in the presence of the GABA reuptake inhibitor, the difference between control and NNC-711 only became significant late in the train (0.8 – 1.2 seconds, n=10, $0.034 < p < 0.05$). Control and NNC-711 conditions also differ as measurements in time (repeated measures, $F = 3.09$, $p < 0.005$). Together these data suggest that GABA release from molecular layer interneurons can excite PF axons and facilitate the amplitude of fiber volleys during trains.

Depolarizing $GABA_AR$ actions in a compartmental model of granule cell and PF axon

To establish whether a regional difference in chloride concentration in axonal compartments could account for increased axonal excitability in PFs, we implemented a NEURON model of a granule cell body and bifurcating PF axon with mammalian Hodgkin-Huxley style conductances (Wang, Liu et al. 2003). The model consists of a

5.8 µm diameter cell with a 0.3 µm diameter axon (**Figure III-9A**). The axon ascends for 70 µm and then bifurcates into two branches, one 750 µm and the other 250 µm. Each axonal compartment is 2.5 µm in length. All compartments have a constant density of leak conductance, voltage-gated potassium conductance and voltage gated sodium conductance. To mimic tonic inhibition all simulations include a constant conductance of 100 µS/cm^2 (E_{rev}= -70 mV) at the cell body in addition to the standard leak conductance.

In order to simulate GABA effects on the axon, gated GABA conductances with user defined reversal potentials designated as $G_{GABA,\ Erev}$, are added selectively to axonal compartments. In this way the model can be used to explore how PF axon excitability is affected by regional activation of axonal conductances with a range of reversal potentials from -55 mV to -75 mV, that is $G_{GABA,\ -55\ mV}$ to $G_{GABA,\ -75\ mV}$.

When $GABA_AR$ conductances (100 µS/cm^2) were activated in the axon, the threshold for spike generation triggered by current injection in the axon was reduced in a manner dependent on the reversal potential. Activation of $G_{GABA,\ -60\ mV}$ in the axon decreased spike threshold to 40% (**Figure III-9B-D**). In contrast, with $G_{GABA,\ -70\ mV,}$ that is, a reversal potential set equal to the resting membrane potential of the axon, spike threshold increased slightly, presumably due to shunting inhibition (**Figure III-9C-D**). Increases in spike threshold were also observed for $G_{GABA,\ -75\ mV}$.

Experiments on single PF axons suggest that axonal G_{GABA} might also affect orthodromic spike initiation (Pugh and Jahr 2011). To test whether the model shows this behavior, currents were injected into the granule cell body to elicit spikes (**Figure**

III-10A). Activation of axonal G_{GABA} also decreased orthodromic spike threshold in a manner dependent on reversal potential (**Figure III-10B-C**). In this case no shunting was seen for the threshold curve when the reversal potential for G_{GABA} was equal to the resting membrane potential. However, a small delay in time to spike was observed when $G_{GABA,\ rev}$ was equal to the resting membrane potential consistent with shunting (**Figure III-10E**, compare control and -70 mV curves). Moreoever, only regional application of gGABA at the molecular layer is necessary for generating spike threshold decreases in the soma (**Figure III-10F**). Activating only $GABA_A$Rs on the segments of the parallel fiber beyond the T-junction is sufficient to see the effect, and even a 200 μm diameter spot 270 μm away from the soma yields a 5 pA decrease in current threshold at E_{rev}= -70 mV, indicating that GABA released from a regional population of interneurons are sufficient to influence granule cell spiking over 200 μm away. Considered together, the modeling results suggest that axonal G_{GABA} decreases threshold for orthodromic spikes facilitating normal spike generation.

We next examined whether activation of axonal G_{GABA} affected conduction velocity by depolarizing the cell body and measuring AP propagation at two sites in the axon (**Figure III-10A**). As was the case for the threshold effect, GABA-induced changes in conduction velocity varied with $G_{GABA,\ rev}$ such that conduction velocity was inhibited by 6.3% $G_{GABA,\ -75}$ and increased by 10.3% at $G_{GABA,\ -60\ mV}$.

To better understand how axonal depolarization increases conduction velocity we explored changes in the properties of the voltage-gated sodium conductance. Given that G_{GABA} is depolarizing the axon we reasoned that increases in conduction velocity

would be sensitive to the voltage dependence of sodium channel availability, as formalized in the h-∞ curve. To test this hypothesis, we modified the mammalian version of sodium conductance (Wang, Liu et al. 2003) used in the earlier simulations so that it would have an h-∞ curve identical to that of the original Hodgkin Huxley (HH) sodium channel (Hodgkin and Huxley 1952). With an HH channel, fewer than half as many sodium channels are available at -60 mV as are available at -75 mV (**Figure III-11B**, green curve) as compared to a loss of only 10% over the same membrane potential range with the mammalian channel (**Figure III-11B**, black curve). In simulations using the HH sodium channel, the resting membrane potential was unchanged (-70 mV in both models with G_{GABA}=0) and G_{GABA} still decreased threshold, albeit to a smaller extent (**Figure III-11C**). However, G_{GABA}–induced increases in conduction velocity were lost; instead conduction velocity was decreased at all chloride reversal potentials (**Figure III-11D**).

To investigate the mechanism of action of the depolarizing effect of GABA, we conducted additional simulations at different E_{rev} in which brief current injections to the granule cell body were used to determine spiking threshold recorded from a nearby axonal compartment. Despite the fact that E_{rev} was well below spike threshold, whenever E_{rev} was more depolarized to the resting membrane potential it facilitated spiking (**Figure III-12A**). There may still be a shunting effect, but the depolarization predominates in this case. It appears that the role of G_{GABA} is to depolarize the resting potential, bringing it closer to the threshold for spiking. Indeed, comparing with the squid giant axon Hodgkin-Huxley inactivation curve model, we find that the threshold

voltage is increased slightly, but remains relatively constant at different E_{rev}. This, along with the smaller depolarization associated with lower sodium channel availability, makes the excitatory effect much smaller.

To understand the relative contributions of shunting and depolarization on the reported effects, we ran simulations in which we varied the magnitude of G_{GABA} with an E_{rev} set at -60 mV (**Figure III-12-B**). Threshold currents injected at the soma were determined as an indication of excitability. Minimal thresholds were found to occur with G_{GABA} approximately equal to 100 μS/cm^2. Threshold remained lower than control (i.e., G_{GABA}=0) until G_{GABA} exceeded 1800 μS/cm^2, at which point the shunting effect of the conductance predominated over the depolarizing effect and G_{GABA} caused net inhibition. We also explored even higher shunting effects and found that even regional increases of G_{GABA} to 240 times the somatic value of 100 μS/cm^2 leads to spike propagation failure. Note that depolarizing effects stated here really depends on the balance of G_{GABA}, G_{LEAK}, and the excitatory conductance (dependent on sodium channel availability). When G_{LEAK} is reduced, the resulting decrease in overall conductance can lead to a larger effect on excitability for a similar range of stimulus intensities (**Figure III-12-C**).

DISCUSSION

We find that transient activation of $GABA_A$Rs on PFs increases axonal excitability and that this is reflected in an increase in the amplitude of fiber volleys and an increase in axonal conduction velocity. Our findings complement previous studies which have

suggested that PF presynaptic excitability is increased by GABA (Stell, Rostaing et al. 2007; Pugh and Jahr 2011; Stell 2011). In the prior work, pressure pipette application of GABA and/or muscimol or iontophoretic application of GABA was found to increase glutamate release from PFs (Stell, Rostaing et al. 2007; Pugh and Jahr 2011) and increase PF calcium transients (Pugh and Jahr 2011; Stell 2011). Calcium imaging of single PF axons as well as whole cell recording from granule cell bodies demonstrated that GABA application to axons reduces the threshold for generating an action potential (Pugh and Jahr 2011). The fiber volley measurements described here extend these observations, demonstrating directly that axonal membrane excitability is altered and that this not only affects presynaptic output but also spike propagation.

The most likely mechanism by which GABA excites PFs is by depolarizing the axonal membrane, thereby bringing the axon closer to AP threshold. In this way the axon could provide passive depolarization to the spike initiation zone, acting in an analogous manner to a dendrite. Experimental evidence is consistent with passive propagation of $GABA_AR$-initiated depolarization over considerable distances in PF axons (Pugh and Jahr 2011). Moreover, modeling studies suggest that APs are initiated in the ascending axon of PFs (Diwakar, Magistretti et al. 2009), supporting the idea that axonal $GABA_ARs$ can influence orthodromic spike generation.

It has been hypothesized that the depolarizing effect of GABA on PFs is due to slightly higher chloride concentrations in the axon (Stell, Rostaing et al. 2007; Pugh and Jahr 2011; Stell 2011). PFs would thus be similar to mossy fiber axons, calyx of Held nerve terminals, and pituitary nerve terminals, preparations in which cell-attached and

perforated patch clamp recordings have demonstrated GABA depolarization of the terminal (Zhang and Jackson 1995; Price and Trussell 2006; Ruiz, Campanac et al. 2010). In the latter two preparations non-invasive recordings have also allowed estimates of internal chloride concentrations of 15-20 mM and corresponding GABA reversal potentials of approximately -50 mV (Zhang and Jackson 1995; Price and Trussell 2006).

The inaccessibility of PFs to patch clamp methods has made it impossible to directly explore whether there are regional differences in chloride reversal potential in PFs. However the pattern of expression of chloride cotransporters in cerebellar granule cells and PF axons suggests that regional differences in chloride reversal potential may exist. Chloride gradients in neurons are determined in large part by the actions of two types of chloride transporters, KCC2, which extrudes chloride, and NKCC1, which accumulates chloride into neurons (Blaesse, Airaksinen et al. 2009). In some brain regions, such as the olfactory neuroepithelium, retina, and suprachiasmatic nucleus, where GABA has been shown to be excitatory, NKCC1 protein has been detected in adult tissue (Kaneko, Putzier et al. 2004; Li, McKernan et al. 2008; Belenky, Sollars et al. 2009). In other neurons such as neocortical pyramidal cells where GABA has been shown to depolarize axons, it is unclear whether NKCC1 is expressed in adults; however, KCC2 protein is excluded from the axonal compartments (Szabadics, Varga et al. 2006). In the adult cerebellar cortex, both KCC2 and NKCC1 mRNA are present in granule cells (Mikawa, Wang et al. 2002), and KCC2 protein appears to be completely absent in PFs (Seja, Schonewille et al. 2012). Thus, either the presence of NKCC1 or the absence of

KCC2 from PFs likely accounts for the compartmental differences in chloride reversal potential.

The $GABA_AR$ subtype responsible for exciting PFs

Our data in slices are consistent with axonal $GABA_A$Rs being entirely responsible for the increase in excitability (**Figure III-2**). Indeed, under our experimental conditions, it is unlikely that activation of somatic $GABA_A$Rs could have contributed. The effect of GABA on granule cell bodies is hyperpolarizing, therefore, if there were any contribution to axonal excitability it would be inhibitory. Moreover, local iontophoresis of GABA onto single PF axons yields a very similar effect to that described here (Pugh and Jahr 2011).

Cerebellar granule cells express a unique isoform of $GABA_A$R containing δ and α_6 subunits which is localized on extrasynaptic membranes and which knockout studies show is responsible for a tonic GABA current (Nusser, Sieghart et al. 1998; Brickley, Revilla et al. 2001; Stell, Brickley et al. 2003; Santhakumar, Hanchar et al. 2006; Meera, Wallner et al. 2011). We found that DS2, a modulator selective for δ subunit-containing $GABA_A$Rs (Wafford, van Niel et al. 2009; Shu, Bracamontes et al. 2011), did not affect the enhancement by GABA on volley amplitude or on volley latency, however it did enhance the inhibitory phase that sometimes followed the initial excitation. If the inhibitory phase arises from persistent activation of PF $GABA_A$Rs, as we argue below, then it is likely the case that δ $GABA_A$Rs are involved in excitation as well as inhibition but in DS2 the inhibitory effect dominates. Nevertheless, GABA mediated excitation of

PFs was present in tissue from mice lacking the δ subunit indicating that while δ subunits may be present on PFs, they are not required for GABA-mediated excitation of PFs.

Immunocytochemistry suggests that δ protein, like α_6, is expressed highly in granule cell somata and at much lower levels, if at all, in the molecular layer (Pirker, Schwarzer et al. 2000). We demonstrate here that etomidate enhances the excitatory effect of GABA uncaging on PFs but that diazepam has no effect. This pharmacological profile, sensitivity to etomidate but not classical benzodiazepines, suggests that PF $GABA_A$Rs either lack a γ subunit or contain α_6 or both (Mohler, Crestani et al. 2001). Considering that α_1 protein is detected in presynaptic terminals in PF boutons by EM (Stell, Rostaing et al. 2007) and that α_6-containing $GABA_A$Rs increase PF release of glutamate (Schmid, Bonanno et al. 1999), a reasonable possibility is that $GABA_A$Rs on PFs are composed of α_1, α_6, $\beta_{2/3,}$ and γ_2 or δ. Biochemical and electrophysiological data support the presence of such a receptor subtype on somatodendritic membranes of granule cells (Jechlinger, Pelz et al. 1998; Santhakumar, Hanchar et al. 2006), although it is also possible that receptors composed only of α and β subunits are involved as has been suggested in hippocampus (Mortensen and Smart 2006). Taken together, our data and published literature are consistent with axonal $GABA_A$Rs of the subunit composition $\alpha_{1/6}\beta_{2/3}\delta$, $\alpha_1\alpha_6\beta_{2/3}\gamma_{2,}$ $\alpha_6\beta_{2/3}\gamma_2$, or $\alpha_{1/6}\beta_{2/3}$.

Inhibition versus excitation of PFs by axonal $GABA_A$Rs

In a minority of experiments, we observed an inhibitory effect of GABA photolysis

on the volley amplitude. This effect is likely similar to the biphasic effect of GABA on PF excitability in response to pressure pipette application of agonists (Stell 2011). We find that the inhibition is smaller but otherwise consistent with that described by Stell; in our average data (e.g. **Figures III-1C, III-6A,** and **III-7A**) we also observe excitation followed by inhibition. Inhibition was not caused by $GABA_B$ receptor activation and was not associated with a reduction in conduction velocity. In a minority of experiments, inhibition could be observed in the absence of excitation; it also appeared to decrease with age (**Figure III-3**). The observations that inhibition develops more slowly than excitation and that it is more prominent under conditions in which receptors are strongly activated suggests that inhibition may result from shifts in ionic gradients.

PF $GABA_A$Rs increase conduction velocity

The reduction in volley latency and increase in the volley velocity seen with $GABA_A$R activation in PFs in both our experiments and our model are reflective of a phenomenon termed "super-normal excitability" (Gardner-Medwin 1972). Increases in PF volley amplitudes were seen in response to trains of stimuli *in vivo* and were accompanied by 10-20% increases in conduction velocity similar to that described here. Subsequent work suggested that K^+ accumulation might play a role (Malenka, Kocsis et al. 1981; Malenka, Kocsis et al. 1983), however the constraints of studying the phenomenon *in vivo* made it difficult to dissect the underlying mechanisms.

Our observations suggest that excitatory $GABA_A$Rs on PF axons may contribute to supernormal excitability. Based on our experiments we cannot rule out the possibility

that K^+ accumulation could contribute to supernormal excitability as well, indeed, the computational model shows that any modest depolarization from the axonal resting potential by a few millivolts will speed conduction velocity.

Why then does this not occur in all axon types? A key determinate in our model of whether depolarization leads to axon excitability are the properties of voltage gated sodium conductance, particularly the voltage dependence of inactivation (the h_∞ curve for a Hodgkin Huxley-type channel). We find that velocity increases are opposed by sodium channel inactivation at depolarized potentials. When the h-∞ curve is shifted to negative potentials, reduced sodium channel availability at depolarized potentials mitigates the increase in axon excitability. In this regard it is intriguing to note that both calyx of Held (Kim, Kushmerick et al. 2010) and cerebellar granule cells (Afshari, Ptak et al. 2004) express an unusual form of voltage-gated sodium current characterized by a resurgent activation behavior, a persistent sodium current fraction, and a right-shifted availability (h-∞) curve (Bant and Raman 2010). This current is mediated by the interaction between NaV1.6, a pore forming voltage-gated sodium channel subunit and an accessory subunit, β_4 (Grieco, Malhotra et al. 2005). Knockdown of the β_4 subunit in cerebellar granule cells leads to a leftward shift of the sodium current inactivation curve (Bant and Raman 2010) indicating that the resurgent gating mechanism is accompanied by an increased steady state availability of sodium channels at membrane potentials in the critical potential range between the resting potential and spike threshold. This may explain why GABAergic depolarization can be found to inhibit propagation in one model system (Jackson and Zhang 1995) and

facilitate propagation in another. These results raise the interesting possibility that this specialized voltage-gated sodium current may be an important determinant of whether axonal depolarization is coupled to increased conduction velocity in axons.

Conclusion

Using extracellular field recordings of evoked population APs our data confirm a robust excitatory effect of GABA on PFs that had been observed with calcium imaging and single neuron electrophysiological approaches (Stell, Rostaing et al. 2007; Pugh and Jahr 2011; Stell 2011). Subunit specific pharmacology and knockout animals suggest that δ subunit-containing $GABA_AR$ subtypes play a minor role in these effects and that they are likely mediated by α_6-and γ_2-containing $GABA_ARs$. We also report that activation of axonal $GABA_ARs$ can increase AP conduction velocity. Endogenous GABA release mimics the excitatory effect consistent with a physiological role. A simplified NEURON model recapitulates our experimental findings and suggests that the excitatory effect will be sensitive to specific features of voltage-gated sodium channels such as the voltage dependence of availability. Through these physiological actions, PF $GABA_ARs$ may exert an important role in signal processing of sensorimotor information in the granule cell layer.

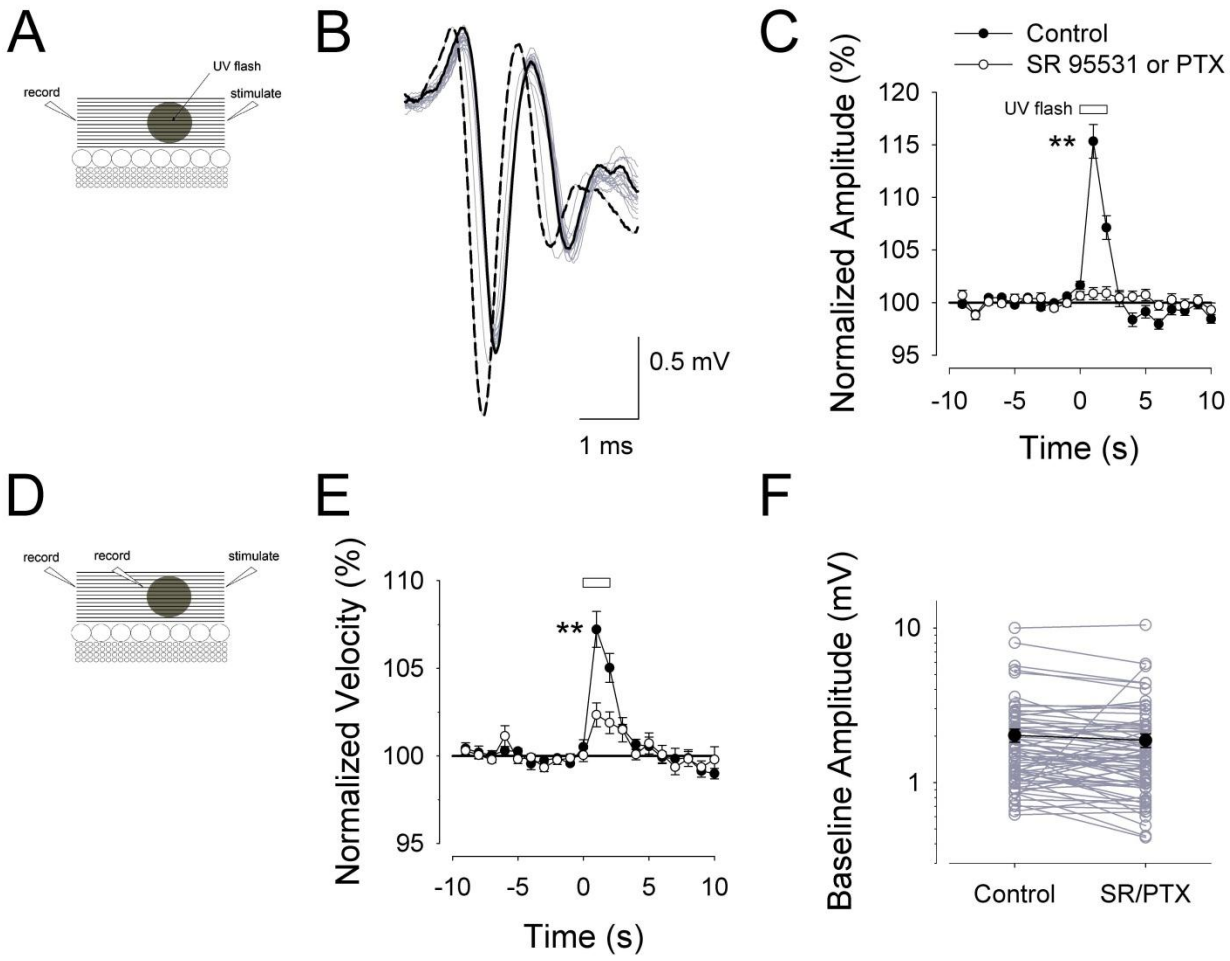

Figure III-1. Local photolysis of GABA excites parallel fibers and speeds up fiber volleys. A) Diagram of the setup of experiments involving one recording and one stimulating electrode. B) Sample traces from a single trial. The solid and dashed black traces are, respectively, the volleys recorded immediately at the beginning and one second into the UV flash. The gray traces are the volleys recorded at all other times during the experimental protocol. C) Summary time course (n = 95 measurements, 70 slices from 60 animals) from experiments as in B, and after blockade of $GABA_A$Rs by SR (n = 28) or PTX (n = 40). The plot is of the volley amplitude normalized to the average of the 9 s control period before the UV flash. D) Diagram of the setup of experiments to measure conduction velocity. E) Summary time course from the velocity experiments in control (n= 16 slices, 14 animals) and after wash in of SR (n = 3) or PTX (n = 10). F) Summary of the pre-UV raw volley amplitudes (gray circles) before and after $GABA_A$R blockade by SR or PTX. Average data are denoted by black diamonds. Ordinate axis is log-scaled.

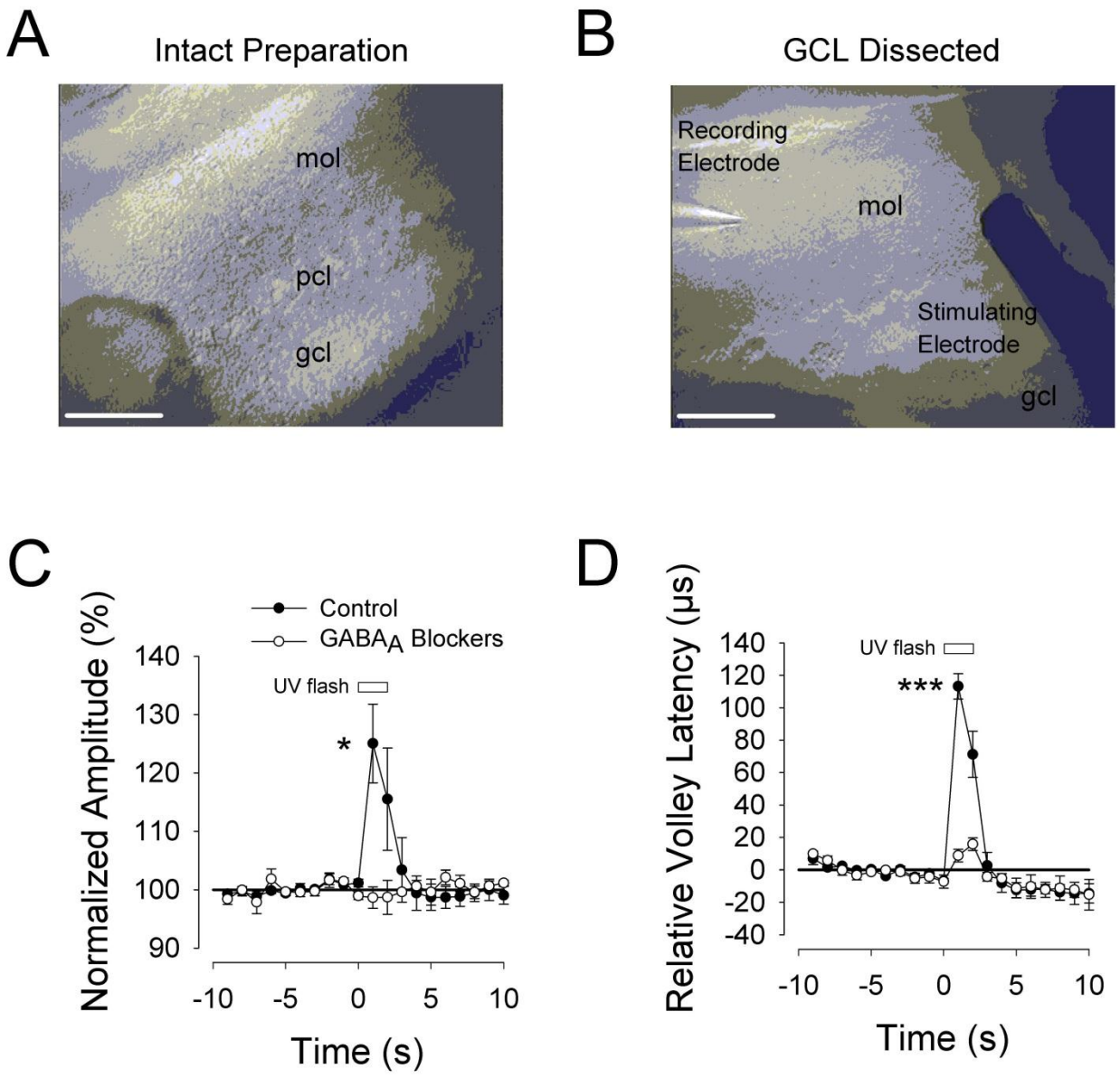

Figure III-2. GABA excitation of PF axons is not due to GABA actions at the granule cell bodies. A) Photograph of an intact slice preparation. The granule cell layer (gcl), purkinje cell layer (pcl), and molecular layer (mol) are labeled. The scale bar here and in B is 100 µm. B) Photograph of a slice preparation with the stimulating electrode and recording electrode in view. The granule cell layer was dissected away from the molecular layer by making an incision between the granule cell layer and the molecular layer with a 27 gauge syringe needle under 30X magnification. C) Summary time course of the normalized volley amplitude (n = 5 measurements, 4 slices from 4 animals) from experiments as in **Figure III-1 B**, and after blockade of $GABA_A$Rs by SR or PTX. D) Summary time course of the volley latency, after subtraction of the average latency in the pre-UV period from the same experiments as in C.

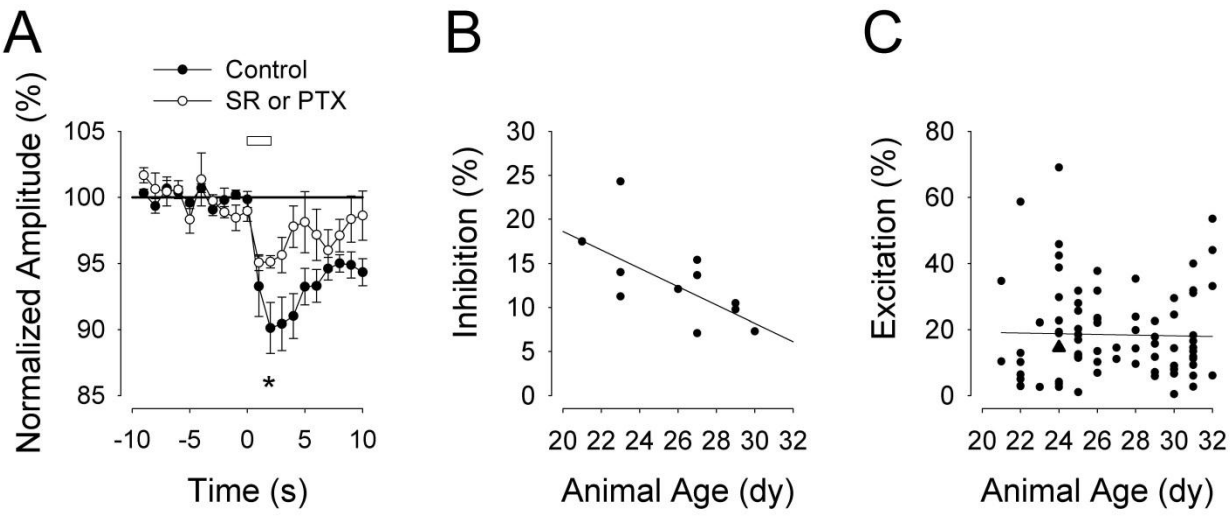

Figure III-3. Summary of excitatory and inhibitory effects of GABA on volley amplitude. A) Summary time course from experiments as in B, but only from those experiments which showed an inhibitory effect on volley amplitude. For the purposes of this figure, inhibition is defined as no increase in volley amplitude by UV and a decrease in volley amplitude to less than 95% of the baseline average in the first 5 s after the UV pulse. (control, n = 11 measurements, 8 slices from 8 animals; SR, n = 3; PTX, n = 3). B) Scatter plot of the volley amplitude inhibition by UV versus the age of the animal from the same experiments reported in A (parameters of the linear fit, $y = 41.24 – 1.09x$, $R^2 = 0.435$). C) Scatter plot of the volley amplitude enhancement by UV versus the age of the animal (linear fit: $y = 22.3 – 0.14x$, $R^2 = 0.0013$). Note that all experiments in **Figure III-1C** are displayed as individual points in either panel C or panel B. The triangle corresponds to the representative trace shown in **Figure III-1B**.

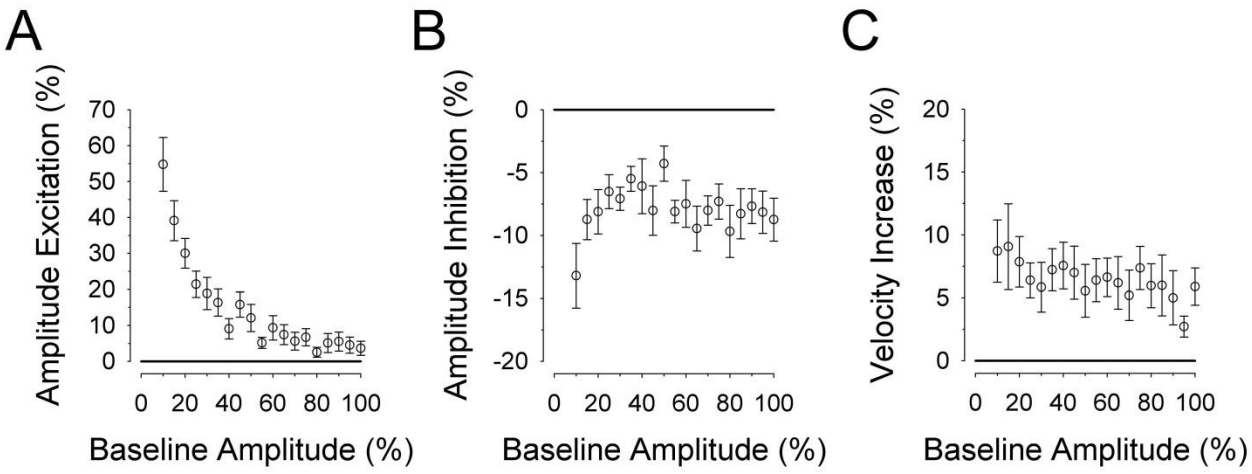

Figure III-4. Relationship of GABA photolysis effects with stimulus intensities. A) Plot of normalized amplitude excitation by GABA versus normalized baseline volley amplitude. Experiments were carried out as in **Figure III-1**, but the stimulus duration was varied systematically between trials. All volley amplitude values for a single experiment were normalized to the peak volley amplitude for the entire experiment, and then the data were binned (5% bin width) and averaged (n = 17 measurements, 9 slices from 9 animals). B) Plot of normalized amplitude inhibition versus baseline volley amplitude (from the same experiments as in A; see Methods for how inhibition was defined). C) Plot of normalized velocity increase versus baseline volley amplitude (n = 8 slices from 8 animals).

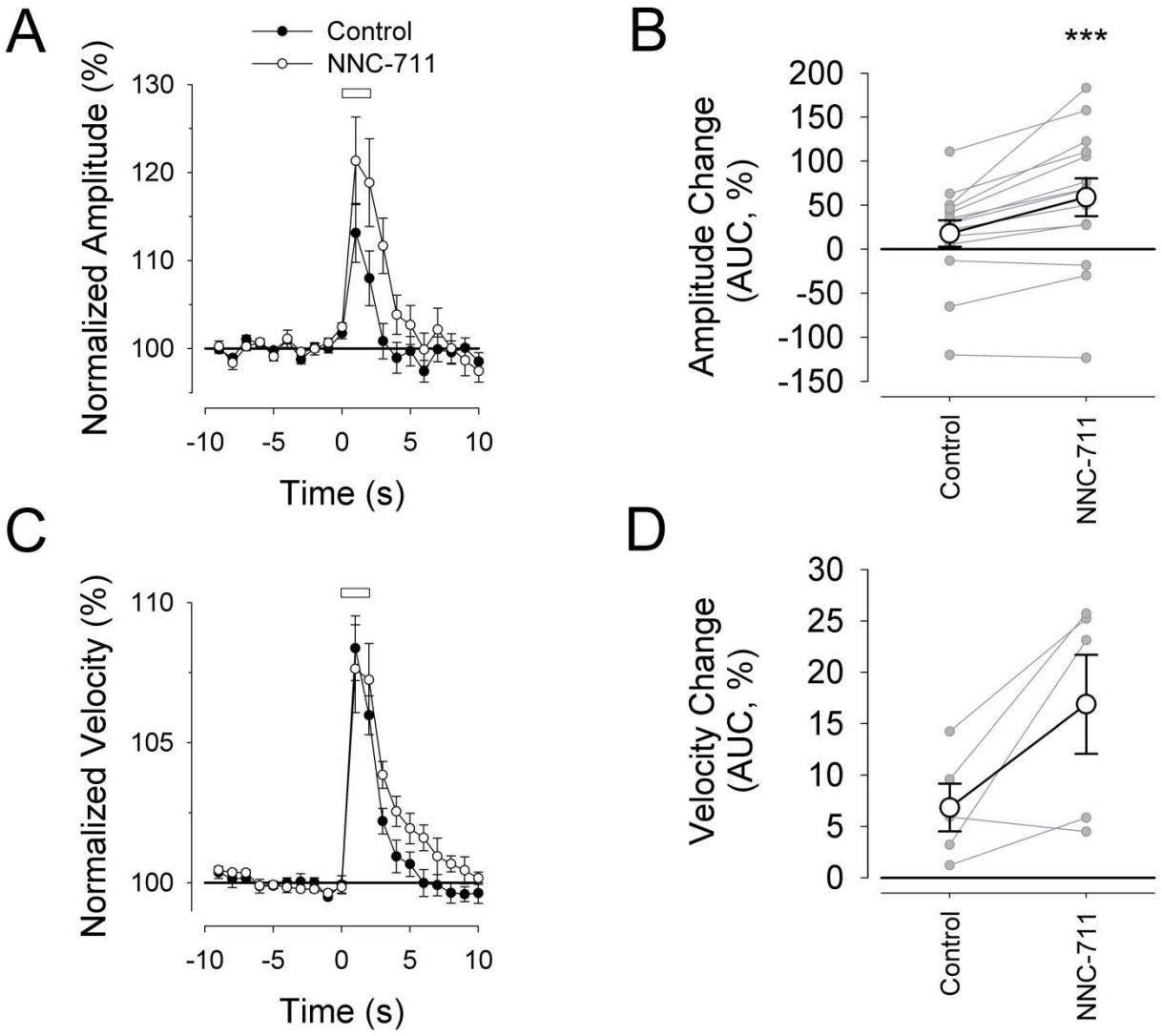

Figure III-5. Blockade of GABA reuptake prolongs the photolysis effect. NNC-711 summary data. A) Time course of volley amplitude (n = 14 measurements, 9 slices from 7 animals). B) Cumulative amplitude change (AUC) are summarized (individual data in gray circles, group average and SEM in open diamonds, see Methods for how these values were calculated). The solid black lines here and in panel D indicate the expected AUC values if there had been no changes from the baseline, therefore values above and below the solid black line represent net excitation and inhibition, respectively. C) Time course of volley velocity (n = 5 slices from 4 animals). D) Velocity AUC summary data as in B.

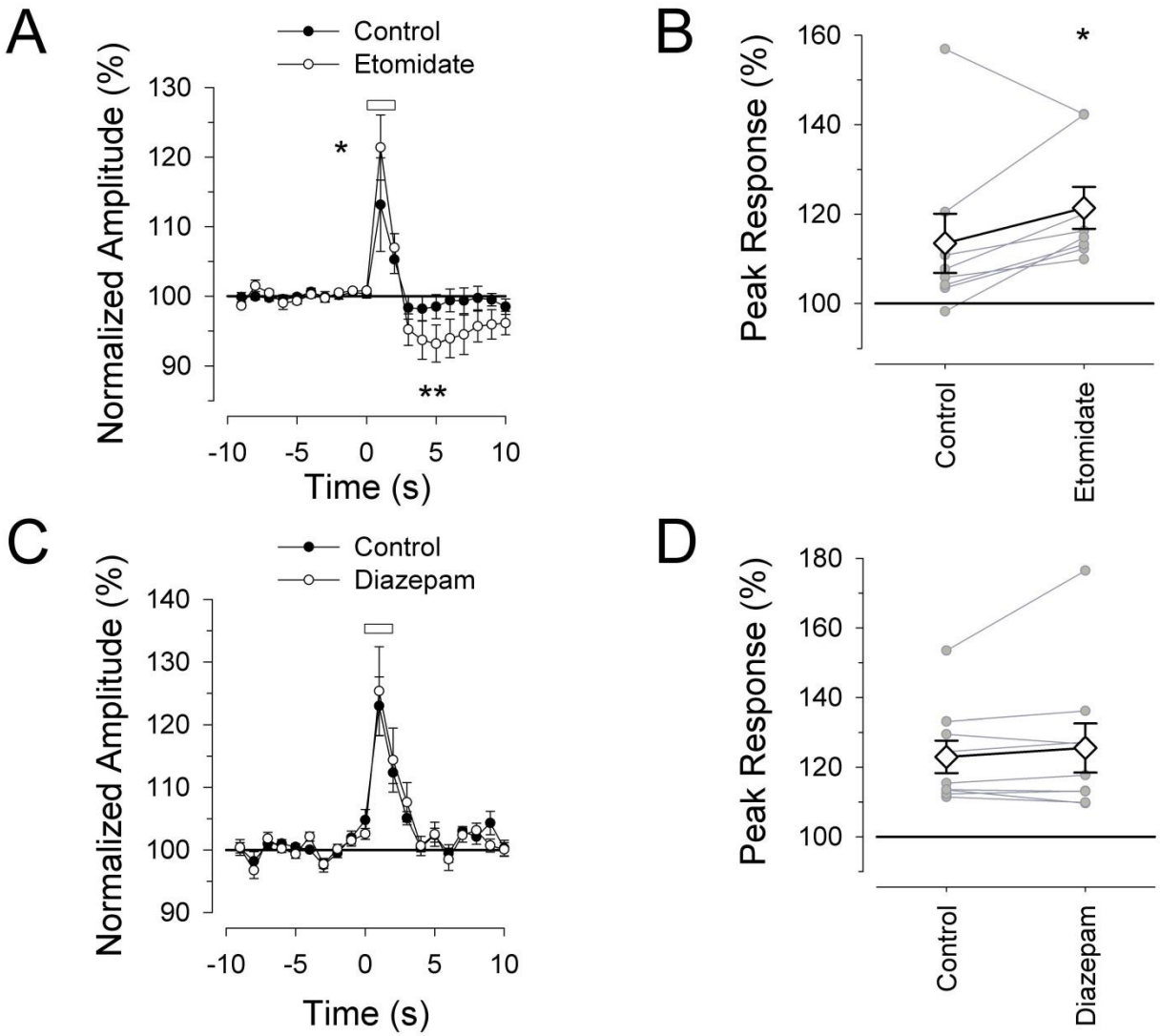

Figure III-6. Axonal GABAARs mediating photolysis effect are sensitive to etomidate but not classical benzodiazepines. A-B) Etomidate summary data. A) Time course of volley amplitude (n = 7 measurements, 7 slices, 7 animals). B) Amplitude summary data. C-D) Diazepam summary data. C) Time course of volley amplitude (n = 8 measurements, 5 slices, 5 animals). D) Amplitude summary data.

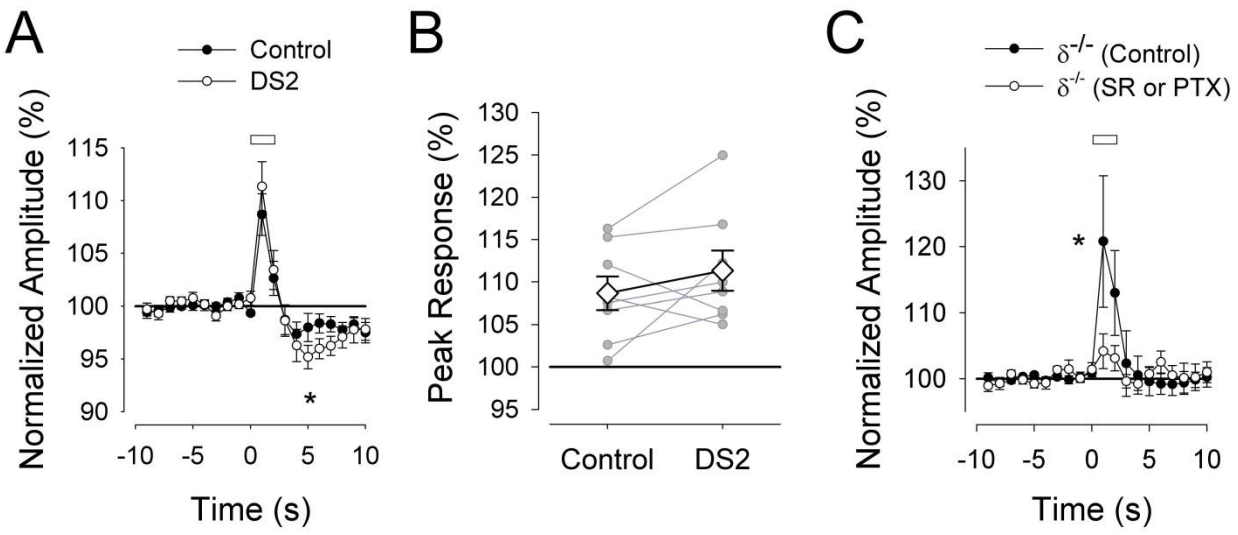

Figure III-7. Excitation of parallel fibers by GABA does not require the GABAAR δ-subunit. A-B) DS2 summary data. A) Time course of volley amplitude (n = 8 measurements, 8 slices, 8 animals). B) Amplitude summary data. C) Time course of volley amplitude in $\delta^{-/-}$ mice (Control, n = 12 slices, 10 animals; SR, n = 3; PTX, n = 7).

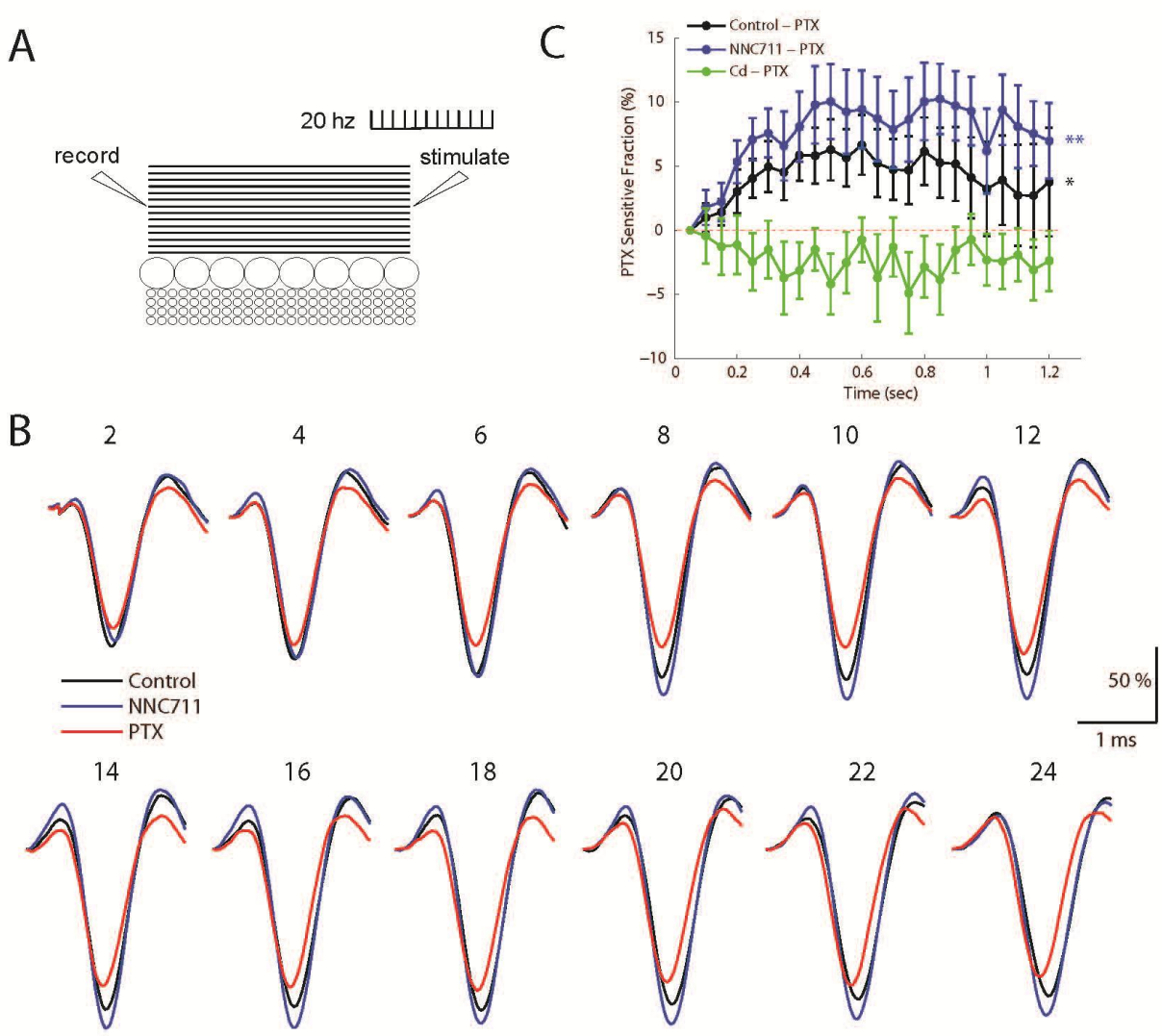

Figure III-8. Endogenously released GABA contributes to parallel fiber excitation. A) Diagram of the experimental design. B) Sample fiber volleys in response to 20 Hz stimulation. Traces have been normalized to the amplitude of the first fiber volley in the train and numbers above traces indicate the pulse number in the train. Black traces are control, blue traces are in the GABA uptake blocker 10 μM NNC-711 and red traces are in 10 μM NNC711 and 100 μM PTX. C) Mean time courses of the PTX-sensitive components in control (black, n = 16), in 100 μM cadmium (green, n = 6) and in 10 μM NNC-711 (blue, n = 10). PTX-sensitive components are expressed as a fraction of the amplitude of the first fiber volley in the train. Control data for cadmium and NNC-711 experiments are pooled in this plot (see Results).

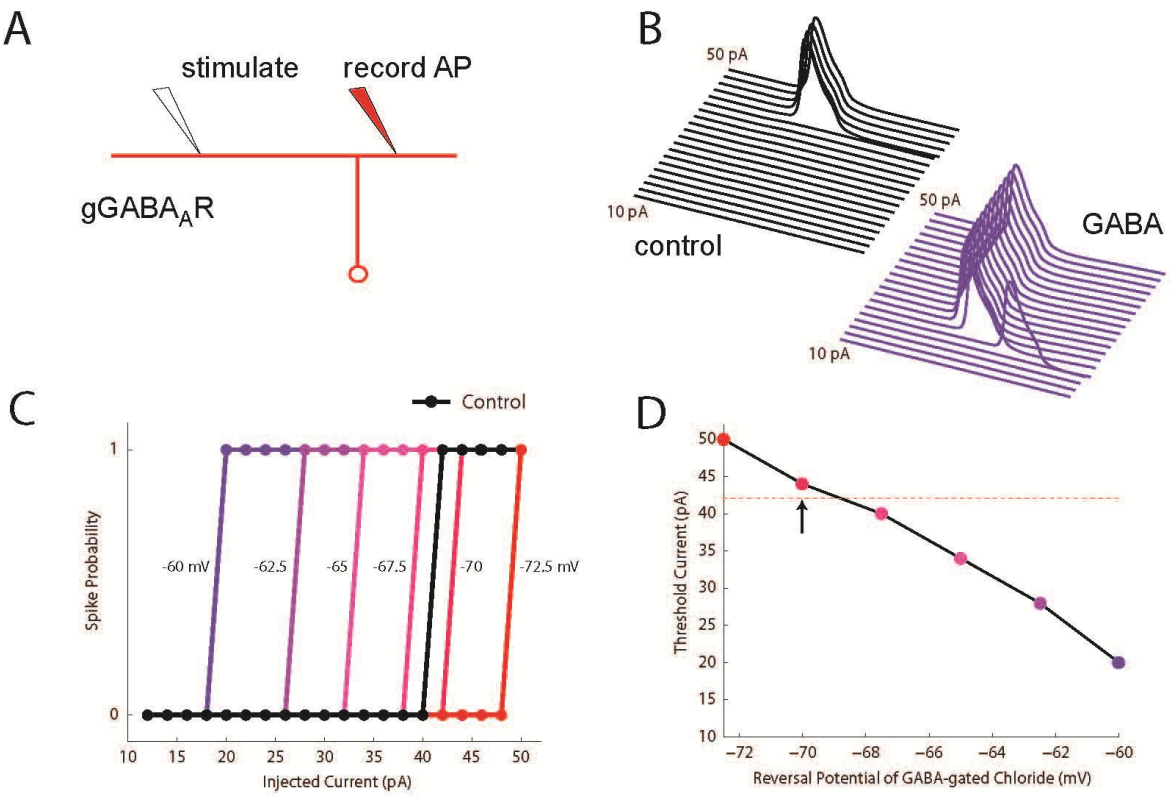

Figure III-9. Simulation of the effect of GABAAR-activation on axonal excitability. A) Diagram of the NEURON simulation. B) A family of responses recorded in the axon in response to an ascending range of current injections (1 ms duration, 10-50 pA) into a site in the axon 600 µm away. Black traces indicate control and purple traces indicate conditions in which an axonal GABA conductance (100 µS/cm^2, -60 mV reversal potential for chloride) is active. Trace durations are 25 ms. C) Spiking probability as a function of stimulus size. Each color shows the effect of a GABA-gated chloride conductance (100 µS/cm^2) with a different reversal potential. D) Threshold current as a function of G_{GABA} reversal potential. Horizontal line shows the threshold current for control condition (G_{GABA} =0). Arrow indicates the resting potential of -70 mV; note that activation of $G_{GABA,\ -70\ mV}$, leads to an increase in threshold.

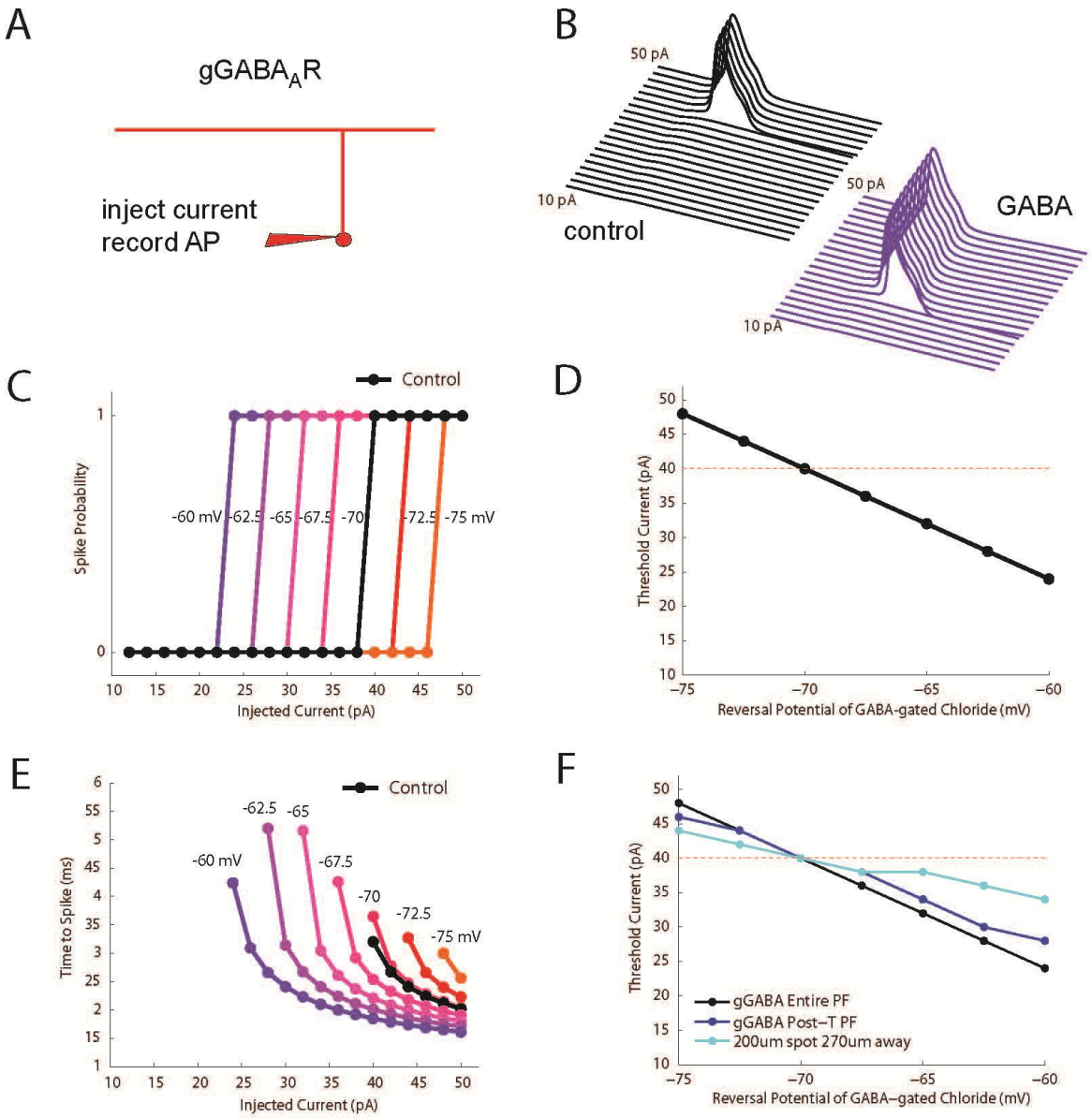

Figure III-10. Simulation of the effect of GABAAR-activation on orthodromic spike initiation. A) Diagram of the NEURON model. B) Traces recorded in the soma in response to a range of stimulus intensities; black are with $G_{GABA} = 0$ and purple with $G_{GABA,\ -60\ mV} = 100\ \mu S/cm^2$. C) Spiking probability curves in response to current injection at the soma. Different colors indicate reversal potentials for G_{GABA}. D) Threshold current as a function of G_{GABA} reversal potential. Horizontal line shows the threshold current for control condition ($G_{GABA} = 0$). E) Time to spike for action potentials at the soma versus stimulus current. Each color represents simulations at different reversal potentials for G_{GABA}. Note the slight shunting effect apparent as a slightly longer delay to spike in comparing $G_{GABA,\ -70\ mV}$ (red) with control (black). F) Threshold current as a function of G_{GABA} reversal when turning on gGABA only on sections of the parallel fiber above the T-junction (purple), or in an activated 200 µm spot of parallel fibers (blue).

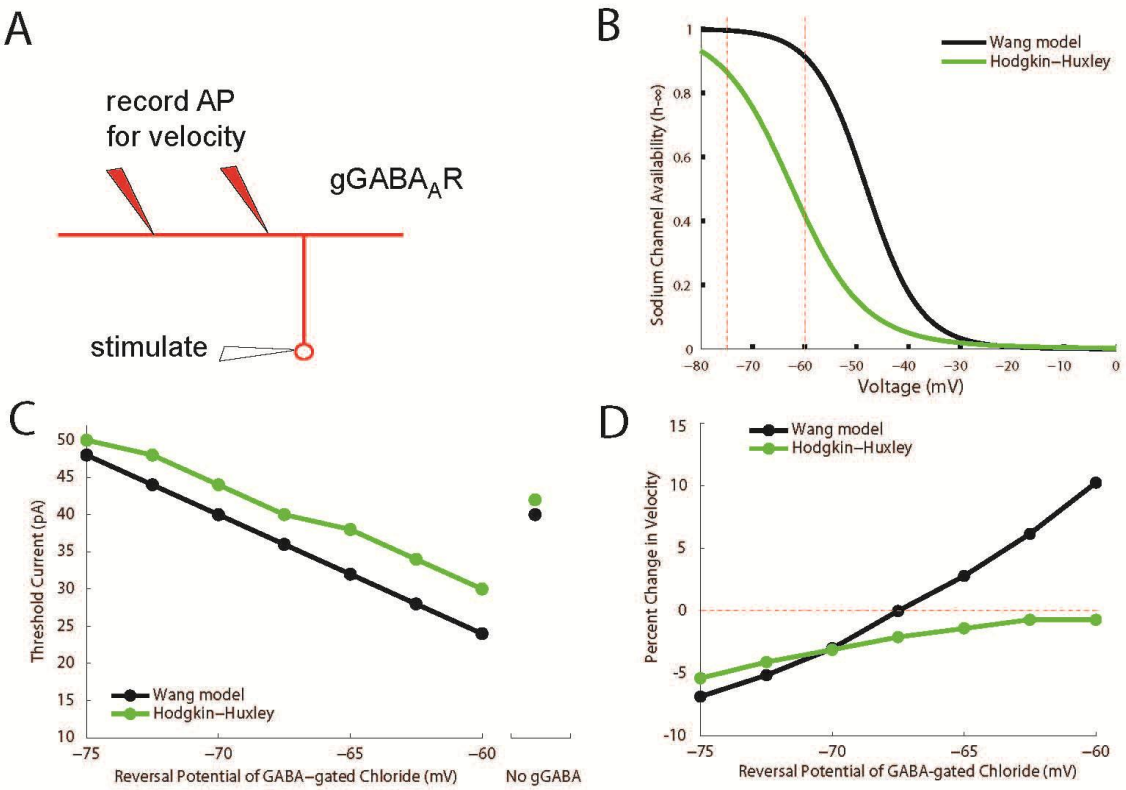

Figure III-11. Sodium channel h-∞ curves influence the effect of depolarizing GABA on conduction velocity. A) Diagram of the NEURON model for studying conduction velocity. The two recording spots are 170 µm and 570 µm away from the cell body. B) Sodium channel availability curves (h-∞) for the mammalian Hodgkin-Huxley model (Wang 2003) and the squid giant axon Hodgkin-Huxley model (Hodgkin-Huxley 1952). The range of $G_{GABA,\ Erev}$ simulated in this study is indicated by the vertical red lines. C) Threshold current for generating an action potential as a function of G_{GABA} reversal potential. Black curve indicates simulations using the h-∞ curve from Wang, 2003 and green curve represents simulations using the Hodgkin Huxley h-∞ curve. Symbols on the right show the threshold current for control conditions (G_{GABA}=0) in the two models. D) Percent change in conduction velocity versus reversal potential for the two models.

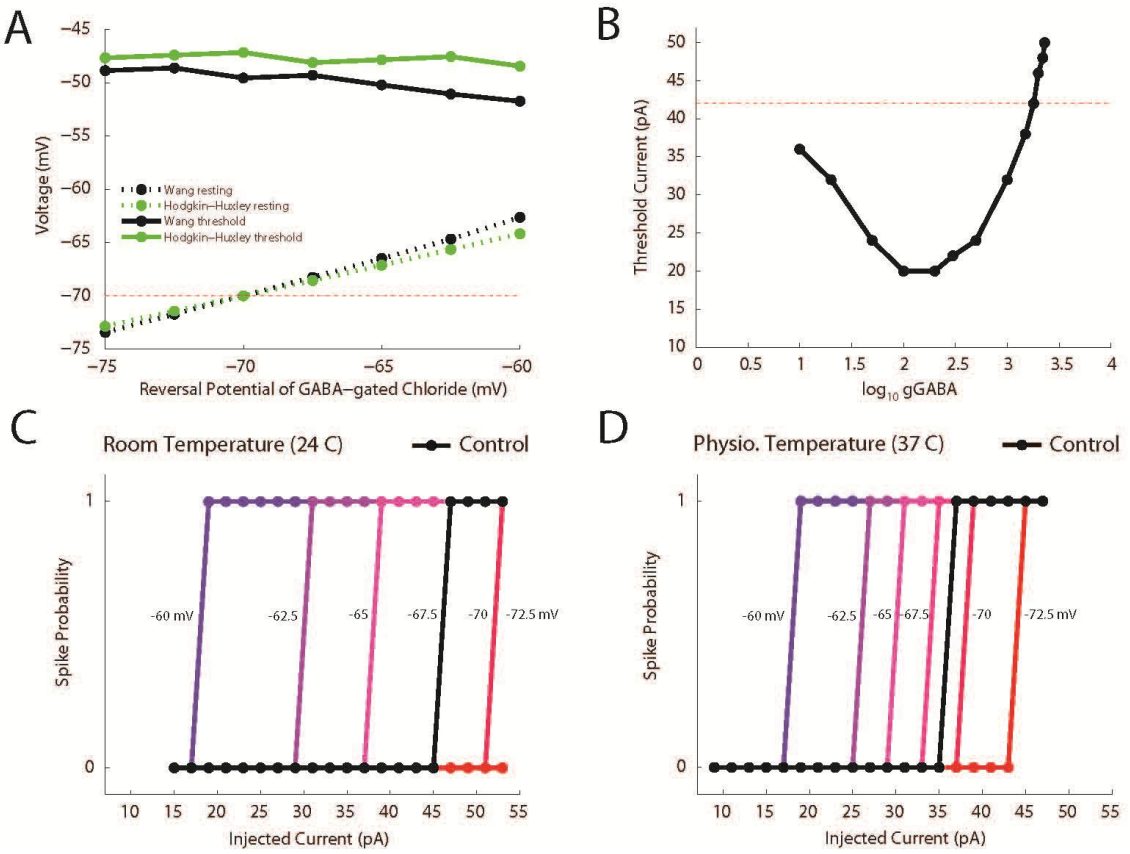

Figure III-12. Depolarizing effect of GABA depends on gGABA conductance, but does not rely on a specific temperature. A) Resting membrane potential in the presence of 100 μS/cm^2 gGABA (dotted) and threshold voltage (solid) of a granule cell as a function of E_{Cl}. Green traces used the Hodgkin Huxley inactivation parameters for squid giant axon and black traces used the Wang model. Threshold voltage is determined in an axonal compartment within 10 μm of the cell body by injecting a range of currents into the cell body and determining the peak membrane potential in the largest subthreshold response. B) Effect on threshold of different gGABA conductances. gGABA values are expressed on a log scale and are in μS/cm^2. Note that the maximum excitatory effect is at gGABA = 100 μS/cm^2, and that for gGABA > 1800 μS/cm^2 shunting predominates and threshold is increased. C) Effect on threshold of gGABA=100 μS/cm^2 at room temperature (24 °C). Stimuli range from 13 to 53 pA and gLEAK = 26 μS/cm^2. D) Effect on threshold of gGABA=100 μS/cm^2 at physiological temperature (37 °C). Stimuli range from 7 to 47 pA and gLEAK = 30 μS/cm^2.

CHAPTER IV

Submillisecond optical reporting of membrane potential *in situ* using a neuronal tracer dye

SUMMARY

A major goal in neuroscience is the development of optical reporters of membrane potential that are easy to use, have limited phototoxicity, and achieve the speed and sensitivity necessary for detection of individual action potentials in single neurons. Here we present a novel, two-component optical approach that attains these goals. By combining DiO, a fluorescent neuronal tracer dye, with dipicrylamine (DPA), a molecule whose membrane partitioning is voltage-sensitive, optical signals related to changes in membrane potential based on Förster resonance energy transfer (FRET) are reported. Using this pair in HEK 293 cells with diffraction-limited laser spot illumination, depolarization-induced fluorescence changes of 56% per 100 mV ($\tau \sim 0.1$ ms) were obtained, while in neuronal cultures and brain slices, action potentials (APs) generated a $\Delta F/F$ per 100 mV of greater than 25%. The high sensitivity provided by DiO/DPA enabled the detection of subthreshold activity and high frequency APs in single trials from somatic, axonal, or dendritic membrane compartments. Recognizing that DPA can depress excitability, we assayed the amplitude and duration of single APs, burst properties, and spontaneous firing in neurons of primary cultures and brain slices and found that they are undetectably altered by up to 2 μM DPA and only slightly perturbed by 5 μM DPA. These findings substantiate a simple, non-invasive method that relies on a neuronal tracer dye for monitoring electrical signal flow, and offers unique flexibility for the study of signaling within intact neuronal circuits.

INTRODUCTION

Electrode-based methods are the principal tools for recording activity from single neurons, yet there are many contexts in which these methods have limited capabilities. For example, it is difficult to monitor electrical signals in sub-cellular compartments such as axons or dendritic spines, to make parallel recordings from several interconnected neurons, or to make long-term (i.e., days) recordings from single neurons. Such limitations have stimulated the development of optical approaches as alternatives (Salzberg, Davila et al. 1973; Cohen, Salzberg et al. 1978). The most widely used involve synthetic fluorescent dyes which allow detection of spatially averaged membrane potential from many neurons (Parsons, Salzberg et al. 1991; Obaid, Koyano et al. 1999; Petersen, Grinvald et al. 2003; Grinvald and Hildesheim 2004), or from small regions of single neurons (Djurisic, Antic et al. 2004; Nuriya, Jiang et al. 2006; Palmer and Stuart 2006; Zhou, Yan et al. 2007; Fisher, Barchi et al. 2008; Zhou, Yan et al. 2008). Unfortunately, the best performing synthetic dyes have significant shortcomings including low aqueous solubility (Fromherz, Hubener et al. 2007) making it difficult to label single neurons, slow diffusional properties (Blunck, Chanda et al. 2005) requiring long staining periods (e.g. (Djurisic, Antic et al. 2004), and high phototoxicity (Obaid, Koyano et al. 1999; Djurisic, Antic et al. 2004).

A promising optical approach makes use of changes in Förster resonance energy transfer (FRET) between two components, one of which partitions between leaflets of the lipid bilayer in response to changes in transmembrane voltage (Gonzalez and Tsien 1995; Gonzalez and Tsien 1997). We have adapted this approach by pairing the

common tracer dye DiO (Cohen, Salzberg et al. 1974; Honig and Hume 1989; Wu, Russell et al. 2003) as a fluorescent donor with dipicrylamine (DPA), a low molecular weight lipophilic anion, as a non-fluorescent, voltage-sensing acceptor (Chanda, Blunck et al. 2005). As a donor, DiO is a bright, non-toxic membrane label that permits repeated imaging of viable neuronal structures (Dailey, Buchanan et al. 1994) and does not perturb electrical activity (Honig and Hume 1986; Ratzliff, Howard et al. 2004). DiO readily labels cultured cells by bath application, or clusters of neurons within live tissue using ballistic application (Gan, Grutzendler et al. 2000), making it a versatile fluorescent membrane label for neurons within a network (Morgan and Wong 2008). As an acceptor/voltage sensor, DPA has attractive properties including extremely rapid kinetics (τ < 0.5 ms) (Fernandez, Taylor et al. 1983; Chanda, Blunck et al. 2005), peak voltage sensitivity within the physiological range, good aqueous solubility, and low phototoxicity. One potential limitation is that DPA can perturb excitability by adding capacitance to the membrane (Fernandez, Taylor et al. 1983; Chanda, Blunck et al. 2005; DiFranco, Capote et al. 2007; Sjulson and Miesenbock 2008).

Using laser spot detection methods, we demonstrate that DiO/DPA can report voltage-dependent fluorescence changes in HEK cells with submillisecond kinetics and a sensitivity of up to 60% $\Delta F/F$ per 100mV, performance equal to or better than any existing voltage sensor. In cultured and brain slice preparations, subthreshold signals are detectable from neurons in average trials and AP-evoked signals in single trials with a signal to noise ratio (SNR) greater than 6. Control experiments confirm that relevant DPA concentrations do not alter AP waveform, high frequency bursting, or spontaneous

firing. These properties make DiO/DPA well suited for use as an *in situ* sensor of neuronal activity.

METHODS

Cell culture preparation and transfection

HEK 293 cells and hippocampal neurons (2-4 weeks *in vitro*) were prepared as previously described (Zhang, Chou et al. 1997; Eugene, Depienne et al. 2007), respectively). eGFP-F was from BD Biosciences Clontech and the kind gift of Dr. Pratap Meera. Transfections were also performed as previously described (Zhang, Chou et al. 1997).

Brain Slice Preparation

Parasagittal slices of cerebellum were prepared from 25-45 day-old BALB or C57Bl6 mice (Nielsen, DiGregorio et al. 2004). Slicing solution was chilled to below 4° C and consisted of (in mM unless otherwise stated): 85 NaCl, 63.4 sucrose, 2.5 KCl, 0.5 $CaCl_2$, 4 $MgCl_2$, 1.25 NaH_2PO_4, 26 $NaHCO_3$, and 25 glucose, saturated with 95% O_2/5% CO_2. Slices were incubated in the same solution at 34° C for 30 minutes to one hour, and then transferred to normal external solution maintained at room temperature (22-24 °C). This external solution was comprised of: 125 NaCl, 2.5 KCl, 2 $CaCl_2$, 1 $MgCl_2$, 1.25 NaH_2PO_4, 26 $NaHCO_3$, and 25 glucose (pH 7.3).

Electrophysiological recording

The external solution for HEK-293 cells was (in mM): 140 NaCl, 5 KCl, 2 $CaCl_2$, 1 $MgCl_2$, 20 HEPES, and 25 glucose (pH 7.4), and for hippocampal cells: 130 NaCl, 2 KCl, 2 $CaCl_2$, 3 $MgCl_2$, 10 HEPES, and 20 glucose (pH 7.4). Fire-polished patch electrodes were back-filled with an internal solution (in mM): 110 K-$MeSO_3$, 40 HEPES, 6 NaOH, 4 $MgCl_2$, 0.3 NaGTP, 4 NaATP, either 5 EGTA and 2 $CaCl_2$, or 2 EGTA alone, and in some recordings 20 μM Alexa 594. Tip resistances were between 3-10 MΩ. Recordings from cultured cells were performed at elevated temperatures (32-34 °C), and neuronal recordings from brain slices were made at slightly elevated temperature (25-27 °C). Voltage-clamp and current clamp recordings from cultured cells were performed with an Axopatch 200B (Molecular Devices), filtered at 5-10 kHz, and then digitized at 20 or 100 kHz. Current clamp recordings from brain slices were performed with a Multiclamp 700B amplifier (Molecular Devices), filtered at 10 kHz, and digitized at 20-100 kHz. Series resistance compensation of HEK-293 cells produced a final series resistance of on average (6.3 ± 0.9 MΩ, n=16). Where indicated, holding current was injected in order to maintain the membrane potential at ~-70 mV (hippocampal neurons) or -60 mV (Purkinje neurons) and 2 or 10 ms current injections were used to elicit single APs or complex spike-like bursts, respectively. AP waveforms used as voltage clamp commands in the HEK-293 cell experiments were provided courtesy of Dr. Yukihiro Nakamura, and were recorded from 7-day-old rat calyx of Held.

DiO and DPA staining

HEK-293 cells on glass coverslips were labeled for 2 minutes by incubation in HEPES-based external solution containing the membrane fluorescent probe DiO, either DiO-C_{18} or DiO-C_{16} (Invitrogen), at a final concentration of 5-10 μM. Cultures of hippocampal neurons were labeled with 4-10 μM DiO_{16}. Increasing the temperature to 37ºC during incubation with DiO_{16} often enhanced labeling. In some sets of cultures (both HEK-293 and hippocampal) bath staining was less reliable. As an alternative, HEK-293 cells or single neurons were labeled by maintaining the cell-attached patch configuration for 15 seconds - 3 minutes with a patch pipette filled with external solution (HEK-293) or internal solution (neurons), to which DiO at a final concentration of 1.8 μM or 5-10 μM, respectively, had been added. Dilutions of DiO were made fresh from a 1.8 mM stock in dimethylformamide (Sigma). Empirically, we found it more efficient to stain with DiO_{16} yet did not observe significantly different response behavior compared to DiO_{18}. We found that cell-attached labeling was quite reliable for staining the soma, proximal axon and dendrites (see Results), particularly when a piece of DiO was visible in the labeling pipette.

DPA (City Chemicals, West Haven, CT, USA) was dissolved to 20 mM in DMSO (Sigma-Aldrich), stored at room temperature, and diluted daily into the external solutions. Superfusion was set to ~1ml/min; optical responses generally could be detected from cultured cells within 3 minutes after switching over to DPA-containing external solution, and became maximal within 10 minutes. For slices, more than 30 minutes of pre-incubation by bath application of DPA was necessary before optical responses showed saturation. For this reason all measurements utilizing DPA in slices

have been made after 45 minutes of pre-incubation and during continuous superfusion by DPA.

Optical recording

An acousto-optical tunable filter (AOTF) was used to control the wavelength (488 nm), amplitude and duration of illumination by laser light produced from an air-cooled krypton-argon laser (Omnichrome). The laser light was coupled into a polarization maintaining optical fiber (Point Source) and delivered to a galvanometer mirror-based scan head (Prairie Technologies Inc.). The laser light was collimated and adjusted to overfill a 60x objective (1.0 NA, Nikon) in order to produce a diffraction-limited spot (full width at half maximum of ~400 nm) in the specimen plane. All optical voltage recordings were made from the illumination spot parked on the plasma membrane guided by a confocal scanned fluorescent image. For cultured cells this was generally in a focal plane several microns above the surface of the coverslip. The fluorescence emission was filtered using a 540/80 nm band pass filter. All the emitted fluorescence was focused onto either a standard side-on multi-alkali photo multiplier tube (PMT; 3896, Hamamatsu) or a gallium arsenide phosphide-based photocathode PMT (GaAsP PMT; H7422P, Hamamatsu; quantum efficiency ~45%) whose current output was passed through a discriminator (C3866, Hamamatsu). For all images and some point recordings, a 60 µm pinhole was inserted in a conjugate image plane using a remotely controlled servo motor. Confocal images of labeled HEK 293 cells were made using the multi-alkali PMT, whereas the GaAsP detector was used for neuronal images. Unless

otherwise stated, spot detection fluorescence recordings were performed without the confocal pinhole in place. Spot detection currents produced by the multi-alkali PMT (used for HEK 293 cells) were directly filtered and acquired as described above. For spot detection measurements in neurons, the voltage output of the discriminator was filtered at 10 kHz using an 8-pole Bessel filter (Frequency Devices) prior to digitization. This discriminator model can typically count linearly up to 4 MHz. However, increases in signal to noise could still be attained by increasing the illumination, and thereby the detected photon flux (range of fluxes were 10-185 MHz). In cases where the photon flux was within this range, signals were corrected for non-linearities (likely due to missed photon counts). This non-linearity was estimated by comparing the output voltage of the discriminator versus the current output of a multi-alkali PMT in response to a range of fluorescence intensities spanning those detected in the experiment. Fluorescence was excited and detected using laser spot illumination of 2 μM fluorescein (Sigma). The relationship was well fit by an exponential function and used to correct (scale) the amplitude of optical responses. Correction factors were typically 1.2 fold (max 1.6 fold). Photon acquisition was performed simultaneously with electrophysiological patch pipette recordings as described above.

Data analysis

Data analysis was performed using the Neuromatic analysis package (www.neuromatic.thinkrandom.com) and custom routines within the Igor Pro environment (Wavemetrics). All values are displayed or expressed ± s.e.m. All

statistical tests were performed using a non-parametric Wilcoxon-Mann-Whitney two sample rank test routine or a Wilcoxon signed-rank test routine for paired comparisons (Igor Pro), unless otherwise indicated. Correlations between data were tested using a Pearson correlation test within Excel software package (Microsoft). Only cells with less than a 15 mV voltage offset resulting from the pipette resistance and the membrane current at the end of the 40 ms voltage pulse were used for analysis of ΔF/F versus voltage plots. Reported membrane voltages were not corrected for liquid junction potential. Fluorescence traces were converted to ΔF/F% by subtracting the baseline fluorescence value, F (obtained by averaging over 5 ms prior to stimulation), from the peak signal value, then dividing by F, and multiplying by 100. For comparison across cell types, values of ΔF/F per 100 mV per AP were calculated by dividing the peak amplitude of fluorescence transients by the ΔV from rest. Of note is that although the holding potentials in current clamp spanned -75 to -55 mV, the DiO/DPA response is linear along this range of voltages (see **Figures IV-1-2**), and therefore such a normalization is valid. For brain slice experiments, the resting fluorescence was adjusted by subtracting the background fluorescence of the slice estimated from a location off the cell but within 10 μm of the recording site. Fluorescence traces were smoothed offline with the binomial smoothing routine such that the final cascaded frequency was 1 to 3.5 kHz. In most cells the fluorescence decayed by ~25% over two components, a rapid (~2 ms) and slow (~20 ms) component. This was corrected for by subtracting a double exponential function to interleaved sweeps without stimuli. For the SNR we measured the variance over a 5-10 ms window just prior to stimulation

from single trial traces that were filtered to a final frequency of 1 kHz for hippocampal responses and 3.5 kHz for Purkinje cell responses. The SNR was calculated from the peak amplitude divided by the square root of that variance. Weighted decays were calculated from the sum of the amplitude weighted time constants. Values for spontaneous firing frequency were obtained from analysis of 30 to 60 second periods of spontaneous firing. Confocal images were analyzed using ImageJ (http://rsbweb.nih.gov/ij).

RESULTS

DiO and DPA function together as a FRET-based voltage sensor

Membrane tethered eGFP (eGFP-F) together with DPA have been shown to function as a voltage-dependent FRET pair in HEK cells, neurons, and muscle fibers (Chanda, Blunck et al. 2005; DiFranco, Capote et al. 2007; Taraska and Zagotta 2007), and controlling the distance between them can regulate the efficiency of energy transfer (Taraska and Zagotta 2007; Sjulson and Miesenbock 2008). We reasoned, therefore, that DiO (a well-established carbocyanine membrane label with a fluorescence emission spectrum very similar to eGFP (Cohen, Salzberg et al. 1974); (Honig and Hume 1986), might act as a higher efficiency substitute for eGFP-F because its location within the lipid bilayer (Axelrod 1979) places it in closer proximity to DPA molecules. In order to test the performance of the DiO/DPA pair, HEK-293 cells were labeled with DiO-C_{18} or DiO-C_{16} by bath application or with a cell-attached patch

electrode (see Methods) resulting in prominent labeling of the plasma membrane as visualized by standard confocal microscopy (**Figure IV-1A**, left and **Figure IV-9**). Isolated, cells were labeled, voltage clamped at -70 mV in whole-cell patch mode, and then exposed to 5 mM DPA. Voltage steps were delivered while monitoring fluorescence from a 'parked' diffraction-limited illumination spot without the use of a confocal pinhole, similar to detection with stage scanning devices (Escobar, Monck et al. 1994; DiGregorio, Peskoff et al. 1999); l = 488 nm, Fig. 1B, top). Upon depolarization, rapid decreases in fluorescence intensity were observed with a relative fractional change (ΔF/F) as large as -64%. The average change was -56 ± 3% ΔF/F per 100 mV (n=6, **Figure IV-1D**, left most bar). Such responses were very stable indicating that phototoxicity was minimal; hundreds of responses could be elicited over several minutes with no apparent decrement in ΔF/F.

For comparison we expressed a farnesylated form of eGFP (eGFP-F) in HEK-293 cells (**Figure IV-1A**, right). As observed previously with this eGFP-F construct, fluorescence appeared on the plasma membrane as well as in intracellular puncta (Chanda, Asamoah et al. 2005). Fluorescence measurements were made using the same spot detection approach, DPA concentration, and voltage clamp stimuli as in the experiments described above with DiO as donor (**Figure IV-1B**, middle). In our hands, the average sensitivity of the eGFP-F/DPA FRET pair was -14 ± 1% ΔF/F per 100mV (n= 7). These values, in line with prior observations (Chanda, Asamoah et al. 2005), are approximately 4-fold smaller than with DiO as donor (**Figure IV-1D**, compare left two bars).

In some systems the increased capacitive load caused by 5 mM DPA might lead to distortion/prevention of regenerative APs (Fernandez, Taylor et al. 1983; Chanda, Asamoah et al. 2005; DiFranco, Capote et al. 2007; Sjulson and Miesenbock 2008). With this in mind we assayed changes in donor fluorescence at 1 μM DPA. Notably, at 1 μM DPA the DiO/DPA pair still reported a larger signal than did eGFP-F / 5 mM DPA (DiO, -22 ± 2% DF/F per 100 mV, n=6; eGFP-F, -14 ± 1% per 100mV, n=7, $p<0.002$; **Figure IV-1D**). Indeed, the performance of the DiO/DPA pair places it among the largest signals of any rapid optical voltage reporter.

In response to large, sustained, depolarizing voltage steps the initial rapid quenching response was followed by a slower increase in fluorescence, hereafter referred to as a relaxation. Although apparent with eGFP-F/DPA, these voltage-dependent relaxations were more prominent with DiO/DPA, and measures of pre-steady state dynamics in 1 and 5 mM DPA showed no differences indicating these voltage-dependent behaviors appear to be independent of DPA concentration (**Figure IV-1B**, top and bottom panels, **Figure IV-2A-C**). We quantified this behavior by measuring ΔF/F at the end of the 40 ms pulse and found that relaxations appear when the membrane potential is depolarized from -70 to potentials greater than 0 mV, such that at +85 mV only 20% of the initial quenched signal remained (**Figure IV-2A-C**, cyan). In responses where a relaxation was evident during the sustained, 40 ms depolarization, an overshoot, or rebound in fluorescence after termination of the voltage stimulus was also present. Additional experiments (**Figure IV-10**) are directed at better understanding the mechanism underlying the slow relaxation and overshoot, which

have been observed in other systems when two dye components are mobile (Chanda, Asamoah et al. 2005). These experiments, as well as those shown below, suggest that under physiological conditions the slower mechanism would make a minimal contribution to signals because of the brevity and limited positive voltages attained by typical action potentials (delimited by the grey areas of the panels in **Figure IV-2**). Taken together, these data indicate that the DiO/DPA FRET pair can report rapid voltage changes over a wide dynamic range from –125 mV to +40 mV, with a maximum ΔF/F per 100 mV of nearly -60%.

DiO/DPA FRET pair reports sub-millisecond voltage changes

To assess whether the DiO/DPA FRET pair would be suitable for detection of AP-like signals, we determined the speed of fluorescence changes in response to voltage steps from -70 mV to +30 mV and ranging from 0.1 to 5 ms in duration (**Figure IV-3A**). A single exponential fit of the onset of the fluorescence-quenching resulted in a time constant of 0.12 ms. A series of similar experiments indicated that the quenching speeds could vary widely, but that this variability strongly correlated with the voltage clamp speed and was independent of the donor (DiO or eGFP-F) or DPA concentration (**Figure IV-3B**). The fastest fluorescence time constants were ~0.12 ms (**Figure IV-3B**). Although this is slightly faster than previous estimates with DPA and membrane tethered fluorescent proteins (~0.5 ms, see Chanda et al., 2005; DiFranco et. al., 2007), it is comparable to the speed of DPA movement in other preparations (~ 0.1 ms, see (Fernandez, Taylor et al. 1983; Lu, Kabakov et al. 1995).

The decay of the fluorescence (weighted τ) following brief pulses was also fast and increased slightly with longer pulses from 0.30 ± 0.08 to 0.48 ± 0.08 ms (n=5), for 0.3 and 5 ms duration pulses, respectively (**Figure IV-3A**). Also associated with the slowing in the decay was the appearance of small rebound fluorescence (0.7 ± 0.2% ΔF/F for the 5 ms pulses) compared with the maximal drop in fluorescence during the depolarization (-24 ± 0.2% ΔF/F; n=4). Thus, the DiO/DPA FRET pair can faithfully report brief depolarizations, similar in duration to neuronal APs, with little temporal distortion.

Since many neurons fire in short bursts of APs at frequencies of hundreds of Hz, we examined the accuracy with which the DiO/DPA FRET pair could report brief trains of voltage steps delivered at different frequencies. In response to a 100 Hz train of 1 ms pulses, the amplitude of the 10^{th} pulse decreased by approximately 10% compared to the amplitude of the first (**Figure IV-3C**; 7 ± 2% reduction; n=12). Decreases were slightly larger for frequencies of 300 and 600 Hz (16 ± 8 and 18 ± 2% reductions, respectively; n=3). For 1000 Hz, the duration of the pulse was reduced to 0.5 ms and the decrement in the response by the 10^{th} pulse (7 ± 2%; n=3) was less pronounced than at 600 Hz. Also apparent was a progressive increase in the rebound fluorescence following the termination of the higher frequency trains (**Figure IV-3C**), similar to that observed for long step durations in **Figure IV-1**. However, for all pulse frequencies the relative amplitude of this rebound was less than 10% of the peak amplitude. Together, these data indicate that the DiO/DPA FRET pair is suitable for tracking single APs and bursts of APs with little temporal distortion.

DiO/DPA FRET pair detects AP-like voltage waveforms in single sweeps

To test whether the DiO/DPA FRET pair can be used to detect individual AP-like signals in single sweeps, we applied an AP waveform as a voltage-clamp command to DiO-C_{16}-labeled HEK-293 cells in the presence of 1 μM DPA. In **Figure IV-4A**, the command voltage is superimposed on an inverted, signal-averaged optical response. Consistent with the 1 ms step pulses (**Figure IV-3**), responses to AP-like waveforms were large (-25 ± 3%; n=4 cells) and faithfully reported the time course of the command voltage. Trains of AP waveforms (**Figure IV-4B**) elicited brief quenching responses that could easily be detected in single sweeps (**Figure IV-4C**, left), with a signal to noise ratio (SNR) of 7.1 (average across cells 6.1 ± 1.7, n=4). Signal-averaged responses (**Figure IV-4C**, right) showed little decrement in the peak amplitude of the optical response to the 5^{th} AP in comparison to the first (average ratio 1.0 ± 0.03; n=5 cells, $p > 0.5$). By comparison, the eGFP-F/DPA FRET pair gave rise to signals that were ~4-fold smaller given identical stimuli and DPA concentration (**Figure IV-4D**), making it difficult to detect AP-induced fluorescence changes in single trials under these conditions (SNR 3.9).

DiO/DPA FRET pair reports neuronal APs and subthreshold signals from cultured neurons

A critical test of the DiO/DPA FRET pair is detection of APs in excitable cells. Previous studies in cultured neurons (Chanda, Asamoah et al. 2005) or skeletal muscle

fibers (DiFranco, Capote et al. 2007) have shown that DPA concentrations between 5 and 20 μM induce a capacitive load on cell membranes reducing the AP peak amplitude and increasing the AP width. We assayed the effects of 1 μM DPA using current-clamp recordings of cultured hippocampal neurons (**Figure IV-5A**). By comparing recordings in the absence (n=12 cells) or preincubated for >10 min in the presence (n=10 cells) of 1 μM DPA, we found no difference in AP width ($p=0.2$) or AP height ($p>0.5$) when the resting membrane potentials were similar ($p>0.5$). These data indicate that 1 μM DPA would be a suitable concentration to report regenerative APs in this preparation.

Hippocampal neurons were labeled with DiO-C_{16} by either bath or pipette methods. Whole-cell current clamp recordings were used to deliver brief current injections to initiate APs in the presence of 1 μM DPA. In the cell shown in **Figure IV-5B** at 7 minutes after DPA application, a 100 Hz train of APs elicited transient decreases in fluorescence with peak amplitudes of -16% ΔF/F (**Figure IV-5B**, traces have been inverted). In this particular cell the holding potential varied slightly from trial to trial such that in 6 out of the 18 trials there was a failure of AP generation in response to the first current pulse (**Figure IV-5B**, middle panel, red). As indicated in the electrical recordings, APs elicited from the more hyperpolarized resting potential were slightly faster than at the depolarized resting potential (**Figure IV-5B**, middle panel, compare red with blue traces). Notably, this slight difference in AP duration was also apparent in the optical recording (**Figure IV-5B**, lower panel, red and blue traces). Indeed, the DiO/DPA fluorescence transients faithfully followed the time course of the electrical membrane potential recording (half-width of membrane potential signals, 2.1 ± 0.7 ms;

half-width of fluorescence signals, 2.2 ± 0.9; paired test, p=0.6). In addition, the SNR of the DiO/DPA FRET signals were large enough so that even subthreshold depolarizations were detected in those sweeps where the first AP failed to be evoked (**Figure IV-5B**, red). Analysis of AP-elicited DiO/DPA FRET signals indicated an average ΔF/F per 100 mV of -24 ± 2% (n=7 cells), greater than a 6-fold improvement over eGFP-F/DPA FRET (Chanda, Asamoah et al. 2005). These results demonstrate that the DiO/DPA voltage sensor yields large and rapid fluorescence changes at concentrations of DPA that have negligible effects on AP shape, allowing high fidelity optical detection of either APs or subthreshold activity.

Another critical test for the DiO/DPA FRET pair is detection of AP signals in single sweeps. The neuronal fluorescence responses shown in **Figure IV-5C** show clearly discernable responses in single trials that, with a peak ΔF/F of -13% and a detected 'resting' photon flux (a critical determinant of SNR (Sjulson and Miesenbock 2007) prior to AP stimulation of 29 MHz, produced a signal to noise ratio of 6.1. The average SNR across cells was 7.2 ± 0.7 (n=7; 29 ± 3. MHz resting photon flux). When using a confocal pinhole, the SNR was reduced to 2.9 ± 1.0 (n=3; 2.6 ± 1.1 MHz resting photon flux) yet the mean signal size improved to -34 ± 3% ΔF/F/100 mV. Signal averaged responses with the DiO/DPA FRET pair (**Figure IV-5C**, lower black trace) showed that the peak amplitude of the fluorescence transients generated by APs were well maintained throughout trains, indicating that in cultured hippocampal neurons, APs can be monitored optically with high fidelity. This, combined with high sensitivity, makes the DiO/DPA voltage reporter amenable to use with other rapid optical detection

devices, such as photodiode arrays and fast CCD cameras (Baker, Kosmidis et al. 2005), which enable rapid multi-site or multi-neuron imaging of network activity (Obaid, Loew et al. 2004).

DiO/DPA FRET pair reports evoked neuronal activity in brain slices

To examine the performance of the DiO/DPA FRET pair *in situ*, Purkinje neurons within a brain slice were labeled with DiO-C_{16} using a cell-attached configuration (**Figure IV-9**). Prior to labeling, slices were pre-incubated in DPA for greater than 45 minutes to ensure the DPA concentration was at equilibrium; DPA was subsequently continuously superfused for the remainder of each experiment. Up to 90% of Purkinje neurons were successfully labeled (i.e. produced preferential membrane labeling) with DiO_{16} if the labeling solution was made < 30 minutes before patching. Preferential membrane staining of the soma, proximal dendrite, and proximal axon was observed within minutes following establishment of a seal with the membrane (see **Figure IV-6B**). After longer periods (~15 min), the staining of spine-like structures could also be observed (data not shown). The cell body, however, progressively lost its membrane staining over tens of minutes after the dye-filled pipette was removed (compare **Figure IV-6B** to image in **Figure IV-6C**). Following staining, a second, dye-free pipette was introduced to obtain a whole-cell recording and to enable simultaneous electrical and optical recordings. The whole cell recording configuration also permitted spontaneous spiking activity to be silenced by slight hyperpolarization of the membrane potential, and injection of brief current pulses from hyperpolarized resting potentials to induce

well timed APs. Under these conditions, and with the illumination spot positioned on the soma membrane, transient decreases in fluorescence were observed in response to single APs in single trials (1 mM DPA, **Figure IV-6C**).

As was the case for the HEK-293 cells, many sweeps could be delivered without noticeable photodamage (up to 100, with < 5s intervals): the electrophysiological parameters remained stable following illumination and there was no evidence of membrane blebbing, significant increase in baseline fluorescence, or decrement in consecutive fluorescence responses. In the cell displayed in **Figure IV-6C**, peak amplitudes and widths of DiO/DPA optical responses were stable over the 20 APs delivered at 5s intervals (**Figure IV-6C**, inset). Note that because of the interleaved trials without AP stimuli, the total number of illumination trials was double that indicated in the **Figure IV-6C** inset. On average DiO/DPA responses to single APs could be stable for >30 min. It is also important to note that of the 90% of neurons showing prominent membrane labeling, all of them produced detectable (>5% ΔF/F) optical responses to APs.

The SNR of the single AP responses (given the peak DF/F of -13% and a resting photon flux of 69 MHz) was 5.0. In another cell, the peak DF/F was -19% and the resting photon flux was 183 MHz yielding a larger SNR of 11.4 (2 mM DPA, **Figure IV-6D**). On average, the peak amplitude of the fluorescence transients in response to single APs recorded with the spot positioned on somatic membrane was -12 ± 1% ΔF/F for 1 mM DPA (n=5), which was significantly different from experiments performed in 2 mM DPA (-19 ± 2% DF/F, n=5; p=0.05). This corresponds to a -19 ± 3 % ΔF/F per

100 mV for 1 mM DPA and 26% ± 2 % per 100 mV for 2 mM DPA (p=0.04). The average SNR of single trial AP-associated somatic transients was 4.6 ± 1.2 (70 ± 21 MHz count rate) and 6.8 ± 1.4 (70 ± 29 MHz count rate) for 1 and 2 mM DPA respectively.

In addition to firing classical APs (often referred to as "simple spikes"), Purkinje neurons also fire "complex spikes," a characteristic discharge in response to strong depolarization by climbing fiber synaptic inputs (Eccles et al., 1966). Somatic injection of current can elicit complex spike-like responses which are remarkably similar to climbing-fiber evoked complex spikes. Both complex spikes and complex spike-like responses are characterized by high frequency bursts of decrementing spikelets (Eccles, Llinas et al. 1966; Llinas and Sugimori 1980; Khaliq and Raman 2005; Davie, Clark et al. 2008). **Figure IV-6E** and **Figure IV-8A** show examples of single complex spike-like responses elicited by current injections similar in total charge to those found to best reproduce true complex spikes (Davie, Clark et al. 2008). As discussed in detail below, our data show that the number and timing of the spikelets in the electrical signal (red traces in **Figure IV-6E** and **Figure IV-8A**) were faithfully represented in the optical signals (black traces in **Figure IV-6E** and **Figure IV-8A**) in all recorded Purkinje neurons (n=3). The signal to noise ratio of the DiO/DPA FRET pair was sufficiently large that fluorescence responses to single APs as well as high frequency bursts could be well resolved in single trials.

Examination of Purkinje neuron firing properties in the presence of DPA

To evaluate whether the membrane capacitance added by these concentrations of DPA depresses neuronal activity in slices, we made a series of measurements from Purkinje neurons pre-incubated in DPA for at least 45 min before recording. We compared single APs recorded in current clamp under control conditions and in 1, 2 or 5 mM DPA and found that DPA concentrations up to 5 mM led to no significant differences in AP amplitude or spike threshold. However, 5 mM DPA led to a moderate, yet significant broadening of the AP from 431 ms to 637 ms (**Figure IV-7A-B** and **Figure IV-11**).

Interestingly, DPA-treated Purkinje neurons did not require larger current injections to elicit a spike within the 2 ms duration current injection window. We found that the minimal amount of current required to elicit a spike within ~1.4 ms was the same as for control at all DPA concentrations (**Figure IV-11**). Notably, these current injections are well within the range of stimuli used in previous studies to elicit well-timed spikes in large neurons (Kole and Stuart, 2008, Zhou et al., 2008).

Analyses of complex-spike like responses elicited by longer duration current injections yielded complementary results in that 1 and 2 mM concentrations of DPA had little effect on excitability. No significant differences as compared to control were observed in the numbers of spikelets per burst or spikelet frequency within a burst (**Figure IV-11**). However, just as for the single AP responses, 5 mM DPA led to a reduction in the number of spikelets and their instantaneous frequency (**Figure IV-7C** and **Figure IV-11**). Thus, in cerebellar slices, concentrations of 1-2 mM DPA do not

interfere in significant ways with the endogenous generation of APs or complex spike-like responses.

Finally, we exploited the fact that Purkinje neurons engage in spontaneous pacemaking activity in brain slice preparations (Dailey, Buchanan et al. 1994; Hausser and Clark 1997) in order to examine the effects of DPA on spontaneous excitability in a minimally invasive manner. Extracellular recordings from individual Purkinje neurons in control versus 1, 2, or 5 mM DPA show that spontaneous spiking is maintained in the presence of DPA (**Figure IV-7D**). Even at 5 mM, the highest DPA concentration tested, there is only a non-significant trend towards a reduced average firing rate (no difference between any groups, one way ANOVA, $p=0.64$). The cumulative plots indicate that there was also no significant difference in the distribution of firing frequencies across cells in any DPA concentration when compared to control (**Figure IV-7E**; $p> 0.05$, Kolmogorov-Smirnov test). Taken together, these data suggest that DPA concentrations necessary for high fidelity optical detection minimally perturb neuronal electrical properties. Beyond our own work these observations also suggest that DPA-based optical reporters may be useful over a much broader range than previously suggested from experiments in *Drosophila* (Sjulson and Miesenbock 2008).

DiO/DPA voltage signals in neuronal subcompartments

Taking advantage of the high spatial resolution, we positioned the diffraction-limited illumination spot (~ 400 nm) on different cellular compartments, and obtained AP or complex spike-like optical signals from somata, dendrites (> 10 mm from somata),

and axons (> 5 mm from somata) of the same Purkinje neuron (**Figure IV-8**; same cell as shown in **Figure IV-6D**). When comparing complex spikes measured in the soma vs. those measured in the dendrite, the amplitudes were smaller in the dendrite with a prominent slow charging component (**Figure IV-8A**), consistent with the lack of invasion of fast spikes into the dendrite (Davie et al., 2008). The largest signals were observed in the axonal compartments (**Figure IV-8B**). Although we have not explored this further, non-homogeneity in intracellular labeling or the relative surface to volume differences between these compartments could be contributing factors. When the optical signals were aligned on the basis of the electrical AP signal (**Figure IV-8B**, lower right) it was clear that the AP in the axon preceded APs in the soma and dendrites by 100 ± 30 ms, (n=4). Moreover, the width of the optical AP signal in the axon was significantly greater than the width of signals recorded either from the somata or the electrically recorded AP (axon, 580 ± 60 ms, n=4; soma, 400 ± 20 ms, n=10; electrical signal, 455 ± 20 ms, n=10; $p<0.05$). These observations are in line with prior electrical measurements in Purkinje neurons, and are consistent with the suggestion that AP initiation occurs in the axon (Stuart and Hausser 1994). Interestingly, there was also a significant difference between the width of DiO/DPA fluorescence responses to an AP and the width of the corresponding electrically recorded AP (above values, $p=0.01$). This is consistent with the electrode-based measurement being influenced by larger membrane regions than the diffraction-limited spot optical measurement (Bean 2007). The use of a diffraction limited spot to optically

monitor membrane potential therefore provides a more localized measurement of electrical signals than can be achieved with electrode-based methods.

DISCUSSION

We describe a novel, FRET-based approach for optical detection of changes in membrane potential. The method relies on energy transfer from a membrane dye (DiO) and a lipophilic anion (DPA) whose membrane partitioning is voltage sensitive. Ironically, DiO was originally synthesized as a potential voltage-sensitive dye, but exhibited no signal (Cohen, Salzberg et al. 1974), and has since been used extensively for neuroanatomical tracing. In comparison to other available methods several features of this approach are worth noting. First, DiO/DPA rapidly reports changes in membrane potential ($\tau \sim 120$ μs); second, it shows a high sensitivity over the physiological range of membrane voltage within neurons in culture and in brain slices (-17 to -40% $\Delta F/F$ per 100 mV for APs); third, there is no apparent phototoxicity; and fourth, DiO has favorable chemical properties (bright signal, rapid dispersion within biological membranes, and negligible fluorescence in aqueous solution). We demonstrate that these properties, combined with laser-illuminated spot detection, represent a very effective method for optical detection of membrane potential from single neurons and/or small neuronal compartments. These same features make the DiO/DPA FRET an

attractive methodology for high throughput screening assays for compounds that give rise to depolarizing or hyperpolarizing changes in membrane potential.

Comparison with existing voltage sensors

The large ΔF/F response to voltage (-56% per 100mV using 5 μM DPA) is, to our knowledge, the largest reported signal for such a rapid, single photon-activated, fluorescent reporter. The improvement over eGFP-F/DPA may in part be due to a closer proximity of the DiO chromophore to DPA within the plasma membrane. Additional factors, such as a more favorable dipole orientation or a larger quantum yield, may also contribute. Comparison with existing voltage sensor dyes shows that only the dyes annine-6 and annine-6plus yield larger signals, up to 70% ΔF/F per 100mV for two-photon excitation (Kuhn, Fromherz et al. 2004; Fromherz, Hubener et al. 2007). These compounds, however, require relatively large illumination intensities that may result in neuronal damage upon repeated measurement and their narrow emission bands limit SNR (Fromherz, Hubener et al. 2007). Among the dyes used to measure APs within neurons, di-3-ANNEPDHQ produces ~8% ΔF/F per 100 mV in response to an AP using two-photon excitation (Fisher, Barchi et al. 2008), while FM-4-64 has been reported to produce AP-induced fluorescence changes of ~8% ΔF/F per 100mV in cultured cells and brain slices using second harmonic generation (Dombeck, Sacconi et al. 2005). In the latter case, low photon fluxes limit the SNR to less than 2 for single sweeps (Dombeck, Blanchard-Desce et al. 2004; Dombeck, Sacconi et al. 2005). By comparison, in response to evoked APs in hippocampal neurons, the DiO/DPA FRET pair produces -34%

ΔF/F per 100 mV with a SNR of ~3 under confocal detection and -26 ± 3% ΔF/F per 100 mV with a SNR of ~7 in non-confocal mode. In brain slices the sensitivity was slightly reduced to -19 ± 3% ΔF/F per 100 mV (1 mM DPA) and -26 ± 2% (2 mM) with a combined average SNR of ~6. While all of these dyes have not been compared on the same preparation with identical methods, a comparison in similar experimental contexts (axonal measurement of APs in brain slices) shows slightly higher SNR and larger peak signals for DiO/DPA as compared to di-3-ANNEPDHQ (10 vs. 39% ΔF/F without the pinhole, compare **Figure IV-8B**, blue trace with Fisher et. al., 2008). While we have not yet tested whether the DiO/DPA FRET pair will produce signals with a similar sensitivity using 2-photon excitation, DiO is readily excited in two-photon mode (Majewska, Yiu et al. 2000). Two-photon excitation would not only allow for deep tissue imaging but would permit the use of new random access acousto-optic deflector-based scanning devices (Duemani Reddy, Kelleher et al. 2008; Otsu, Bormuth et al. 2008), which are ideally suited for rapid monitoring of single neurons or network activity in 3 dimensional space.

Another class of recently described synthetic dye compounds has been used to monitor AP propagation in pyramidal cell dendrites and axons (Antic 2003; Palmer and Stuart 2006; Zhou, Yan et al. 2007; Zhou, Yan et al. 2008). The largest signals reported by these dyes have been ~12% DF/F (i.e., the JPW 4090 dye, Zhou et. al., 2007). However, all DiO/DPA data reported here have been collected with diffraction-limited spot illumination and SNRs have been calculated from single trials, whereas other investigators calculated peak DF/F and SNR values from spatially (15-20 mm) and

temporally averaged traces. Interestingly, Zhou and colleagues (2007) have noted decreased photodamage when using spot laser illumination in comparison to whole cell illumination; this would also be the case for the submicron detection volumes used here.

Regarding speed of response, DPA serves as an extremely rapid voltage sensor in a FRET based system, yet it is likely slower than the microsecond response times of the commonly used synthetic dyes such as merocyanines (Salzberg, Obaid et al. 1993) or styryl dyes (Rohr and Salzberg 1994). It should also be noted that conventional voltage sensitive dyes tend to be linear reporters of membrane voltage, without any visible hysteresis (Cohen and Salzberg 1978).

Although genetically-encoded voltage sensors are extremely desirable, proteins engineered to report voltage have significant shortcomings as compared to synthetic dyes. These include relatively small ΔF/F (Sjulson and Miesenbock 2007), kinetics much slower than single APs (Sjulson and Miesenbock 2007; Tsutsui, Karasawa et al. 2008), limited dynamic range (Blunck, Chanda et al. 2005), and intracellular targeting defects resulting in poor or mislocalized expression (Baker, Lee et al. 2007). "Hybrid" voltage sensor methods, that is those that make use of a fluorescent protein combined with DPA (Chanda, Blunck et al. 2005; DiFranco, Capote et al. 2007; Sjulson and Miesenbock 2008), show excellent promise due to the combination of high membrane specificity, extremely rapid kinetics ($t < 0.5$ ms) and low phototoxicity (Sjulson and Miesenbock 2007). Improvements to the hybrid voltage sensor method have already been demonstrated by shortening the stretch of amino acids tethering the fluorescent protein to the membrane (Sjulson and Miesenbock 2008) and by changing the donor from

green to cyan fluorescent protein, which increases the spectral overlap with DPA (DiFranco, Capote et al. 2007). To date, however, AP-elicited signals have been reported only for cultured neurons (-4% ΔF/F per 100 mV using eGFP-F and 3 mM DPA, Chanda et al., 2005) and muscle cells (~7% ΔF/F per 100 mV using eCFP-F and 5 mM DPA, DiFranco et al., 2007). Attempts to make optical recordings of APs from single neurons *in situ* in *Drosophila* have been unsuccessful (Sjulson and Miesenbock 2008).

Effects of DPA on neuronal excitability

One potential shortcoming of DPA-based methods, and for that matter any method relying on a mobile voltage sensing element located in the transmembrane electric field, arises due to the added electrical capacitance. The measurements of single AP and AP burst parameters as well as spontaneous spiking activity in the present work demonstrate that there is very little effect of 1-2 mM DPA on regenerative excitability in primary neuronal cultures and Purkinje cells in cerebellar slices. These conclusions are in general agreement with prior work. Both the voltage range over which DPA moves, as well as the fractional increase in capacitance within this voltage range, have been well documented in various systems in the presence of low micromolar concentrations of DPA (Fernandez, Taylor et al. 1983; Oberhauser and Fernandez 1995; Chanda, Asamoah et al. 2005; DiFranco, Capote et al. 2007; Sjulson and Miesenbock 2008). At concentrations of 5-10 mM, DPA depresses regenerative excitability in most cells, as reflected by AP slowing and reductions in peak amplitude (Fernandez, Taylor et al. 1983; Chanda, Asamoah et al. 2005; DiFranco, Capote et al.

2007). In contrast, a recent study concluded that DPA concentrations of 2 mM severely depress axonal excitability in a *Drosophila* antennal lobe preparation (Sjulson and Miesenbock 2008). However, to assay excitability this study relied on a synaptophluorin reporter construct to report exocytosis. Given that DPA might quench synaptophluorin fluorescence, this reduction may not result from DPA depressing excitability. Other possibilities to explain these discrepant results are that Drosophila neurons are more sensitive to added capacitance by DPA, or exhibit specific pharmacological sensitivity to DPA (Sjulson and Miesenbock 2008). Nevertheless, the concentrations of DPA attained in brain slices were sufficient to observe large DiO/DPA FRET responses provided the bath concentration was 2 mM or less. The lack of change in the AP shape also suggests that AP propagation may remain intact since changes in the rate of rise of the AP determine the speed of propagation, as observed for 10 mM DPA (Fernandez, Taylor et al. 1983; Chanda, Asamoah et al. 2005; DiFranco, Capote et al. 2007).

In any event, our observations regarding the limited effects of low micromolar concentrations of DPA on excitability of Purkinje cells in cerebellar slices are encouraging for any DPA-based voltage sensing methods. Although the effects of DPA on each preparation will have to be determined, DPA-based approaches do have an additional advantage over, for example, most transmembrane protein-based sensors in that the capacitive load for a given DPA concentration should be spatially uniform and can be accurately measured (Fernandez, Taylor et al. 1983; Chanda, Asamoah et al. 2005; DiFranco, Capote et al. 2007). Standard computational methods will then prove useful for predicting effects on excitability.

Unique advantages for DiO/DPA as a voltage sensor

In addition to rapid responsiveness and large sensitivity, the DiO/DPA FRET pair has other unique properties. First, depolarization causes decreases in fluorescence from a large resting fluorescence, which is important because in most imaging systems optical signal detection is dependent on the base-line photon flux (Sjulson and Miesenbock 2007). Second, the brightness of DiO permits detection of rapid changes in membrane potential from subcellular compartments using spot (versus scanning or full field) illumination methods, reducing the excitation load per cell, thereby lowering phototoxicity. Finally, a number of different DiO labeling methods exist, which yield rapid diffusion of DiO in plasma membranes within tens of minutes. Although in certain contexts it is challenging to obtain labeling confined to surface membranes (see Methods), prior studies have used ballistic methods (Gan, Grutzendler et al. 2000; O'Brien and Lummis 2006) or protocols resulting in anterograde and retrograde staining of specific groups of neurons (Lichtman and Fraser 2001; Ratzliff, Howard et al. 2004). Notably, these methods do not perturb neuronal function and in fact have enabled time-lapse microscopy of living neurons over extended time periods (Lichtman and Fraser 2001). Thus, the DiO/DPA FRET pair may serve as an attractive non-genetic approach to sparsely label operationally defined groups of neurons within tissue and may prove useful in the study of neuronal networks in genetically-intractable contexts such as primates (Luo, Callaway et al. 2008).

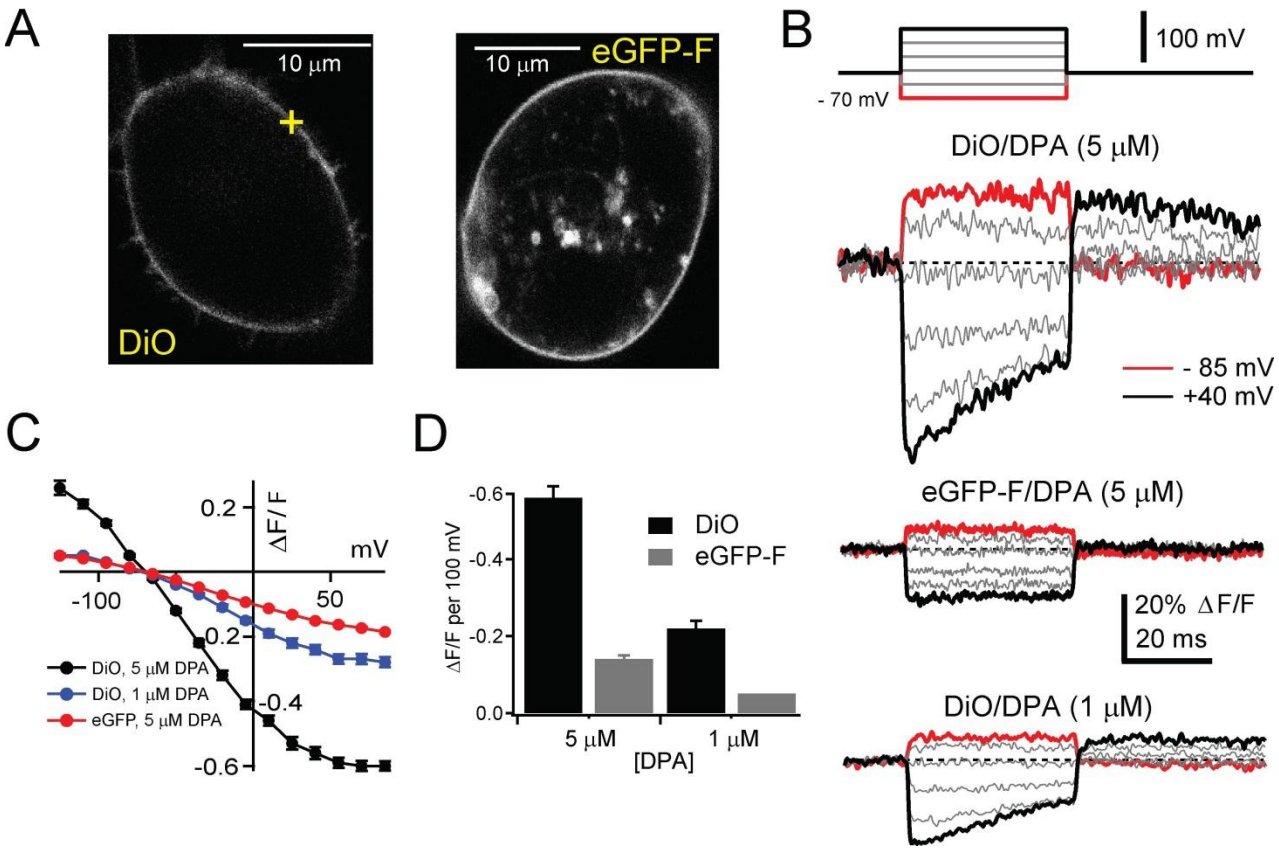

Figure IV-1. Fluorescence changes of DiO/DPA and eGFP/DPA FRET pairs in response to voltage steps. A) Confocal images of a HEK-293 cell labeled by incubation with DiO-C_{18} (left), and a HEK-293 cell transiently expressing eGFP-F (right). Yellow cross is an example of a typical spot detection site. B) Fluorescence signals in response to voltage steps (indicated above) from cells in whole-cell patch-clamp mode either labeled with DiO-C_{18} (upper), eGFP-F (middle), and DiO-C_{16} (lower), and superfused with an extracellular solution containing 5 μM DPA (upper and middle), or 1 μM DPA (lower). All traces are averages of 5 sweeps. Dotted line indicates zero change in fluorescence. C) Summary plots of peak amplitude fluorescence changes within 2 ms of the start of the voltage step. D) Summary bar graph showing average maximal ΔF/F for a 100 mV step from a holding potential (hp) of -70 mV. DiO labeled cells, black bars; 5 μM DPA, n=6; 1 μM DPA, n=7. eGFP-F cells, grey bars; 5 μM DPA, n=5; 1 μM DPA, n=2.

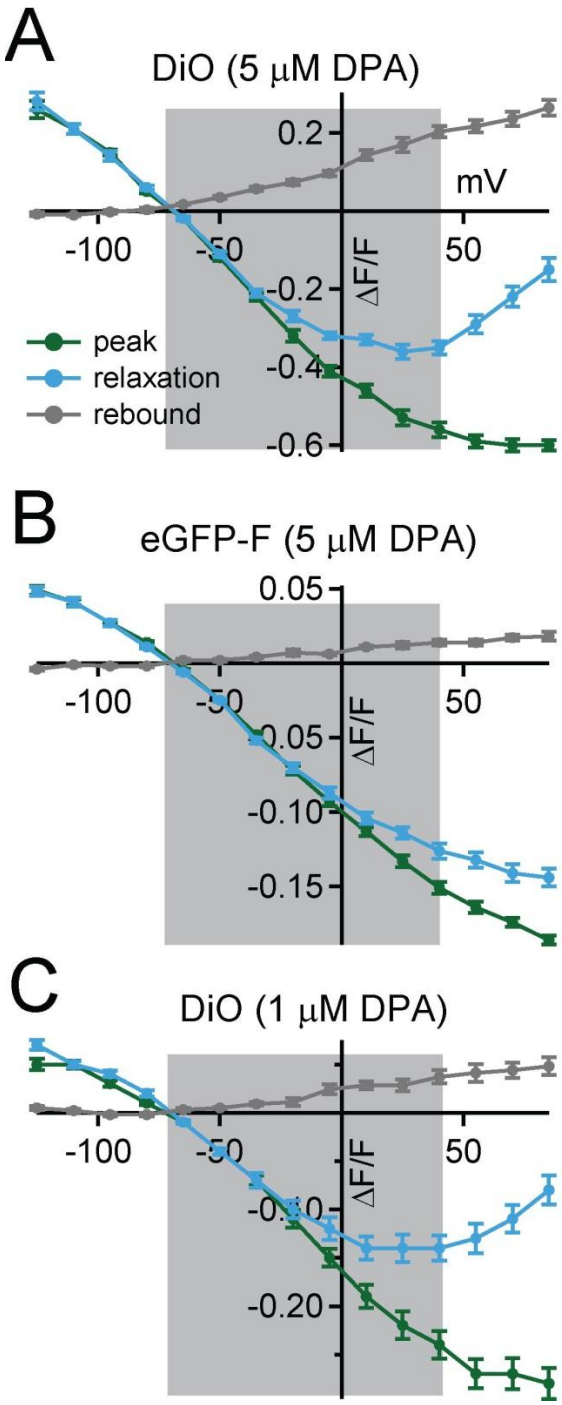

Figure IV-2. Quantification of voltage dependent relaxation and rebound under sustained voltage steps. Summary plots of fluorescence amplitudes measured at 3 time points in **Figure IV-1B**: the initial peak signal within 2 ms of voltage step (green), relaxation at the end of the voltage step (cyan), and rebound just following repolarization of the membrane (grey). Shaded grey area indicates the physiological voltage range from -70 mV to +40 mV.

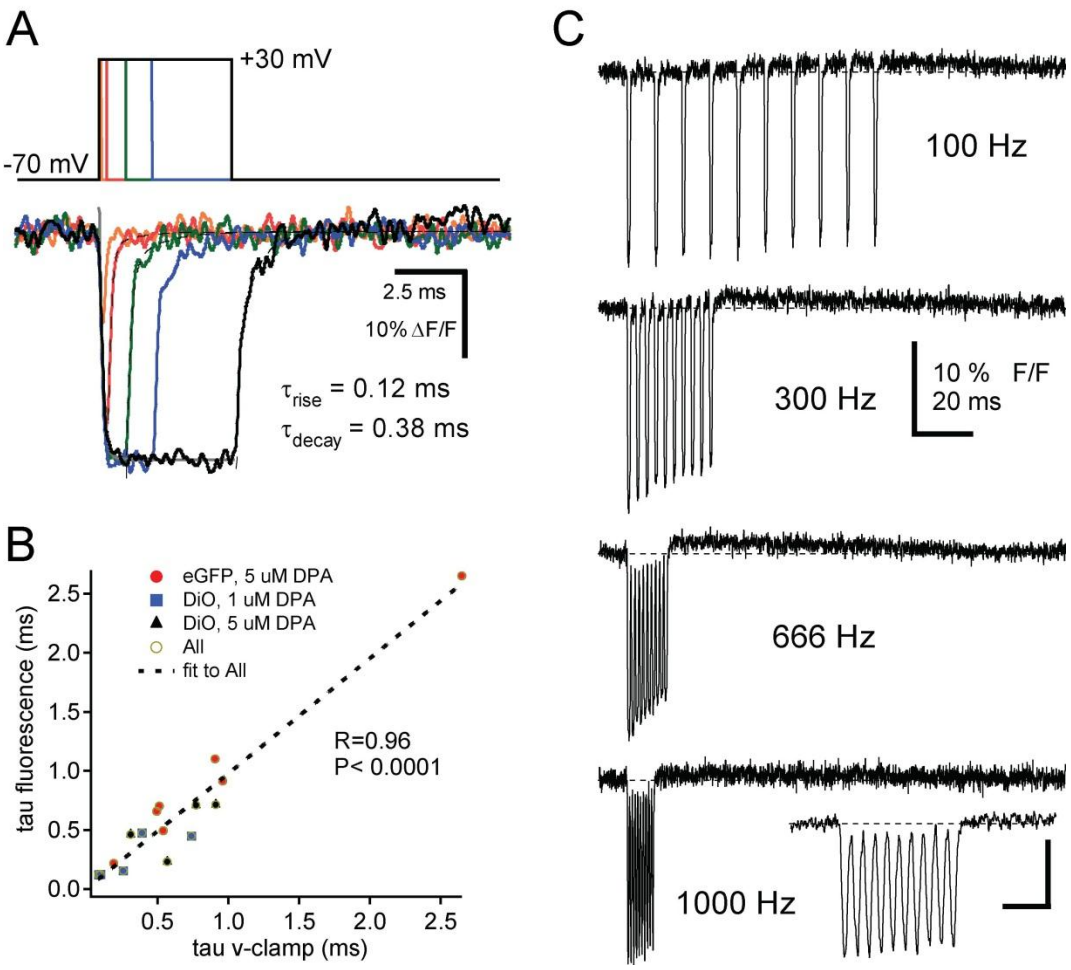

Figure IV-3. Temporal fidelity of DiO-DPA FRET pair. A) Fluorescence quenching responses to brief depolarizations from a HEK-293 cell bath labeled with DiO and incubated with 1 μM DPA. Membrane potential was stepped to +100 mV from a hp of -70 mV for durations of 0.1, 0.3, 1, 2, and 5 ms, yielding peak ΔF/F amplitudes of -14, -25, -28, -28, and -29%, respectively. Grey trace (‥rise) is a single exponential fit to the initial quenching response of the 5 ms pulse. Black dashed traces (‥decay) are double exponential fits of 0.17, 0.29, and 0.38 to the recovery of the quenched fluorescence response following termination of the 0.3, 1, and 5 ms step pulses, respectively. Each trace is an average of 10 sweeps and was filtered offline to 2 kHz. B) Correlation plot of the ‥rise of fluorescence (+100 mV pulse for 5 ms) vs. the weighted time constant of a double exponential fit of the capacitance transients in response to a 5 mV step. Dashed line is a linear fit to all the data (Pearson correlation). The y-intercept is 0.12 ms and approximates the intrinsic time constant of the voltage dependent quenching of the DiO fluorescence. C) Fluorescence quenching responses to trains of 1ms, 100 mV depolarizations (hp = -70 mV) delivered at various frequencies (1000 Hz stimuli used 0.5 ms pulses). Traces were filtered offline to 3.5 kHz, and are averages of 10 and 15, trials for the 100 Hz and 300 Hz trains, respectively, and 17 trials for both 666 and 1000 Hz. DPA concentration was 1 μM.

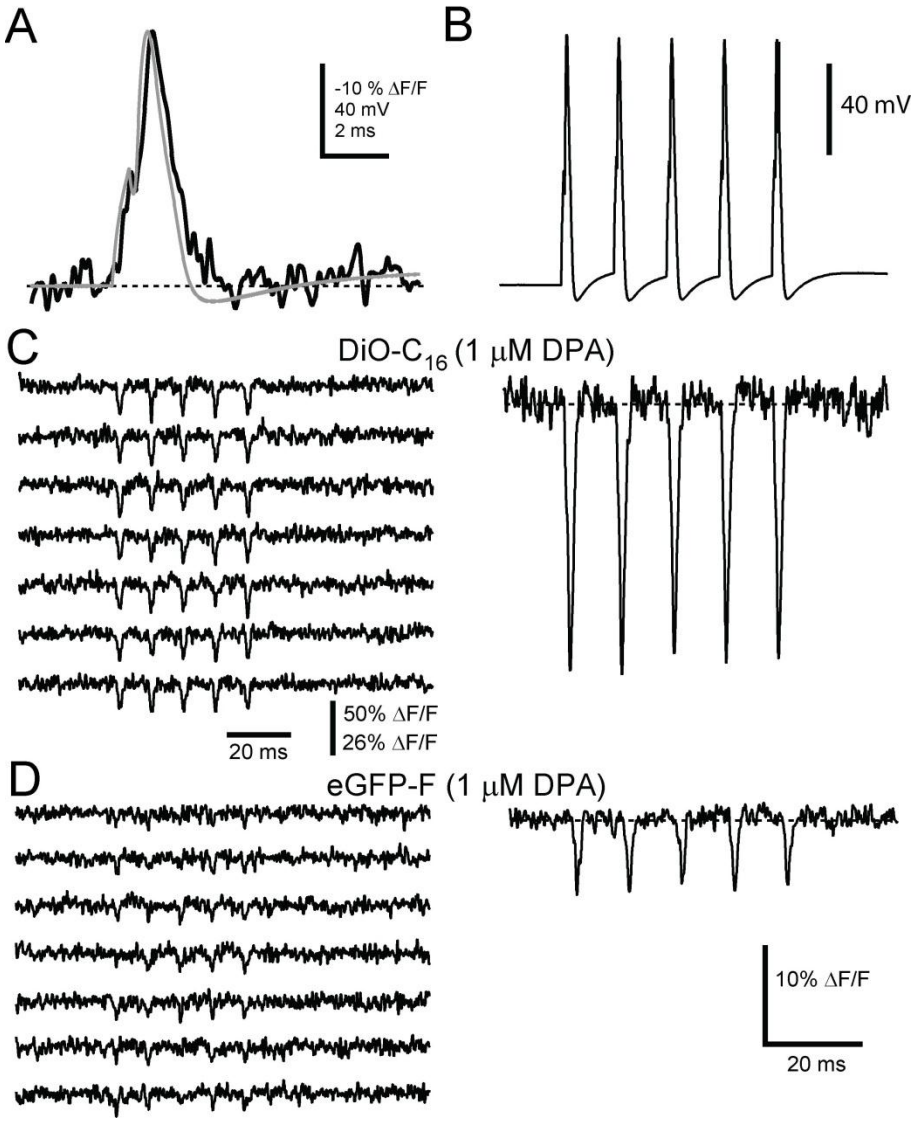

Figure IV-4. Optical responses of the DiO/DPA FRET pair faithfully follow AP voltage waveforms in single sweeps. A) Averaged fluorescence response (black trace; n=17 sweeps) from a voltage-clamped HEK-293 cell labeled with DiO-C_{16} and in the presence of 1 μM DPA to an AP waveform used as command voltage (grey trace). Record was filtered offline to 2 kHz and inverted for comparison to AP waveform. B) 100 Hz AP train waveform used as the command voltage for C and D. C) Seven consecutive fluorescence quenching responses to the train of AP waveforms (C), in the presence of 1 μM DPA. Right is the averaged trace (n=11 sweeps). D) Seven consecutive eGFP-F fluorescence quenching responses to the train of AP waveforms (B), in the presence of 1 μM DPA. Right is the averaged trace (n=11 sweeps). Single sweeps were filtered off line to 1 kHz. Scale bar lower right of D corresponds to averaged traces in C and D.

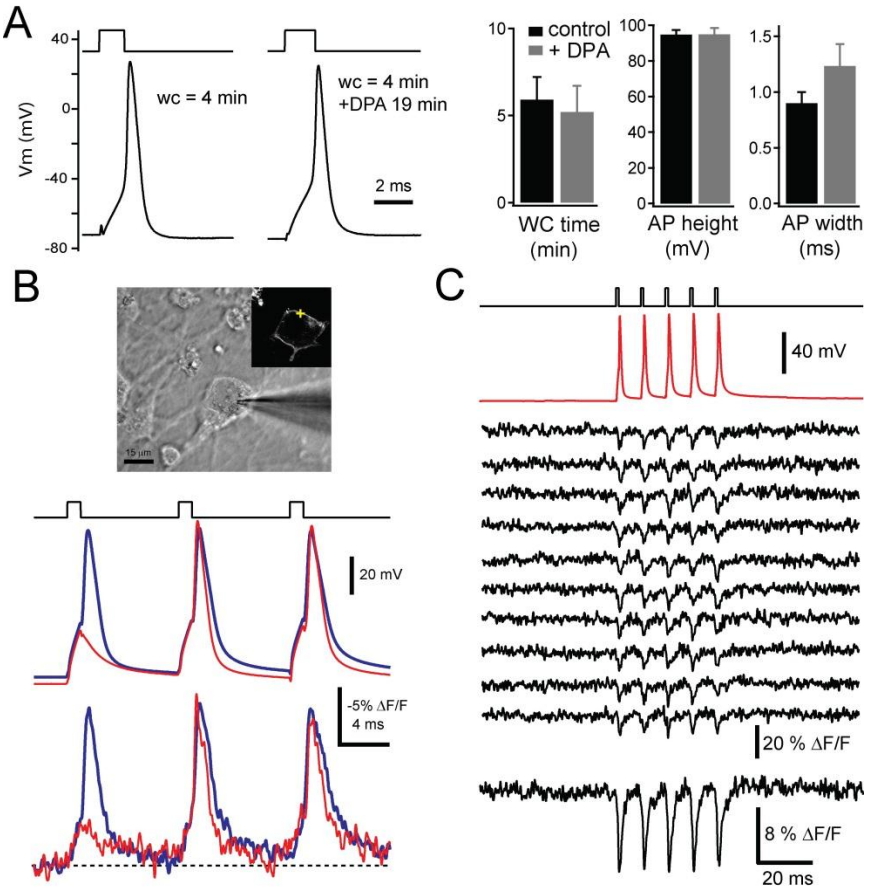

Figure IV-5. DiO/DPA FRET pair reports high frequency APs in cultured hippocampal neurons. Properties of APs recorded under current clamp in the presence of DPA A) Records of APs from two different hippocampal neurons 4 minutes after the formation of the whole cell configuration, either in the absence of DPA (left, current injection 2200 pA), or after preincubation in 1 µM DPA for 19 minutes (right, current injection 1600 pA). Far right, summary bar graphs of AP properties recorded in the absence of DPA (n=12 cells) or after the 1 µM DPA preincubation (≥10 minutes, mean= 20 ± 4 min, n=10). 'WC time' is the average time at which APs were recorded following whole cell formation, 'AP height' is the difference between the peak amplitude and resting potential, and 'AP width' is the width of the AP at half its maximal amplitude. No significant differences were observed ($p>0.1$). DiO/DPA reports APs in neurons. B) DIC image of the cultured hippocampal neuron and recording pipette (upper panel), inset, confocal image of the same neuron and the location of the optical recording (yellow cross) made during a 100 Hz train of current injections (1400 pA) to initiate APs. Shown are electrical recordings (middle) and corresponding optical recordings (bottom). Red traces are averages of 6 sweeps where there was a failure of AP generation in response to the first current injection. Blue traces are averages of 12 sweeps, where each current pulse successfully generated an AP. C) DiO/DPA reports APs in single trials. APs (red) were evoked by a train of five 1900 pA current pulses at 100 Hz (top). Ten consecutive single sweeps are shown with the average below.

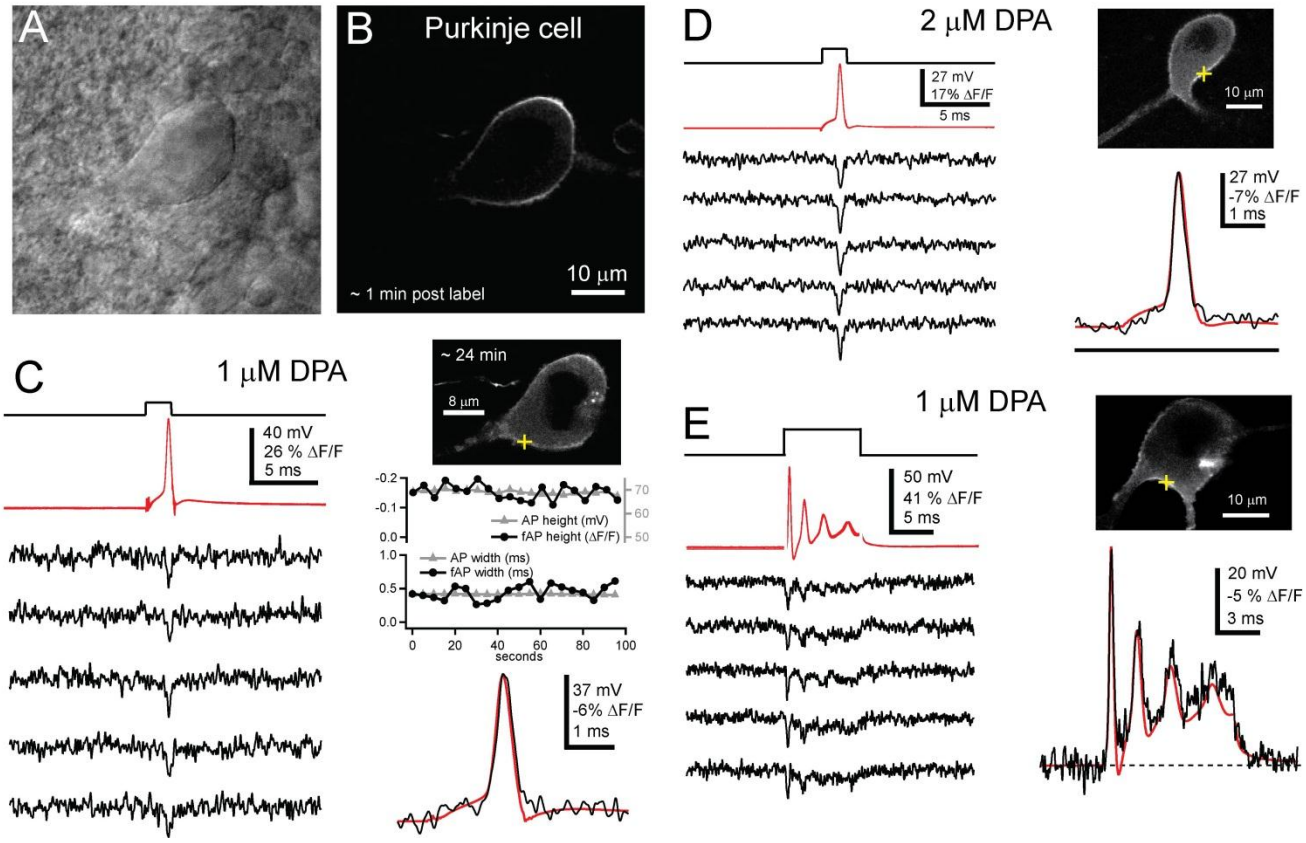

Figure IV-6. DiO/DPA FRET pair reports simple and complex cerebellar Purkinje neuron activity in brain slices. A) DIC and B) confocal fluorescence images of a Purkinje neuron located in a brain slice preincubated and superfused with 1 µM DPA and 1 minute after cell-attached labeling with DiO-C_{16}. C) Single sweep AP-associated DiO/DPA responses (left) and their average (n=19; lower right) obtained from the Purkinje neuron displayed in A and B. Single APs were elicited by whole-cell current injection (2500 pA, 2 ms). Red traces are the current clamp voltage recordings. Confocal image shows decreased membrane staining 24 minutes after DiO labeling, and yellow cross indicates the location of optical recordings. Right middle are two plots of the amplitudes and widths, as a function of time, of the individual electrical (grey) and optical (black) AP recordings (scale of lower plot is in ms). D) DiO/DPA optical responses to single APs elicited by whole-cell current injection in the presence of 2 µM DPA. Lower right is an average of 19 responses superimposed on the average electrical recording (red). E) Single and averaged (n=10) optical responses to complex spike-like bursts elicited by larger current injections (3500 pA, 10 ms) from a different cell. All optical traces shown were filtered offline at 3.5 kHz.

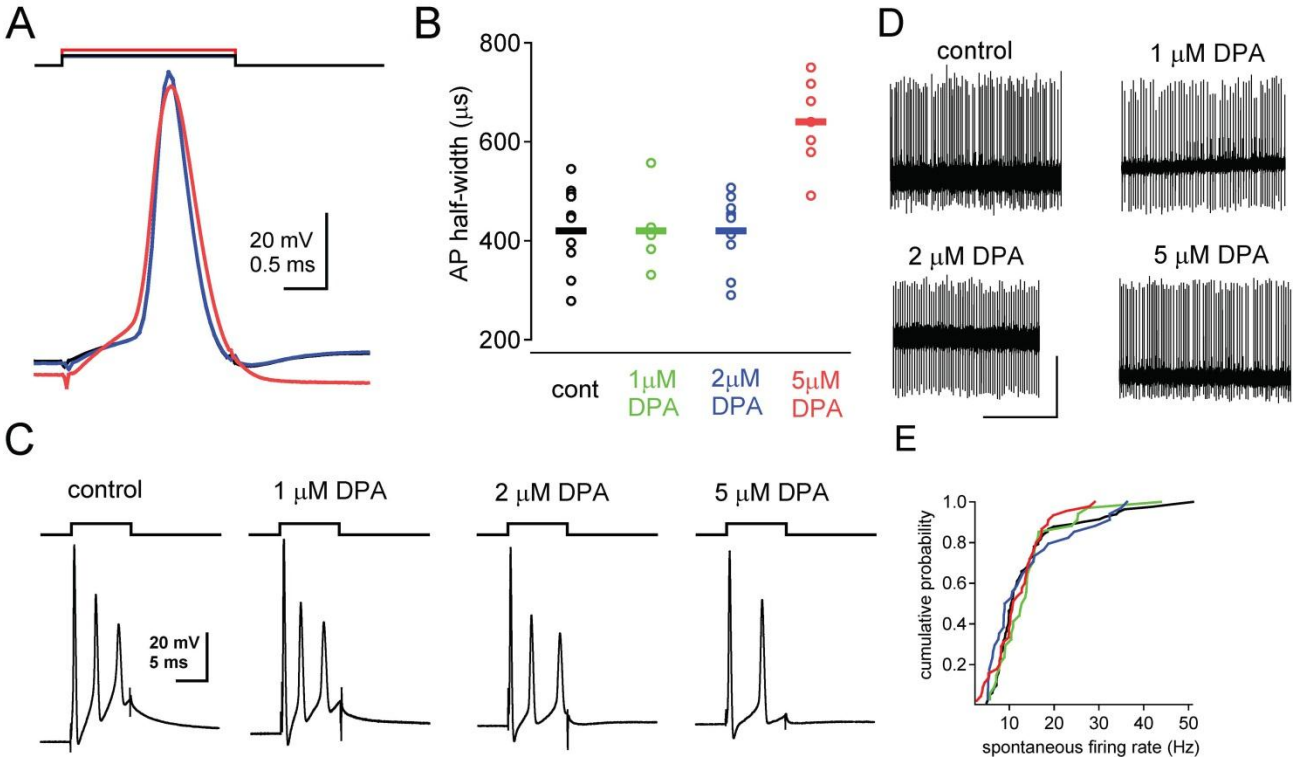

Figure IV-7. DPA does not disrupt firing properties of Purkinje neurons. A) Superimposed whole-cell current-clamp recordings of Purkinje neuron action potentials in response to a 2 ms step current injection. Displayed are single sweeps from 3 different neurons (control black, 2 μM DPA blue and 5 μM DPA red). Note that the AP duration is prolonged in 5 μM DPA. B) Summary plot of AP duration measurements (full width at half-maximal amplitude) as a function of DPA concentration. Each data point corresponds to a different Purkinje neuron. Horizontal lines indicate mean values. C) Complex spike-like responses elicited with longer/larger current injections (10 ms, 3.5 nA) recorded in the indicated concentrations of DPA. Note that 5 μM DPA is associated with a loss of spikelets in the burst. D) Extracellular recordings made from Purkinje neurons in slices incubated in control solutions or indicated DPA concentrations. Note that regular spontaneous firing rates are maintained in slices equilibrated in DPA. Vertical scale bar represents 45 pA for control, 15 pA for 1 μM DPA, and 30 pA for 2 and 5 μM DPA; horizontal scale bar is 2 s. E) Cumulative probability plots of Purkinje neuron spontaneous firing rates measured with extracellular electrophysiological methods in control (n=82 cells) and DPA-treated conditions (1 μM, n=34; 2 μM n=34; 5 μM n=45). All measurements have been made on Purkinje neurons in slices equilibrated in the indicated concentration of DPA for greater than 45 minutes. No significant differences were observed (pairwise Komolgorov Smirnov tests, $p>0.05$).

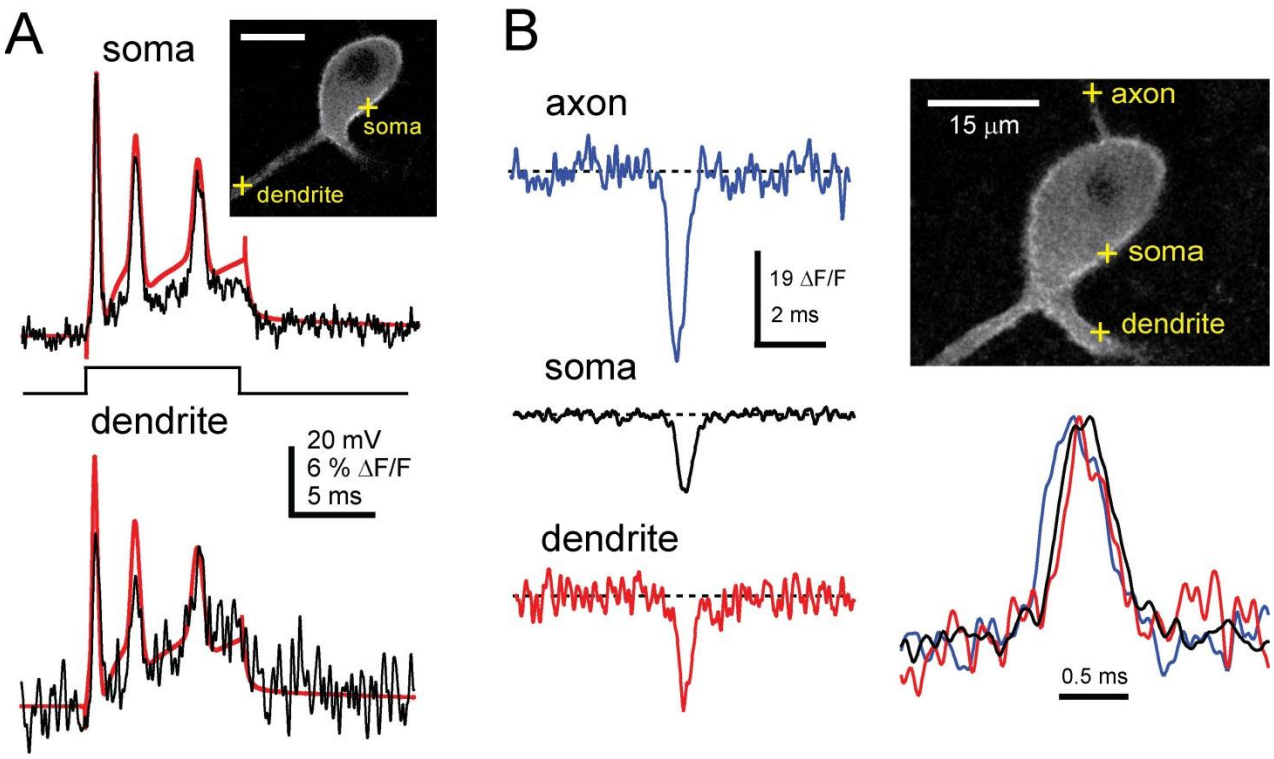

Figure IV-8. Spot detection of soma, dendrite, and axonal voltage responses. A) Averaged optical responses (black traces) to complex spike-like bursts (red traces) recorded from the soma (n=16 sweeps) and dendrite (n=13 sweeps) of a Purkinje neuron indicated in the confocal image (yellow crosses). B) Optical responses to single APs recorded from different locations (yellow crosses) within the same cell. Averaged responses from the axon (blue, n=9 sweeps), soma (black; n=14), and dendrite (red, n=10) are shown to the left. Traces have been temporally aligned with respect to the electrically recorded AP and superimposed below the micrograph. Responses were recorded in 2 μM DPA.

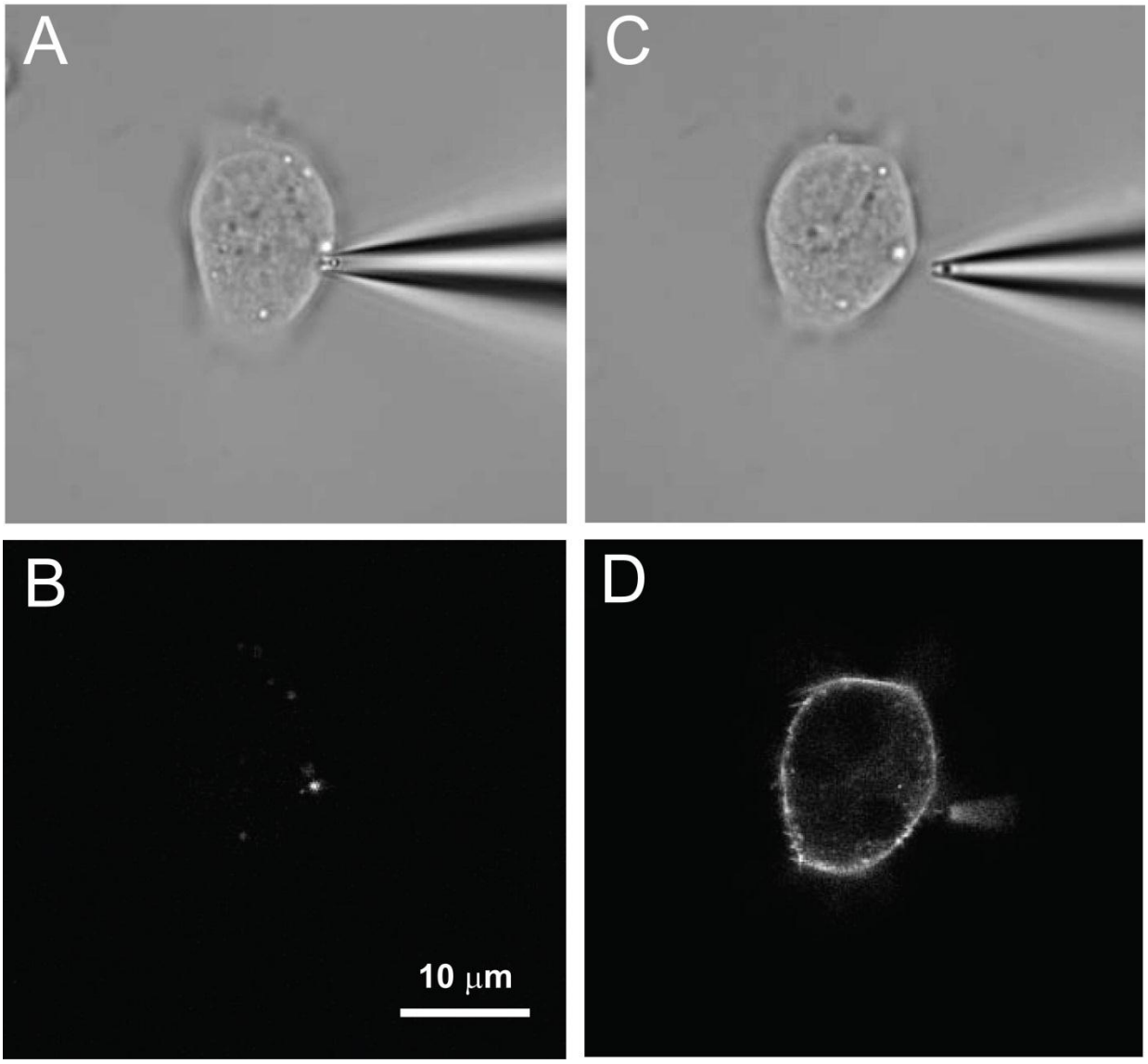

Figure IV-9. Labeling of cells by cell-attached patch pipette method. A and C) DIC, and B and D) fluorescent images of a HEK-293 cell before suction was applied through a patch pipette containing DiO-C_{16} (A and D), and after 15 seconds of suction was applied and the pipette backed away (C and D).

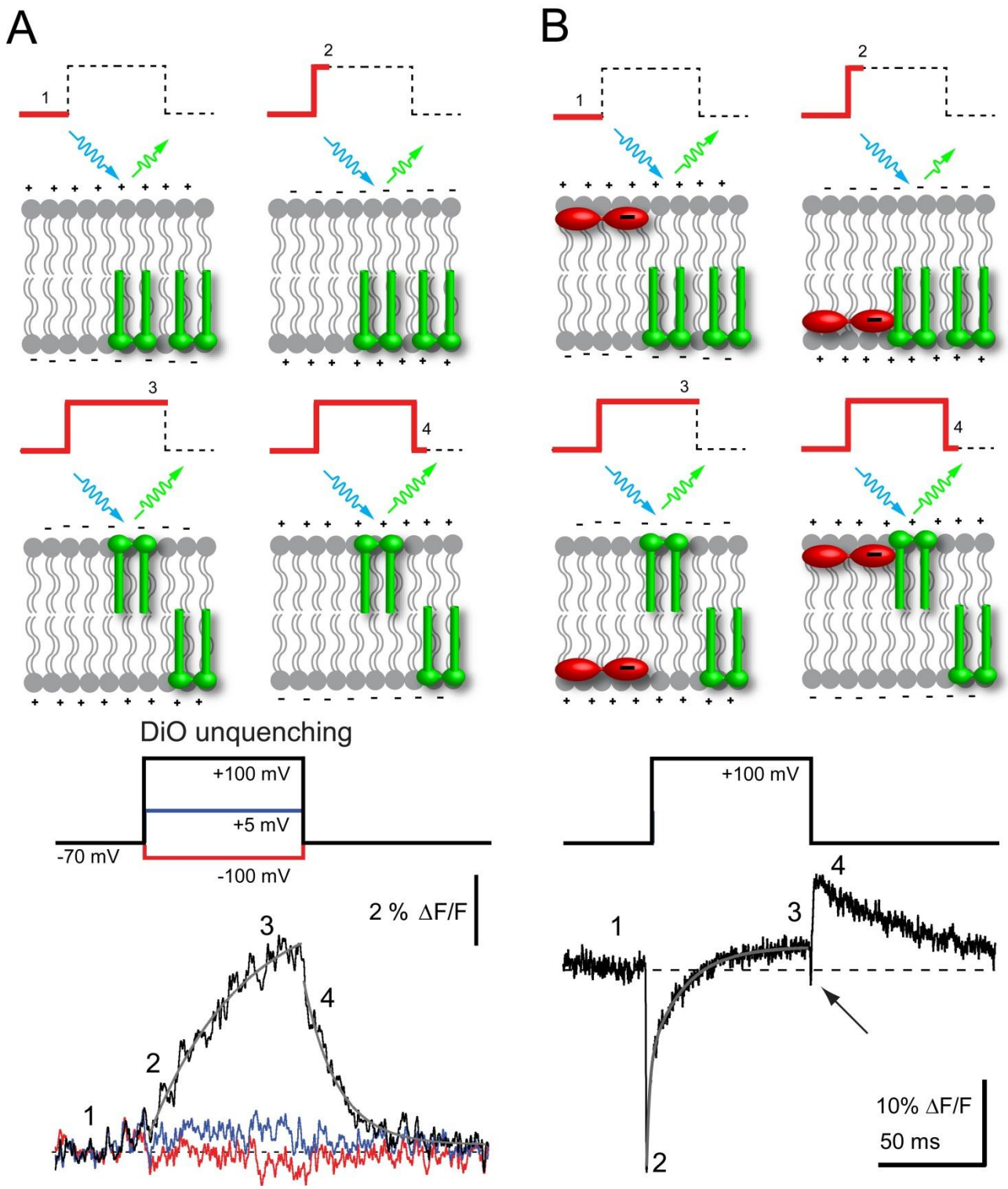
A
B
1
2
3
4
DiO unquenching
+100 mV
+5 mV
-70 mV
-100 mV
2 % ΔF/F
+100 mV
10% ΔF/F
50 ms

Figure IV-10A. DiO labeled HEK-293 cells show an increase in fluorescence in response to step depolarizations. Upper four panels, schematic diagram describing our interpretation of DiO fluorescence changes at different times (numbers) during a step depolarization (thick red line) in the absence of DPA. Grey symbols represent membrane phospholipids, large green symbols represent DiO molecules. Arrows represent 488 nm excitation (blue) and DiO emission (green). The length of the green arrows represents the amount of relative fluorescence emitted at the time indicated by the number. Lower two panels, Fluorescence signals in response to voltage steps (above), from a HEK-293 cell labeled with DiO_{16}, and patch-clamped in whole-cell mode at a holding potential of -70mV. Traces are averages of 50 sweeps per step (step duration = 80 ms) and filtered to (2000 point binomial smoothing, Igor Pro, Wavemetrics; <0.5 kHz equivalent Bessel filtering). Single exponential fits (grey) to the rising and falling phase of the +100 mV step (black trace) produced time constants of 48 and 17 ms, respectively.

Figure IV-10B. Schematic diagram outlining DiO/DPA FRET responses to a step depolarization. Upper four panels, schematic diagram describing our interpretation of DiO fluorescence changes at different times during a step depolarization in the presence of DPA. Dynamic changes in DiO fluorescence during sustained step depolarizations (from -70 mV to > 0 mV) result predominantly from a rapid repartitioning of DPA molecules to the inner leaflet (fluorescence quenching) followed by a slower repartition of DiO molecules (relaxation of quenching). Symbols are as in **Figure IV-10A**, with the red symbol here representing DPA molecules. Lower panel, Fluorescence signal from a voltage-clamped HEK-293 cell labeled with DiO_{16} in the presence of 1 μM DPA in response to a step depolarization from -70 mV to +100 mV (above). Numbers correspond to the approximate time represented in the voltage command in the upper panels. Double exponential fit (solid grey) to the +100 mV pulse is 1.5 and 17 ms with relative amplitudes of 0.46 and 0.54, respectively.

Properties of single APs				
	control (10)	1 ·M DPA (5)	2 ·M DPA (10)	5 ·M DPA (7)
AP height (mV)	79.3 ± 1.5	74.9 ± 6.6	77.3 ± 3	76.8 ± 2.9
AP half-width (·s)	431 ± 29	422 ± 42	422 ± 24	637 ± 36 **
AP threshold (mV)	-54.9 ± 1.2	-52.3 ± 2.4	-53.6 ± 1	-52.6 ± 2.7
threshold stimulus	1.3 ± 0.17	1.2 ± 0.13	1.3 ± 0.11	1.1 ± 0.23
Properties of complex spike-like bursts				
	control (7)	1 ·M DPA (6)	2 ·M DPA (6)	5 ·M DPA (7)
# of spikelets per	3.7 ± 0.2	3.7 ± 0.2	3.3 ± 0.2	2.3 ± 0.2 *
intra-burst freq. (Hz)	362 ± 19	334 ± 17	329 ± 17	219 ± 29 *

Figure IV-11. Summary of DPA effects on Purkinje neuron excitability. Single APs or complex spike-like bursts were elicited in Purkinje neurons by current injection in whole cell current clamp mode under control conditions, or after incubating the slice in the indicated concentration of DPA for greater than 45 minutes. Numbers in parentheses are number of cells. *AP half-width* was measured at the half-maximal amplitude of the AP. *AP threshold* was measured by calculating the membrane potential at the time point corresponding to the minimum of the differentiated membrane potential versus time. The *threshold stimulus* is defined as the minimal current necessary to elicit an AP within 1.3 to 1.4 ms after the current step onset. Number of spikelets per burst and intraburst frequency were measured from complex-spike like bursts. The ** indicates significance of the 5 μM group from all others at $p \leq 0.005$ and the * indicates significance of the 5 μM group from control at $p<0.005$ based on a one-way ANOVA with a post-hoc Kruskal-Wallis test.

CHAPTER V

Conclusion

If we liken individual cells as individual people, then the circuit is the community and the parts of a cell that make it work are the different faculties of a human that allows her to interact and take action. Scientifically probing the different parts of a cell requires finer methods than merely single cell recordings and bulk imaging methods. The temporal and spatial precision required demands a reliable and fast voltage sensor, the ability to activate and record from subcellular compartments, and using computational modeling to undertake experiments that would normally not be possible *in vitro* or *in vivo*.

We have described here an attempt to understand a specific receptor's effect on the axonal compartments of a cell in the cerebellar cortex responsible for transmitting and broadcasting contextual motor information to the ultimate output, where learning takes place. Although $GABA_A$Rs are inhibitory on granule cell bodies, we have shown them to be excitatory on their axons the parallel fibers. This excitation is manifest in imaging calcium signals at presynaptic terminals as well as recording fiber volleys in the molecular layer. $GABA_A$R activation has been achieved both by using a an agonist as well as uncaging a synthetic GABA-like compound. We have found that the effects of GABA on parallel fibers are broad, increasing conduction velocity, amplifying stimulus-evoked signals, and decreasing spike threshold both in the axon itself and in the cell body from which it emanates. The biphasic effect of GABA on the cell body and its processes suggests fine regulation of chloride transport in different parts of the cell, as well as geometric differences that make it possible for small subcellular compartments to accumulate chloride.

Turning to the question of why $GABA_AR$ excitation is necessary, we note that faithful transmission of signals from mossy fibers to the Purkinje cells is necessary to preserve the redundant coding that granule cells in the circuit may undertake. The divergence of information from contextual motor cues may have to be coded for in a distributed manner in order for the fine tuning of the cerebellar cortex to have an effect. While spike failures in parallel fibers have not been demonstrated to occur regularly, the speed of transmission may contribute to the precise firing pattern of the Purkinje cell (as seen in the EPSC effects), and hence to downstream motor output. In a neuronal machine dedicated to fine tuning, even the smallest effects matter. What's more, the excitatory effect of GABA on parallel fibers would drive interneurons to release more GABA, hence further exciting the axons. This positive feedback system may play a larger role in tuning both the arrival times of spikes at the presynaptic terminal and the release of transmitters influencing Purkinje cell firing. Moreover, as shown, GABA action on parallel fibers may act to change the spike output from granule cell bodies, further increasing the amplitude of signal transmission. We have only begun to explore the parameters that affect transmission of information from mossy fibers to Purkinje cells in the cerebellar circuit.

It is important to note that the techniques which we used and proposed to investigate and analyze GABA excitation of parallel fibers can be generalized to other systems where a cell and its fine process are segregated in terms of structure and function. The two-component voltage sensing method can be used to record from axons, dendrites, or parts of a cell, allowing us to visualize the flow of information

through the cell in submillisecond manner. The promise of noninvasive voltage imaging of subcellular structures opens up possibilities for experiments for probing action potential initiation, the effect of receptors on spike shape, superposition of signals, precise timing of orthodromic and antidromic spikes, and much more. Even at the places that we cannot record from or even sense voltage from, computational modeling provides a tool for understanding the parameters and constraints underlying a physiological system. The compartmental model we applied was a relatively simple and hence general consideration that attempts to recover general principles rather than providing details on the exact channel distribution of a cell. With a model such as this, our conclusions are limited to general statements. For example, if reversal potentials for certain ions are different in somatic and axonal compartments, it is possible for axonal depolarization to affect somatic spiking in geometries where long processes emanate from a compact cell body. The compartmental model is a tool and not an all-encompassing replica of the cell. We get as much from it as we put in, but it allows us to make predictions that can be tested by experiment. In this case, we ask whether sodium inactivation parameters are the main determinants of whether $GABA_AR$ activation leads to excitation or inhibition. What we have discovered about the lowly parallel fiber may serve us well when we encounter another small cell type with long processes that respond differently somatically and axonally to a given molecule.

Working in different levels in neuroscience may ultimately take us to an understanding that we desire. At one level is the cell, and at another level is the circuit. At one level is the individual, and at another level is the community. Bridging the gap

between one level and the next allows us to make predictions from the general to the specific, and also from the specific to the general. In the grand scheme of attempting to understand ourselves, we start by understanding who we interact with, why we do something, who we do it for, and then what is our core common drive. The latter leads to sociological questions like how a community evolves and why conflicts between groups are so difficult to resolve. These questions in turn return us back to the lower level, asking how certain individuals in history moved communities, and what were their unique characteristics that made them so crucial in the evolution of our species. The individual, her temperaments, and her group are inextricably linked, just as the cell, its subcompartments, and its circuit belong together in a rigorous study of what function characterizes a circuit, as well as what makes us human.

Perhaps the most remarkable thing about being human is that we can study ourselves. Whether it is love, war, or reflection, we may not always do the right thing, but we can look into ourselves and wonder if we are what we think we are.

REFERENCES

Afshari, F. S., K. Ptak, et al. (2004). "Resurgent Na currents in four classes of neurons of the cerebellum." J Neurophysiol 92(5): 2831-2843.

Albus, J. S. (1971). "A Theory of Cerebellar Function." Mathematical Biosciences 10: 25-61.

Alle, H. and J. R. Geiger (2007). "GABAergic spill-over transmission onto hippocampal mossy fiber boutons." J Neurosci 27(4): 942-950.

Antic, S. D. (2003). "Action potentials in basal and oblique dendrites of rat neocortical pyramidal neurons." J Physiol 550(Pt 1): 35-50.

Axelrod, D. (1979). "Carbocyanine dye orientation in red cell membrane studied by microscopic fluorescence polarization." Biophys J 26(3): 557-573.

Baker, B. J., E. K. Kosmidis, et al. (2005). "Imaging brain activity with voltage- and calcium-sensitive dyes." Cell Mol Neurobiol 25(2): 245-282.

Baker, B. J., H. Lee, et al. (2007). "Three fluorescent protein voltage sensors exhibit low plasma membrane expression in mammalian cells." J Neurosci Methods 161(1): 32-38.

Bant, J. S. and I. M. Raman (2010). "Control of transient, resurgent, and persistent current by open-channel block by Na channel beta4 in cultured cerebellar granule neurons." Proc Natl Acad Sci U S A 107(27): 12357-12362.

Bean, B. P. (2007). "The action potential in mammalian central neurons." Nat Rev Neurosci 8(6): 451-465.

Belelli, D., J. J. Lambert, et al. (1997). "The interaction of the general anesthetic etomidate with the gamma-aminobutyric acid type A receptor is influenced by a single amino acid." Proc Natl Acad Sci U S A 94(20): 11031-11036.

Belenky, M. A., P. J. Sollars, et al. (2009). "Cell-type specific distribution of chloride transporters in the rat suprachiasmatic nucleus." Neuroscience 165(4): 1519-1537.

Bender, K. J. and L. O. Trussell (2012). "The Physiology of the Axon Initial Segment." Annu Rev Neurosci.

Blaesse, P., M. S. Airaksinen, et al. (2009). "Cation-chloride cotransporters and neuronal function." Neuron 61(6): 820-838.

Bliss, T. V. and T. Lomo (1973). "Long-lasting potentiation of synaptic transmission in the dentate area of the anaesthetized rabbit following stimulation of the perforant path." J Physiol 232(2): 331-356.

Blunck, R., B. Chanda, et al. (2005). "Nano to micro -- fluorescence measurements of electric fields in molecules and genetically specified neurons." J Membr Biol 208(2): 91-102.

Bradley, J., R. Luo, et al. (2009). "Submillisecond optical reporting of membrane potential in situ using a neuronal tracer dye." J Neurosci 29(29): 9197-9209.

Brickley, S. G., S. G. Cull-Candy, et al. (1996). "Development of a tonic form of synaptic inhibition in rat cerebellar granule cells resulting from persistent activation of $GABA_A$ receptors." J Physiol 497 753-759.

Brickley, S. G., V. Revilla, et al. (2001). "Adaptive regulation of neuronal excitability by a voltage-independent potassium conductance." Nature 409(6816): 88-92.

Bright, D. P., M. Renzi, et al. (2011). "Profound desensitization by ambient GABA limits activation of delta-containing GABAA receptors during spillover." J Neurosci 31(2): 753-763.

Bucher, D. and J. M. Goaillard (2011). "Beyond faithful conduction: Short-term dynamics, neuromodulation, and long-term regulation of spike propagation in the axon." Prog Neurobiol 94(4): 307-346.

Bullock, T. H. (1951). "Facilitation of conduction rate in nerve fibers." J Physiol 114(1-2): 89-97.

Chanda, B., O. K. Asamoah, et al. (2005). "Gating charge displacement in voltage-gated ion channels involves limited transmembrane movement." Nature 436(7052): 852-856.

Chanda, B., R. Blunck, et al. (2005). "A hybrid approach to measuring electrical activity in genetically specified neurons." Nat Neurosci 8(11): 1619-1626.

Chang, Y., Y. Xie, et al. (2001). "Positive allosteric modulation by ultraviolet irradiation on GABA(A), but not GABA(C), receptors expressed in Xenopus oocytes." J Physiol 536(Pt 2): 471-478.

Clark, J. A., A. Y. Deutch, et al. (1992). "Functional expression and CNS distribution of a beta-alanine-sensitive neuronal GABA transporter." Neuron 9(2): 337-348.

Cohen, L. B. and B. M. Salzberg (1978). "Optical measurement of membrane potential." Rev Physiol Biochem Pharmacol 83: 35-88.

Cohen, L. B., B. M. Salzberg, et al. (1974). "Changes in axon fluorescence during activity: molecular probes of membrane potential." J Membr Biol 19(1): 1-36.

Cohen, L. B., B. M. Salzberg, et al. (1978). "Optical methods for monitoring neuron activity." Annu Rev Neurosci 1: 171-182.

Dailey, M. E., J. Buchanan, et al. (1994). "Mossy fiber growth and synaptogenesis in rat hippocampal slices in vitro." J Neurosci 14(3 Pt 1): 1060-1078.

Davie, J. T., B. A. Clark, et al. (2008). "The origin of the complex spike in cerebellar Purkinje cells." J Neurosci 28(30): 7599-7609.

Debanne, D., N. C. Guerineau, et al. (1997). "Action-potential propagation gated by an axonal I(A)-like K+ conductance in hippocampus." Nature 389(6648): 286-289.

Dellal, S. S., R. Luo, et al. (2012). "GABAA receptors increase excitability and conduction velocity of cerebellar parallel fiber axons." J Neurophysiol.

DiFranco, M., J. Capote, et al. (2007). "Voltage-dependent dynamic FRET signals from the transverse tubules in mammalian skeletal muscle fibers." J Gen Physiol 130(6): 581-600.

DiGregorio, D. A., A. Peskoff, et al. (1999). "Measurement of action potential-induced presynaptic calcium domains at a cultured neuromuscular junction." J Neurosci 19(18): 7846-7859.

DiGregorio, D. A., J. S. Rothman, et al. (2007). "Desensitization properties of AMPA receptors at the cerebellar mossy fiber granule cell synapse." J Neurosci 27(31): 8344-8357.

Dittman, J. S. and W. G. Regehr (1997). "Mechanism and kinetics of heterosynaptic depression at a cerebellar synapse." J Neurosci 17(23): 9048-9059.

Diwakar, S., J. Magistretti, et al. (2009). "Axonal Na+ channels ensure fast spike activation and back-propagation in cerebellar granule cells." J Neurophysiol 101(2): 519-532.

Djurisic, M., S. Antic, et al. (2004). "Voltage imaging from dendrites of mitral cells: EPSP attenuation and spike trigger zones." J Neurosci 24(30): 6703-6714.

Dombeck, D. A., M. Blanchard-Desce, et al. (2004). "Optical recording of action potentials with second-harmonic generation microscopy." J Neurosci 24(4): 999-1003.

Dombeck, D. A., L. Sacconi, et al. (2005). "Optical recording of fast neuronal membrane potential transients in acute mammalian brain slices by second-harmonic generation microscopy." J Neurophysiol 94(5): 3628-3636.

Dreosti, E. and L. Lagnado (2011). "Optical reporters of synaptic activity in neural circuits." Exp Physiol 96(1): 4-12.

Duemani Reddy, G., K. Kelleher, et al. (2008). "Three-dimensional random access multiphoton microscopy for functional imaging of neuronal activity." Nat Neurosci.

Durkin, M. M., K. E. Smith, et al. (1995). "Localization of messenger RNAs encoding three GABA transporters in rat brain: an in situ hybridization study." Brain Res Mol Brain Res 33(1): 7-21.

Dzhala, V. I., D. M. Talos, et al. (2005). "NKCC1 transporter facilitates seizures in the developing brain." Nat Med 11(11): 1205-1213.

Eccles, J., Ito, M., Szentagothal, J. (1967). *The Cerebellum as a Neuronal Machine*. Berlin, Heidelberg, New York, Springer-Verlag. 335.

Eccles, J. C., R. M. Eccles, et al. (1961). "Central inhibitory action attributable to presynaptic depolarization produced by muscle afferent volleys." J Physiol 159: 147-166.

Eccles, J. C., R. Llinas, et al. (1966). "The excitatory synaptic action of climbing fibres on the purinje cells of the cerebellum." J Physiol 182(2): 268-296.

Eccles, J. C., R. Schmidt, et al. (1963). "Pharmacological Studies on Presynaptic Inhibition." J Physiol 168: 500-530.

Escobar, A. L., J. R. Monck, et al. (1994). "Localization of the site of Ca2+ release at the level of a single sarcomere in skeletal muscle fibres." Nature 367(6465): 739-741.

Eugene, E., C. Depienne, et al. (2007). "GABA(A) receptor gamma 2 subunit mutations linked to human epileptic syndromes differentially affect phasic and tonic inhibition." J Neurosci 27(51): 14108-14116.

Farrant, M. and Z. Nusser (2005). "Variations on an inhibitory theme: phasic and tonic activation of GABA(A) receptors." Nat Rev Neurosci 6(3): 215-229.

Farrant, M. and Z. Nusser (2005). "Variations on an inhibitory theme: phasic and tonic activation of $GABA_A$ receptors." Nat Rev Neurosci 6(3): 215-229.

Fernandez, J. M., R. E. Taylor, et al. (1983). "Induced capacitance in the squid giant axon. Lipophilic ion displacement currents." J Gen Physiol 82(3): 331-346.

Fisher, J. A., J. R. Barchi, et al. (2008). "Two-photon excitation of potentiometric probes enables optical recording of action potentials from Mammalian nerve terminals in situ." J Neurophysiol 99(3): 1545-1553.

Fromherz, P., G. Hubener, et al. (2007). "ANNINE-6plus, a voltage-sensitive dye with good solubility, strong membrane binding and high sensitivity." Eur Biophys J.

Gan, W. B., J. Grutzendler, et al. (2000). "Multicolor "DiOlistic" labeling of the nervous system using lipophilic dye combinations." Neuron 27(2): 219-225.

Gardner-Medwin, A. R. (1972). "An extreme supernormal period in cerebellar parallel fibres." J Physiol 222(2): 357-371.

Glickfeld, L. L., J. D. Roberts, et al. (2009). "Interneurons hyperpolarize pyramidal cells along their entire somatodendritic axis." Nat Neurosci 12(1): 21-23.

Glickstein, M., P. Strata, et al. (2009). "Cerebellum: history." Neuroscience 162(3): 549-559.

Gonzalez, J. E. and R. Y. Tsien (1995). "Voltage sensing by fluorescence resonance energy transfer in single cells." Biophys J 69(4): 1272-1280.

Gonzalez, J. E. and R. Y. Tsien (1997). "Improved indicators of cell membrane potential that use fluorescence resonance energy transfer." Chem Biol 4(4): 269-277.

Grieco, T. M., J. D. Malhotra, et al. (2005). "Open-channel block by the cytoplasmic tail of sodium channel beta4 as a mechanism for resurgent sodium current." Neuron 45(2): 233-244.

Grinvald, A. and R. Hildesheim (2004). "VSDI: a new era in functional imaging of cortical dynamics." Nat Rev Neurosci 5(11): 874-885.

Haines, D. E. (2008). *Neuroanatomy : an atlas of structures, sections, and systems*. Philadelphia, Wolters Kluwer Health/Lippincott Williams & Wilkins.

Hausser, M. and B. A. Clark (1997). "Tonic synaptic inhibition modulates neuronal output pattern and spatiotemporal synaptic integration." Neuron 19(3): 665-678.

Herz, A. V., T. Gollisch, et al. (2006). "Modeling single-neuron dynamics and computations: a balance of detail and abstraction." Science 314(5796): 80-85.

Hodgkin, A. L. and A. F. Huxley (1952). "A quantitative description of membrane current and its application to conduction and excitation in nerve." J Physiol 117(4): 500-544.

Honig, M. G. and R. I. Hume (1986). "Fluorescent carbocyanine dyes allow living neurons of identified origin to be studied in long-term cultures." J Cell Biol 103(1): 171-187.

Honig, M. G. and R. I. Hume (1989). "Carbocyanine dyes. Novel markers for labelling neurons." Trends Neurosci 12(9): 336-338.

Honig, M. G. and R. I. Hume (1989). "DiI and diO: versatile fluorescent dyes for neuronal labelling and pathway tracing." Trends Neurosci 12(9): 333-335, 340-331.

Ito, M. (1984). *The cerebellum and neural control*. New York, NY, Raven Press.

Ito, M., M. Sakurai, et al. (1982). "Climbing fibre induced depression of both mossy fibre responsiveness and glutamate sensitivity of cerebellar Purkinje cells." J Physiol 324: 113-134.

Jackson, M. B. and S. J. Zhang (1995). "Action potential propagation and propagation block by GABA in rat posterior pituitary nerve terminals." J Physiol 483 (Pt 3): 597-611.

Jaeger, D., E. De Schutter, et al. (1997). "The role of synaptic and voltage-gated currents in the control of Purkinje cell spiking: a modeling study." J Neurosci 17(1): 91-106.

Jang, I. S., M. Nakamura, et al. (2006). "Presynaptic $GABA_A$ receptors facilitate spontaneous glutamate release from presynaptic terminals on mechanically dissociated rat CA3 pyramidal neurons." Neuroscience 138(1): 25-35.

Jechlinger, M., R. Pelz, et al. (1998). "Subunit composition and quantitative importance of hetero-oligomeric receptors: $GABA_A$ receptors containing a6 subunits." J Neurosci 18(7): 2449-2457.

Jorntell, H. and C. F. Ekerot (2002). "Reciprocal bidirectional plasticity of parallel fiber receptive fields in cerebellar Purkinje cells and their afferent interneurons." Neuron 34(5): 797-806.

Kandel, E., Schwartz, J. H., Jessell, T. M. (2000). *Principles of Neural Science*. New York, McGraw-Hill. 1135.

Kaneda, M., M. Farrant, et al. (1995). "Whole-cell and single-channel currents activated by GABA and glycine in granule cells of the rat cerebellum." J Physiol 485 (Pt 2): 419-435.

Kaneko, H., I. Putzier, et al. (2004). "Chloride accumulation in mammalian olfactory sensory neurons." J Neurosci 24(36): 7931-7938.

Khaliq, Z. M. and I. M. Raman (2005). "Axonal propagation of simple and complex spikes in cerebellar Purkinje neurons." J Neurosci 25(2): 454-463.

Khirug, S., J. Yamada, et al. (2008). "GABAergic depolarization of the axon initial segment in cortical principal neurons is caused by the Na-K-2Cl cotransporter NKCC1." J Neurosci 28(18): 4635-4639.

Kim, J. H., C. Kushmerick, et al. (2010). "Presynaptic resurgent Na+ currents sculpt the action potential waveform and increase firing reliability at a CNS nerve terminal." J Neurosci 30(46): 15479-15490.

Kim, J. J. and R. F. Thompson (1997). "Cerebellar circuits and synaptic mechanisms involved in classical eyeblink conditioning." Trends Neurosci 20(4): 177-181.

Klein, R. L. and R. A. Harris (1996). "Regulation of GABAA receptor structure and function by chronic drug treatments in vivo and with stably transfected cells." Jpn J Pharmacol 70(1): 1-15.

Kuhn, B., P. Fromherz, et al. (2004). "High sensitivity of Stark-shift voltage-sensing dyes by one- or two-photon excitation near the red spectral edge." Biophys J 87(1): 631-639.

Lapicque, L. (2007). "Quantitative investigations of electrical nerve excitation treated as polarization. 1907." Biol Cybern 97(5-6): 341-349.

Li, B., K. McKernan, et al. (2008). "Spatial and temporal distribution patterns of Na-K-2Cl cotransporter in adult and developing mouse retinas." Vis Neurosci 25(2): 109-123.

Lichtman, J. W. and S. E. Fraser (2001). "The neuronal naturalist: watching neurons in their native habitat." Nat Neurosci 4 Suppl: 1215-1220.

Llinas, R. and M. Sugimori (1980). "Electrophysiological properties of in vitro Purkinje cell somata in mammalian cerebellar slices." J Physiol 305: 171-195.

Lu, C. C., A. Kabakov, et al. (1995). "Membrane transport mechanisms probed by capacitance measurements with megahertz voltage clamp." Proc Natl Acad Sci U S A 92(24): 11220-11224.

Lu, T. and L. O. Trussell (2001). "Mixed excitatory and inhibitory GABA-mediated transmission in chick cochlear nucleus." J Physiol 535(Pt 1): 125-131.

Luo, L., E. M. Callaway, et al. (2008). "Genetic dissection of neural circuits." Neuron 57(5): 634-660.

Magee, J. C. and D. Johnston (1997). "A synaptically controlled, associative signal for Hebbian plasticity in hippocampal neurons." Science 275(5297): 209-213.

Majewska, A., G. Yiu, et al. (2000). "A custom-made two-photon microscope and deconvolution system." Pflugers Arch 441(2-3): 398-408.

Malenka, R. C., J. D. Kocsis, et al. (1981). "Modulation of parallel fiber excitability by postsynaptically mediated changes in extracellular potassium." Science 214(4518): 339-341.

Malenka, R. C., J. D. Kocsis, et al. (1983). "The supernormal period of the cerebellar parallel fibers effects of [Ca2+]o and [K+]o." Pflugers Arch 397(3): 176-183.

Marr, D. (1969). "A theory of cerebellar cortex." J Physiol 202(2): 437-470.

Mauk, M. D., J. E. Steinmetz, et al. (1986). "Classical conditioning using stimulation of the inferior olive as the unconditioned stimulus." Proc Natl Acad Sci U S A 83(14): 5349-5353.

Medina, J. F., K. S. Garcia, et al. (2000). "Timing mechanisms in the cerebellum: testing predictions of a large-scale computer simulation." J Neurosci 20(14): 5516-5525.

Meera, P., R. W. Olsen, et al. (2009). "Etomidate, propofol and the neurosteroid THDOC increase the GABA efficacy of recombinant alpha4beta3delta and alpha4beta3 GABA A receptors expressed in HEK cells." Neuropharmacology 56(1): 155-160.

Meera, P., M. Wallner, et al. (2011). "Molecular basis for the high THIP/gaboxadol sensitivity of extrasynaptic GABAA receptors." J Neurophysiol 106(4): 2057-2064.

Mikawa, S., C. Wang, et al. (2002). "Developmental changes in KCC1, KCC2 and NKCC1 mRNAs in the rat cerebellum." Brain Res Dev Brain Res 136(2): 93-100.

Mohler, H., F. Crestani, et al. (2001). "$GABA_A$-receptor subtypes: a new pharmacology." Curr Opin Pharmacol 1(1): 22-25.

Moradmand, K. and M. D. Goldfinger (1995). "Computation of long-distance propagation of impulses elicited by Poisson-process stimulation." J Neurophysiol 74(6): 2415-2426.

Morgan, J. L. and R. O. Wong (2008). "Ballistic labeling with fluorescent dyes and indicators." Curr Protoc Neurosci Chapter 2: Unit 2 11.

Mortensen, M. and T. G. Smart (2006). "Extrasynaptic alphabeta subunit GABAA receptors on rat hippocampal pyramidal neurons." J Physiol 577(Pt 3): 841-856.

Mutoh, H., A. Perron, et al. (2011). "Optogenetic monitoring of membrane potentials." Exp Physiol 96(1): 13-18.

Nielsen, T. A., D. A. DiGregorio, et al. (2004). "Modulation of glutamate mobility reveals the mechanism underlying slow-rising AMPAR EPSCs and the diffusion coefficient in the synaptic cleft." Neuron 42(5): 757-771.

Nuriya, M., J. Jiang, et al. (2006). "Imaging membrane potential in dendritic spines." Proc Natl Acad Sci U S A 103(3): 786-790.

Nusser, Z., W. Sieghart, et al. (1998). "Segregation of different $GABA_A$ receptors to synaptic and extrasynaptic membranes of cerebellar granule cells." J Neurosci 18(5): 1693-1703.

O'Brien, J. A. and S. C. Lummis (2006). "Diolistic labeling of neuronal cultures and intact tissue using a hand-held gene gun." Nat Protoc 1(3): 1517-1521.

Obaid, A. L., T. Koyano, et al. (1999). "Spatiotemporal patterns of activity in an intact mammalian network with single-cell resolution: optical studies of nicotinic activity in an enteric plexus." J Neurosci 19(8): 3073-3093.

Obaid, A. L., L. M. Loew, et al. (2004). "Novel naphthylstyryl-pyridium potentiometric dyes offer advantages for neural network analysis." J Neurosci Methods 134(2): 179-190.

Oberhauser, A. F. and J. M. Fernandez (1995). "Hydrophobic ions amplify the capacitive currents used to measure exocytotic fusion." Biophys J 69(2): 451-459.

Ohyama, T. and M. Mauk (2001). "Latent acquisition of timed responses in cerebellar cortex." J Neurosci 21(2): 682-690.

Otsu, Y., V. Bormuth, et al. (2008). "Optical monitoring of neuronal activity at high frame rate with a digital random-access multiphoton (RAMP) microscope." J Neurosci Methods 173(2): 259-270.

Palay, S. L. and V. Chan-Palay (1974). *Cerebellar Cortex: Cytology and Organization*. New York, Springer-Verlag.

Palmer, L. M. and G. J. Stuart (2006). "Site of action potential initiation in layer 5 pyramidal neurons." J Neurosci 26(6): 1854-1863.

Paradiso, K. and L. G. Wu (2009). "Small voltage changes at nerve terminals travel up axons to affect action potential initiation." Nat Neurosci 12(5): 541-543.

Parsons, T. D., B. M. Salzberg, et al. (1991). "Long-term optical recording of patterns of electrical activity in ensembles of cultured Aplysia neurons." J Neurophysiol 66(1): 316-333.

Perrett, S. P., B. P. Ruiz, et al. (1993). "Cerebellar cortex lesions disrupt learning-dependent timing of conditioned eyelid responses." J Neurosci 13(4): 1708-1718.

Petersen, C. C., A. Grinvald, et al. (2003). "Spatiotemporal dynamics of sensory responses in layer 2/3 of rat barrel cortex measured in vivo by voltage-sensitive dye imaging combined with whole-cell voltage recordings and neuron reconstructions." J Neurosci 23(4): 1298-1309.

Pirker, S., C. Schwarzer, et al. (2000). "$GABA_A$ receptors: immunocytochemical distribution of 13 subunits in the adult rat brain." Neuroscience 101(4): 815-850.

Pouille, F. and M. Scanziani (2001). "Enforcement of temporal fidelity in pyramidal cells by somatic feed-forward inhibition." Science 293(5532): 1159-1163.

Price, G. D. and L. O. Trussell (2006). "Estimate of the chloride concentration in a central glutamatergic terminal: a gramicidin perforated-patch study on the calyx of Held." J Neurosci 26(44): 11432-11436.

Pugh, J. R. and C. E. Jahr (2011). "Axonal GABAA receptors increase cerebellar granule cell excitability and synaptic activity." J Neurosci 31(2): 565-574.

Rall, W. (1959). "Branching dendritic trees and motoneuron membrane resistivity." Exp Neurol 1: 491-527.

Ramón y Cajal, S. (1905). *Manual de anatomia pathologica y fundamentos de bacteriologia*. Madrid, Imprenta y Liberia de Nicolas Moya.

Rancillac, A. and F. Crepel (2004). "Synapses between parallel fibres and stellate cells express long-term changes in synaptic efficacy in rat cerebellum." J Physiol 554(Pt 3): 707-720.

Ratzliff, A. H., A. L. Howard, et al. (2004). "Rapid deletion of mossy cells does not result in a hyperexcitable dentate gyrus: implications for epileptogenesis." J Neurosci 24(9): 2259-2269.

Raymond, J. L., S. G. Lisberger, et al. (1996). "The cerebellum: a neuronal learning machine?" Science 272(5265): 1126-1131.

Regehr, W. G. and P. P. Atluri (1995). "Calcium transients in cerebellar granule cell presynaptic terminals." Biophys J 68(5): 2156-2170.

Rivera, C., J. Voipio, et al. (1999). "The K+/Cl- co-transporter KCC2 renders GABA hyperpolarizing during neuronal maturation." Nature 397(6716): 251-255.

Rohr, S. and B. M. Salzberg (1994). "Multiple site optical recording of transmembrane voltage (MSORTV) in patterned growth heart cell cultures: assessing electrical behavior, with microsecond resolution, on a cellular and subcellular scale." Biophys J 67(3): 1301-1315.

Rudomin, P. and R. F. Schmidt (1999). "Presynaptic inhibition in the vertebrate spinal cord revisited." Exp Brain Res 129(1): 1-37.

Ruiz, A., E. Campanac, et al. (2010). "Presynaptic GABAA receptors enhance transmission and LTP induction at hippocampal mossy fiber synapses." Nat Neurosci 13(4): 431-438.

Ruiz, A., R. Fabian-Fine, et al. (2003). "GABAA receptors at hippocampal mossy fibers." Neuron 39(6): 961-973.

Sabatini, B. L. and W. G. Regehr (1997). "Control of neurotransmitter release by presynaptic waveform at the granule cell to Purkinje cell synapse." J Neurosci 17(10): 3425-3435.

Salin, P. A., R. C. Malenka, et al. (1996). "Cyclic AMP mediates a presynaptic form of LTP at cerebellar parallel fiber synapses." Neuron 16(4): 797-803.

Salzberg, B. M., H. V. Davila, et al. (1973). "Optical recording of impulses in individual neurones of an invertebrate central nervous system." Nature 246(5434): 508-509.

Salzberg, B. M., A. L. Obaid, et al. (1993). "Microsecond response of a voltage-sensitive merocyanine dye: fast voltage-clamp measurements on squid giant axon." Jpn J Physiol 43 Suppl 1: S37-41.

Santhakumar, V., H. J. Hanchar, et al. (2006). "Contributions of the $GABA_A$ receptor a6 subunit to phasic and tonic inhibition revealed by a naturally occurring polymorphism in the a6 gene." J Neurosci 26(12): 3357-3364.

Schmid, G., G. Bonanno, et al. (1999). "Enhanced benzodiazepine and ethanol actions on cerebellar $GABA_A$ receptors mediating glutamate release in an alcohol-sensitive rat line." Neuropharmacology 38(9): 1273-1279.

Seja, P., M. Schonewille, et al. (2012). "Raising cytosolic Cl(-) in cerebellar granule cells affects their excitability and vestibulo-ocular learning." EMBO J.

Sharpee, T. O., H. Sugihara, et al. (2006). "Adaptive filtering enhances information transmission in visual cortex." Nature 439(7079): 936-942.

Shu, H. J., J. Bracamontes, et al. (2011). "Characteristics of alpha4/delta-containing concatemeric GABA(A) receptors expressed in Xenopus oocytes." Br J Pharmacol.

Sjulson, L. and G. Miesenbock (2007). "Optical recording of action potentials and other discrete physiological events: a perspective from signal detection theory." Physiology (Bethesda) 22: 47-55.

Sjulson, L. and G. Miesenbock (2008). "Rational optimization and imaging in vivo of a genetically encoded optical voltage reporter." J Neurosci 28(21): 5582-5593.

Smith, E. C. and M. S. Lewicki (2006). "Efficient auditory coding." Nature 439(7079): 978-982.

Spruston, N., Y. Schiller, et al. (1995). "Activity-dependent action potential invasion and calcium influx into hippocampal CA1 dendrites." Science 268(5208): 297-300.

Steinmetz, J. E., D. J. Rosen, et al. (1986). "Classical conditioning of the rabbit eyelid response with a mossy-fiber stimulation CS: I. Pontine nuclei and middle cerebellar peduncle stimulation." Behav Neurosci 100(6): 878-887.

Stell, B. M. (2011). "Biphasic action of axonal GABA-A receptors on presynaptic calcium influx." J Neurophysiol 105(6): 2931-2936.

Stell, B. M., S. G. Brickley, et al. (2003). "Neuroactive steroids reduce neuronal excitability by selectively enhancing tonic inhibition mediated by d subunit-containing $GABA_A$ receptors." Proc Natl Acad Sci U S A 100(24): 14439-14444.

Stell, B. M., P. Rostaing, et al. (2007). "Activation of presynaptic $GABA_A$ receptors induces glutamate release from parallel fiber synapses." J Neurosci 27(34): 9022-9031.

Stuart, G. and M. Hausser (1994). "Initiation and spread of sodium action potentials in cerebellar Purkinje cells." Neuron 13(3): 703-712.

Stuart, G. and N. Spruston (1998). "Determinants of voltage attenuation in neocortical pyramidal neuron dendrites." J Neurosci 18(10): 3501-3510.

Szabadics, J., C. Varga, et al. (2006). "Excitatory effect of GABAergic axo-axonic cells in cortical microcircuits." Science 311(5758): 233-235.

Taraska, J. W. and W. N. Zagotta (2007). "Cyclic nucleotide-regulated ion channels: spotlight on symmetry." Structure 15(9): 1023-1024.

Trigo, F. F., M. Chat, et al. (2007). "Enhancement of GABA release through endogenous activation of axonal GABA(A) receptors in juvenile cerebellum." J Neurosci 27(46): 12452-12463.

Tsutsui, H., S. Karasawa, et al. (2008). "Improving membrane voltage measurements using FRET with new fluorescent proteins." Nat Methods 5(8): 683-685.

Turecek, R. and L. O. Trussell (2002). "Reciprocal developmental regulation of presynaptic ionotropic receptors." Proc Natl Acad Sci U S A 99(21): 13884-13889.

Vranesic, I., T. Iijima, et al. (1994). "Signal transmission in the parallel fiber-Purkinje cell system visualized by high-resolution imaging." Proc Natl Acad Sci U S A 91(26): 13014-13017.

Wafford, K. A., M. B. van Niel, et al. (2009). "Novel compounds selectively enhance delta subunit containing GABA A receptors and increase tonic currents in thalamus." Neuropharmacology 56(1): 182-189.

Wang, X. J., Y. Liu, et al. (2003). "Adaptation and temporal decorrelation by single neurons in the primary visual cortex." J Neurophysiol 89(6): 3279-3293.

Williams, J. R., J. W. Sharp, et al. (1999). "The neuron-specific K-Cl cotransporter, KCC2. Antibody development and initial characterization of the protein." J Biol Chem 274(18): 12656-12664.

Wilson, H. R. and J. D. Cowan (1972). "Excitatory and inhibitory interactions in localized populations of model neurons." Biophys J 12(1): 1-24.

Woodruff, A. R., H. Monyer, et al. (2006). "GABAergic excitation in the basolateral amygdala." J Neurosci 26(46): 11881-11887.

Wu, C. C., R. M. Russell, et al. (2003). "Tracing developing pathways in the brain: a comparison of carbocyanine dyes and cholera toxin b subunit." Neuroscience 117(4): 831-845.

Xiao, C., C. Zhou, et al. (2007). "Presynaptic $GABA_A$ receptors facilitate GABAergic transmission to dopaminergic neurons in the ventral tegmental area of young rats." J Physiol 580(Pt.3): 731-743.

Zhang, S. J. and M. B. Jackson (1993). "GABA-activated chloride channels in secretory nerve endings." Science 259(5094): 531-534.

Zhang, S. J. and M. B. Jackson (1995). "GABAA receptor activation and the excitability of nerve terminals in the rat posterior pituitary." J Physiol 483 (Pt 3): 583-595.

Zhang, Y., J. H. Chou, et al. (1997). "The Caenorhabditis elegans seven-transmembrane protein ODR-10 functions as an odorant receptor in mammalian cells." Proc Natl Acad Sci U S A 94(22): 12162-12167.

Zhou, W. L., P. Yan, et al. (2007). "Intracellular long-wavelength voltage-sensitive dyes for studying the dynamics of action potentials in axons and thin dendrites." J Neurosci Methods 164(2): 225-239.

Zhou, W. L., P. Yan, et al. (2008). "Dynamics of action potential backpropagation in basal dendrites of prefrontal cortical pyramidal neurons." Eur J Neurosci 27(4): 923-936.